Sites NGHP-01-18

By T. Collett, M. Riedel, J. Cochran, R. Boswell, J. Presley, P. Kumar, A. Sathe,
A. Sethi, M. Lall, and the National Gas Hydrate Program Expedition 01 Scientists

Scientific Investigations Report 2012–5054

U.S. Department of the Interior
U.S. Geological Survey

Contents

Figures

Tables

Site NGHP-01-18

By T. Collett, M. Riedel, J. Cochran, R. Boswell, J. Presley, P. Kumar, A. Sathe, A. Sethi, M. Lall, and the National Gas Hydrate Program Expedition 01 Scientists

Background and Objectives

Site NGHP-01-18 (Prospectus Site MNGH-REL 5) is located at 19° 09.1452'N, 85° 46.3758'E in the Mahanadi Basin (fig. 1). The water depth is ~1374 m. All seismic data were made available through Reliance Ltd., and were extracted from a larger 3D seismic volume (locations are shown in figs. 2 and 3).

- The objectives of the work carried out at this site follow the general objectives of the India NGHP Expedition 01:
- Determine if gas hydrate is present at this site and if the seismic reflection is a gas-hydrate-related BSR;
- Study the occurrence of gas hydrate and establish the background geochemical, geological, geophysical and microbiological baselines for gas-hydrate proxy studies;
- Define the relationship between the sedimentology and structure of the sediments and the occurrence and concentration of gas hydrate;
- Calibrate remote sensing data such as seismic data by acquiring wire-line log data;
- Verify the depositional environment at Site NGHP-01-18.
- The seismic data shown in figures 4 and 5 are characterized by relatively uniform, almost seafloor-parallel sediments with little seismic amplitude variation. The sediments below ~250 ms TWT below the seafloor show a sharp increase in reflectivity. However, this high reflectivity is bound to a band of ~70 ms TWT thickness. Underneath this high-reflectivity band, the reflection amplitudes appear again relatively uniform along the available seismic lines. Although no strong, isolated BSR can be identified at this Site, the top of the high-reflectivity band is interpreted to represent the base of the gas-hydrate stability zone with free gas accumulations below, causing the bright reflectivity. The seismic data at this site show complex structures and geometries suggestive of channelized deposition.

Along the NW-SE oriented seismic line (“Line 1”), a prominent pull-up structure can be seen near trace 440 (fig. 4). This pull-up feature originates at a depth of at least 2.3 sec TWT, well below the base of the inferred gas-hydrate stability zone. The pull-up is apparently stopped at 1.9 s TWT, ~50 ms short of the seafloor, and is marked by a short-lived high-amplitude cap reflection. This pull-up of seismic reflections is most likely an effect of the presence of high-velocity *in situ* gas hydrate.

Operations

This operations summary covers the Leg 4 transit from Site NGHP-01-17 (ANGH01) to Site NGHP-01-18 (MNGH-Reliance 5) and drilling/coring operations for Hole NGHP-01-18A (fig. 6). Schedule details and statistics for this site can be found as Appendixes:

- Appendix 1: NGHP Expedition 01 Operations Schedules
- Appendix 2: NGHP Expedition 01 Operations Statistics

Included in the “Methods” chapter and the glossary is a list of standard or commonly used operations terms and acronyms.

Hole NGHP-01-18A

Hole NGHP-01-18A was occupied on Leg 4 of Expedition 01 and this was the only hole drilled at this site. The 726.0 NMI transit from Site NGHP-01-17 (ANGH01) was completed in 88.0 hr at an average speed of 8.2 kt. The transit took 0.8 days longer than anticipated due to a severe low pressure cell that enveloped nearly the entire Bay of Bengal. Strong head winds (40–50 kt) and heavy seas/swells (15–20 ft) were experienced during the last two days of the transit limiting speed to an average of 6.6 kt. The vessel was switched from cruise mode to DP control at 1234 hr on August 2, 2006 and a positioning beacon was deployed at 1314 hr with the vessel over the site coordinates. The ice bath was installed in the moon pool and the drill collars were picked up from the storage rack. The same BHA as had been used on all previous cored sites was made up and deployed.

Hole NGHP-01-18A was planned as a continuous APC/XCB cored hole to 190.0 mbsf with two packages of pressure cores targeting the gas-hydrate stability zone. Temperature measurements were also to be taken using the APCT–3 and DVTP systems to define a thermal gradient from seafloor to total depth. A complete suite of wire-line logs (Triple Combo, FMS-Sonic, and VSP) were also scheduled for this hole; however, to help make up for some of the time lost on the slow transit, the VSP logging suite was cancelled.

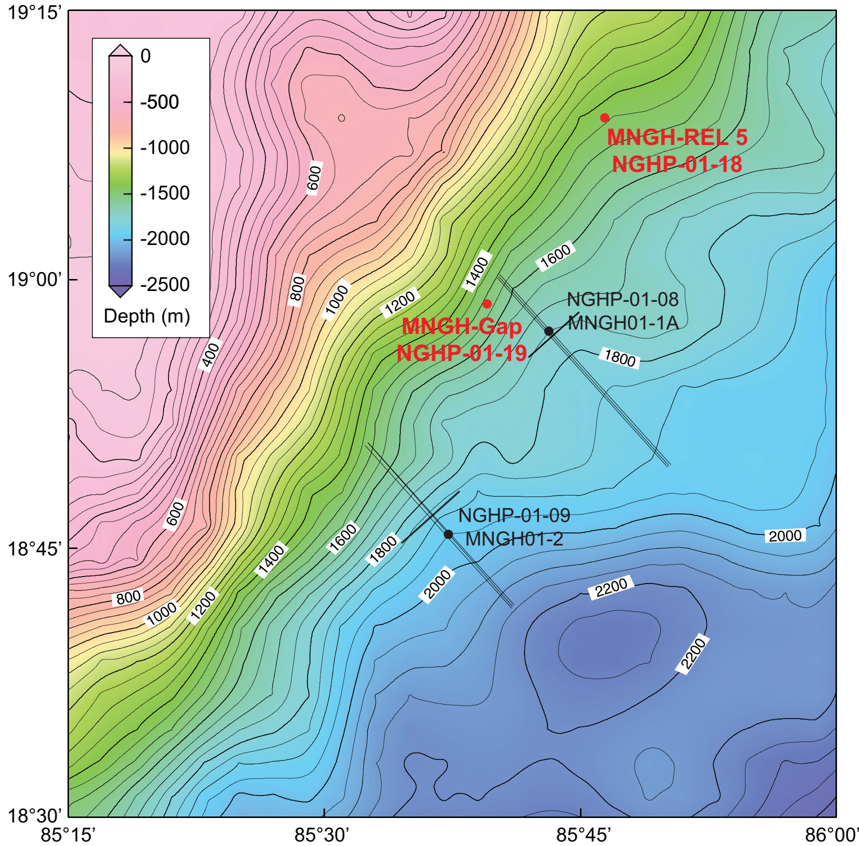

Figure 1. Bathymetric map showing the area of the Mahanadi Basin and Site NGHP-01-18 (Prospectus Site MNGH-REL 5). Also shown is Site NGHP-01-08 (Prospectus MNGH01-1A) and Site NGHP-01-09 (Prospectus Site MNGH01-2); both sites established during LWD (Leg 2) program. [LWD, logging while drilling]

The drill string was tripped to the seafloor and the top drive was picked up in preparation for spudding; however, this activity was deferred because of positioning difficulties. High winds (40+ kt) and an extraordinarily strong current (3+ kt) were aligned, resulting in an inability to maintain station even with both of the main propulsion motors at full power. It should be noted that when configured in DP mode the main propulsion motors cannot provide the same amount of power (or thrust) as they do when configured in cruise mode. With the ship SW (bearing of 210°) of the target location by ~330 m the decision was made to lay out five-stands and secure the drill pipe. The next 2.5 hr were spent waiting-on-weather (WOW). The drill pipe was subsequently run back to 1384.0 mbrf and at 0040 hr on August 3, 2006, Hole NGHP-01-18A was spudded establishing a seafloor depth of 1,386.1 mbrf. The PDR depth for this site, corrected to the rig floor DES, was 1391.4 mbrf.

APC Core NGHP-01-18A-01H was on-deck at 0050 hr and APC coring continued under marginal conditions until 0145 hr through Core NGHP-01-18A-06H to a depth of 54.9 mbsf. Coring was temporarily suspended at that time due to excessive heave (6+ meters). The drill pipe was pulled two-singles off bottom and WOW began again. After some adjustments to heading were made, the vessel heave was reduced to the 4.0 to 4.5 m range and the decision was made to resume APC coring. The bit was run back to TD and Core NGHP-01-18A-07H was on-deck at 0830 hr from 64.4 mbsf. Coring continued using the APC, again under marginal coring conditions, through Core NGHP-01-18A-12H to a depth of 115.9 mbsf. APC coring was halted at this depth due to an incomplete stroke and also because of concern that, due to the high heave conditions, we might not be seeing the true over pull required to extract the core barrels from the formation. During the APC cored interval, a short 4.0 meter drilled advance was made from 73.9 mbsf to 77.9 mbsf. This occurred after Core NGHP-01-18A-08H and prior to Core NGHP-01-18A-09H in order to adjust the drilling kelly.

Successful temperature measurements were taken using the APCT-3 shoe on Cores NGHP-01-18A-03H (at 26.4 mbsf) and NGHP-01-18A-05H (at 23.5 mbsf). The originally scheduled APCT-3 temperature measurement for Core NGHP-01-18A-07H (at 64.4 mbsf) was cancelled due to the severe sea state and because two successful measurements had already been obtained.

Coring continued with the XCB coring system recovering Cores NGHP-01-18A-13X through NGHP-01-18A-20X to a total depth of 190.0 mbsf. DVTP temperature measurements were taken after Cores NGHP-01-18A-14X (unsuccessful) and NGHP-01-18A-20X (successful) at 135.2 mbsf and 190.0 mbsf respectively.

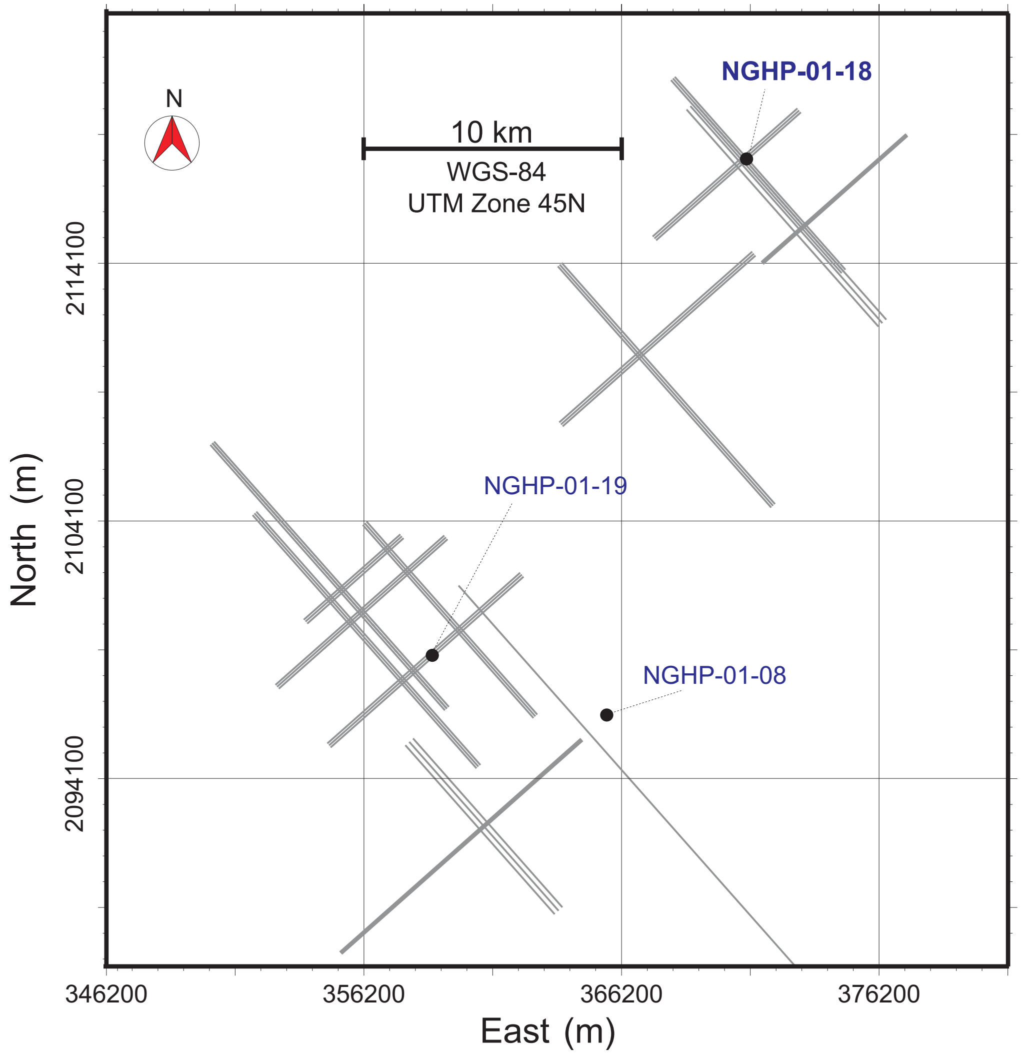

Figure 2. Map of the area in the Mahanadi Basin showing available seismic data and proposed drill sites. Site NGHP-01-18 is the northernmost site of all sites drilled in the Mahanadi Basin. All of the available seismic data were extracted from a 3D seismic volume.

Whirlpaks (microbeads) commonly used for assessing microbiological contamination control were not used. Accelerated core barrel handling protocols were used for all APC/XCB core barrels deployed in this hole. All core barrels were laid down immediately upon arrival at the rig floor before making another drill pipe connection or deploying the next core barrel.

Because of the excessive heave conditions (4+ to 6+ m) the scheduled pressure coring (FPC, HRC, and PCS) and the wire-line logging portions of the operating plan were cancelled. Operations at this site were hampered from start to finish by heavy seas, large swells, excessive heave, moderate to high winds (25+ to 40+ kt), and strong (up to 3+ kt) current. Because of these conditions and safety issues the decision was made to move to the next site in DP mode.

With the BHA racked back in the derrick and the rig floor secured, the ~11.5 NMI transit to Site NGHP-01-19 (MNGH-Gap Site), officially began at 0200 hr on August 4, 2006.

Lithostratigraphy

Site NGHP-01-18 was the first of two sites cored and drilled in the Mahanadi Basin located along the eastern continental margin of India. At Site NGHP-01-18, one hole (NGHP-01-18A) was drilled and cored to a depth of 190 mbsf; pressure coring and wire-line logging were not attempted due to severe weather conditions. (see “Operations”).

The sedimentary sequence recovered at Hole NGHP-01-18A is classified as one lithostratigraphic unit (Unit I) based on sedimentological criteria (for example variations in sedimentary structure and grain size or biogenic and lithologic components) and physical properties (for example magnetic susceptibility and gamma density; fig. 7 and Site NGHP-01-18 Visual Core Descriptions). The core data were integrated with the available seismic data to help define and interpret the stratigraphic section cored at Site NGHP-01-18. The lack of *Discoaster* spp. at this site leads us to suspect the stratigraphy recovered at Site NGHP-01-18 is Quaternary in age.

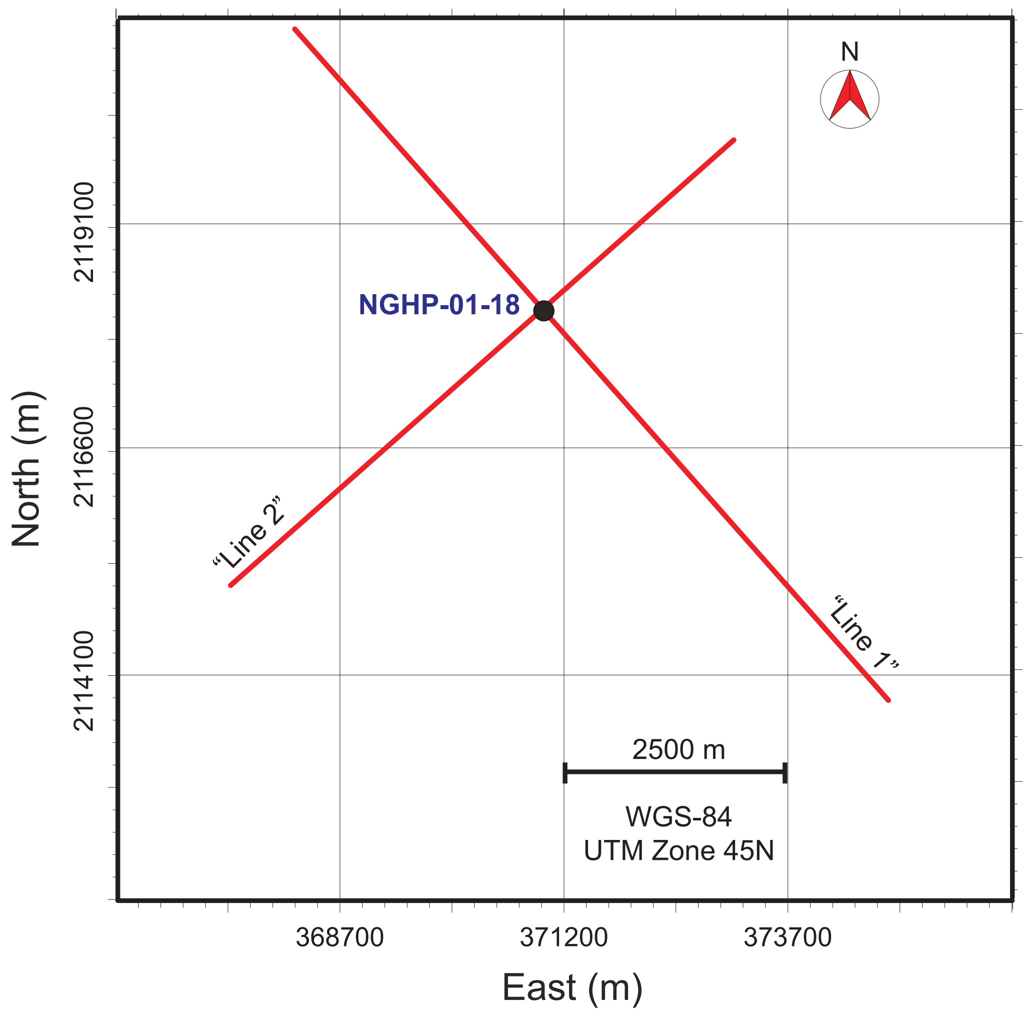

Figure 3. Close-up map of location of Site NGHP-01-18 with two key-seismic lines shown in figures 4 ("Line 1") and 5 ("Line 2").

Lithostratigraphic Units

Lithostratigraphic Unit I

Intervals: Hole NGHP-01-18A, Sections NGHP-01-18A -01H-1 to NGHP-01-18A -20X-CC

Depth: Hole NGHP-01-18A, 0–190 mbsf

Age: Quaternary

Core recovery was generally good at Hole NGHP-01-18A; slightly less than 100 percent recovery occurred only in Cores NGHP-01-18A-07H through NGHP-01-18A-09H and Cores NGHP-01-18A-13X and NGHP-01-18A-15X through NGHP-01-18A-19X (fig. 7 and Site NGHP-01-18 Visual Core Descriptions). Lithostratigraphic Unit I is composed of a variety of calcareous and siliceous biogenic-bearing to -rich clays, volcanic glass-bearing to -rich clays, and clay. All of these lithologies range in color from dark grayish brown (2.5Y 4/2) and dark greenish grey (5GY 4/1) to very dark greenish grey (5GY 3/1 or 10Y 3/1; fig. 7 and Site NGHP-01-18 Visual Core Descriptions). As mentioned above, Lithostratigraphic Unit I at Site NGHP-01-18 is likely Quaternary to recent in age.

Shell fragments and visible foraminifera tests occur sporadically throughout the Unit (figs. 7 and 8, and Site NGHP-01-18 Visual Core Descriptions) and are consistently present in the coarse fractions and smear slides (fig. 9 and table 2). Woody debris is observed in Core NGHP-01-18A-17X (fig. 7 and Site NGHP-01-18 Visual Core Descriptions). A single occurrence of authigenic carbonate was also observed in Core NGHP-01-18A-11X-2 (figs. 7 and 10, and Site NGHP-01-18 Visual Core Descriptions). Occurrences of volcanic ash are visible throughout Core NGHP-01-18A-07H as subcentimeter patches (likely burrows filled with ash) and larger, possibly pumice, fragments (fig. 11 and Site NGHP-01-18 Visual Core Descriptions). Detrital volcanic glass shards were also observed in smear slides taken throughout the Unit and are typically present as trace to 30 percent (fig. 10 and table 1). No distinct beds of ash were observed at Site NGHP-01-18.

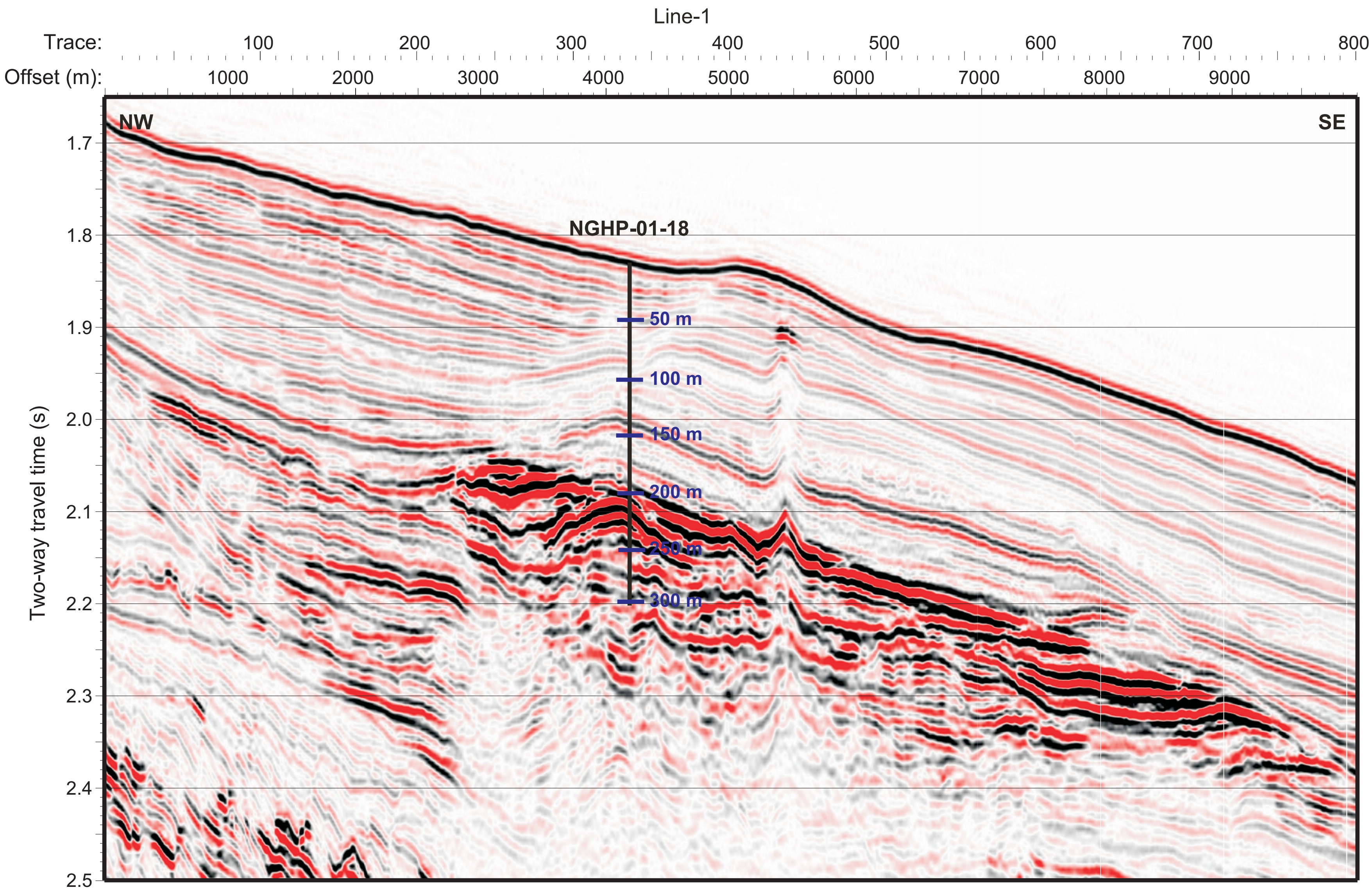

Figure 4. NW-SE oriented seismic line ("Line 1") extracted from a 3D volume crossing Site NGHP-01-18 at trace 330.

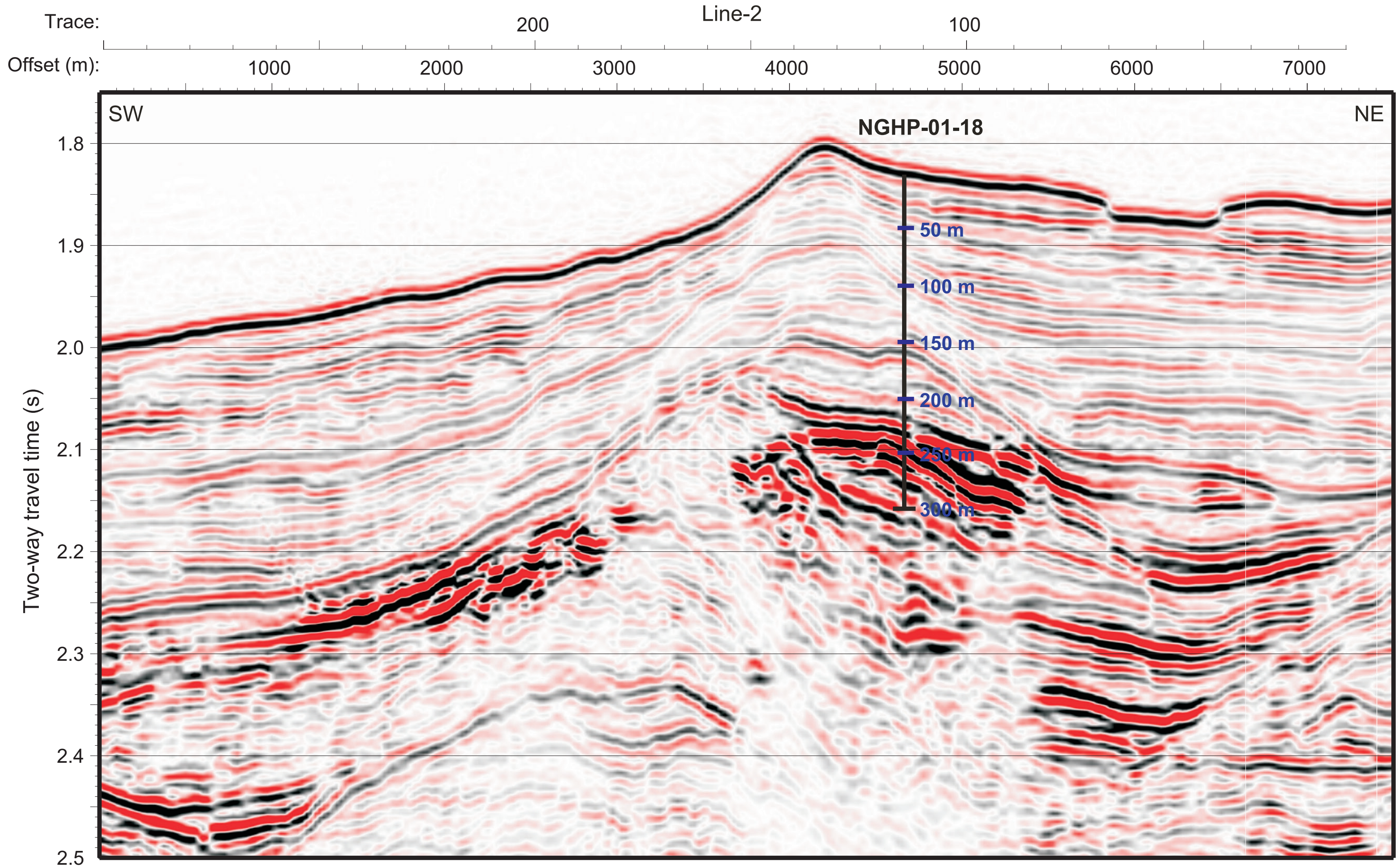

Figure 5. SW-NE oriented seismic line (“Line 2”) extracted from a 3D volume crossing Site NGHP-01-18 at trace 115.

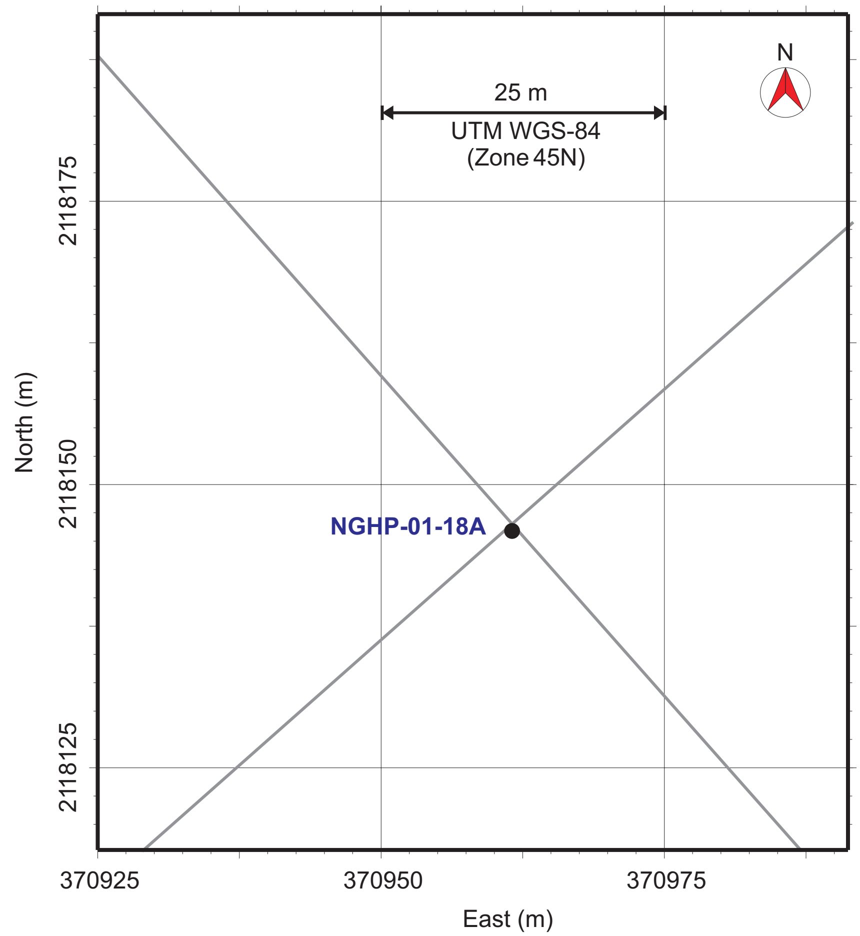

Figure 6. Map showing all holes occupied at Site NGHP-01-18 (MNGH-Reliance 3).

Bioturbation is rare to abundant throughout the interval between 0 mbsf to 125 mbsf. Bioturbation was difficult to identify in the sediments below 125 mbsf and is probably attributable to increased core disturbance related to the switch to XCB coring. Bioturbated zones are also most easily seen in lighter colored portions of the cores where highlighted by dark grey to black colored iron sulfide precipitates. Visual observation of cores shows pyrite and other iron sulfides are present throughout Unit I and coincident with the occurrence of bioturbation, except in the XCB cored interval (figs. 7 and 10, and Site NGHP-01-18 Visual Core Descriptions). Pyrite and other iron sulfides are also present in coarse fractions (trace up to 50 percent) throughout the Unit (table 2).

Downcore magnetic susceptibility measurements (fig. 7) throughout the unit show the greatest variability in Cores NGHP-01-18A-01H through NGHP-01-18A-03H, and also show subtle highs in Cores NGHP-01-18A-06H through -08H, -10H, -13X and -14X (fig. 7). The majority of the cores, however, show a uniform magnetic susceptibility pattern. The density data also show a generally constant bulk density throughout Unit I (fig. 7). Magnetic iron sulfides (for example gregite and(or) pyrrhotite) have been observed in gas-hydrate-bearing sediments offshore western North America (Musgrave and others 2006) and may be responsible for some of the magnetic susceptibility highs observed here. However, subtle changes in magnetic mineral grains present in the more clay rich (biogenic poor) zones may also explain some of this subtle variability.

The major lithologies of Lithostratigraphic Unit I determined from smear slides consist primarily of clay-sized (75–99 percent) grains with minor amounts of silt-sized grains (up to 25 percent; table 1). Minor lithologies described in smear slide included burrow fills and anomalous lighter colored clay regions (table 1). The major non-biogenic components of Lithostratigraphic Unit I are quartz, feldspar, mica, and clay minerals. Opaque grains, mostly iron sulfides in irregular and framboidal forms, are common in all grain sizes, and comprise typically trace to 3 percent of the total sediment (table 1). The total biogenic component of the sediment is dominated by calcareous nannofossils, which comprise trace to 60 percent of the total (biogenic and non-biogenic) sediment grains (table 1). Foraminifera occur (trace to 40 percent) in smear slides, however, they are more abundant (trace to 80 percent) in the coarse fractions of the sediments (table 2) throughout the hole. Foraminifera are often visible with the naked eye on the split core surfaces as well. Terrestrial organic matter is common (trace to 10 percent) in smear slides taken throughout Unit I (table 1).

Gas-Hydrate Occurrence

At Site NGHP-01-18A, the entire core was collected above the level of the BSR and thus, most likely within the gas-hydrate stability zone. Several small IR anomalies were observed in the cores and may indicate disseminated gas hydrate was present within clay sediments at 55 mbsf to 65 mbsf, at 115 mbsf, and at 180 mbsf (see “Physical Properties”). Moussey texture was observed in the split cores at several locations throughout the hole (fig. 7); however, these regions generally did not correspond to IR anomalies. Porewaters measured from two of the areas of moussey texture (see “Inorganic Geochemistry”) showed abundant sulfate, suggesting seawater sulfate contamination which was likely induced by the XCB coring combined with the rough sea state during coring (see “Operations”). Thus, although some of the moussey textures may have formed from the dissociation of gas hydrate, others may have been coring-induced seawater infiltration/contamination. Porewater geochemistry data also showed subtle porewater freshening coincident with the IR anomalies at 115 mbsf and 180 mbsf. Unfortunately, pressure cores were not deployed at Site NGHP-01-18 due to the rough sea state.

Inorganic Geochemistry

This is one of two sites cored in the Mahanadi Basin. The main goals of the inorganic geochemistry program in this region were to constrain the biogeochemical and hydrological characteristics of this basin in order to evaluate the gas-hydrate distribution and abundance. In particular, the objectives were to (1) document the influence of the oblique fault that intersects the drilled section at ~100 mbsf on the interstitial water chemistry, and (2) document the gas-hydrate distribution and content in the “channel-fill” sediments between ~150 mbsf and the depth of the seismic BSR, using infrared (IR) imaging and chloride concentrations. The IW chemical data are tabulated in tables 3 and 4, and illustrated in figures 12, 13, and 14.

A total of 41 whole-round samples were collected and processed for interstitial water (IW) analyses at Site NGHP-01-18, in coordination with both the organic geochemistry and microbiology sampling programs. No pressure cores were collected at this site. Whole-round lengths for the conventional core samples ranged from 10 to 30 cm, with longer sections sub-sampled from cores recovered deeper within the hole. The higher resolution sampling of fourteen whole rounds in the upper 25 mbsf was aimed at characterizing the sulfate-methane interface (SMI) and providing supporting data and samples for studies on the microbial dynamics of the SMI. Three whole round samples were taken in Core NGHP-01-18A-04H, two samples were collected from Core NGHP-01-18A-05H (38.8 mbsf) to Core NGHP-01-18A-09H (83.7 mbsf), and one to two samples were collected in the remaining cores to TD (186.2 mbsf).

All cores were scanned by IR imaging on the catwalk, in an effort to identify the presence of gas hydrate. There is a slight decrease in the background temperature imaged by the IR camera from Core NGHP-01-18A-13X (110 mbsf) to the bottom of the hole (see “Physical Properties”). Within this slightly ‘colder’ depth interval minor variations in the intensity of the IR signal were observed, as for example in Section NGHP-01-18A-19X-2 at ~175 mbsf. The salinity and chlorinity of this sample were similar to the corresponding values obtained in an adjacent background sample from the same core (table 4). The minor IR anomaly in sample NGHP-01-18A-19X-2 was associated with a higher quality sediment sample recovered, thus the sample contained more intact ‘biscuits’. Intact biscuits apparently better maintain the slightly colder temperature from gas-hydrate dissociation than the background sample.

Interstitial Water Chloride and Salinity

Chloride concentrations were measured by titration with $AgNO_3$, with the percent precision of chloride values averaging 0.2 percent, and salinity was determined by refractometry. The Cl^- concentration and salinity data are presented in table 4 and illustrated in figure 12A and 12B.

The salinity depth profile shows a steady decrease with depth from 34.5 to a minimum of 30.2 at 170 mbsf (fig. 12B). In the uppermost ~30 mbsf, the profile is influenced by the diagenetic loss of sulfate. Deeper in the section salinity mostly mimics the chlorinity profile discussed below.

Figure 7 (following page). Lithostratigraphic summary of Hole NGHP-01-18A. [BSR, bottom-simulating reflector; SMI, sulfate-methane interface] Note: Colored intervals exceed symbol size when there is a range in the occurrence. Center point of each symbol represents depth of occurrence; therefore colored bars may slightly exceed core recovery; see Site NGHP-01-18 Visual Core Descriptions for the expanded scale, detailed core descriptions; see Site NGHP-01-18 Oversized Figure for the enlarged version of this summary.

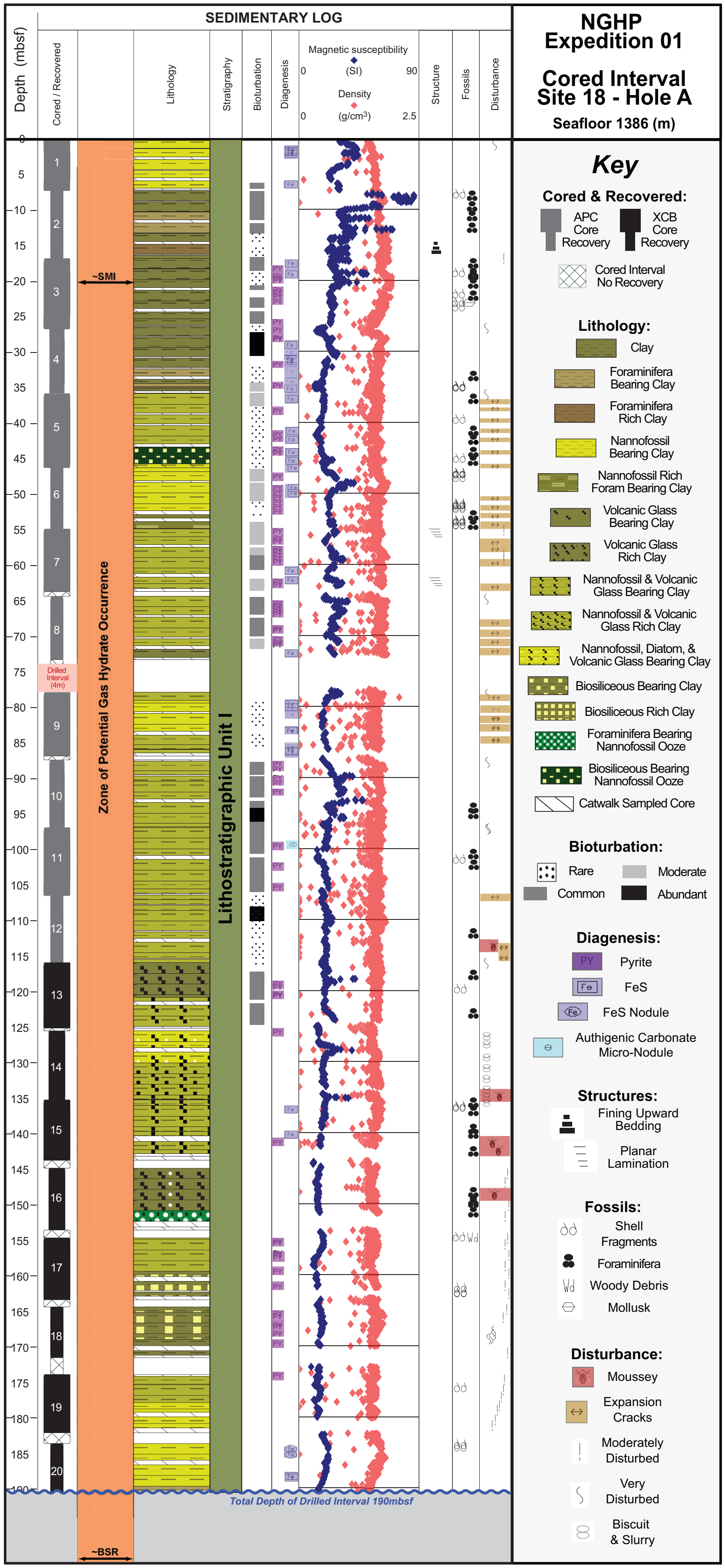
SEDIMENTARY LOG
Depth (mbsf)
Cored / Recovered
Lithology
Stratigraphy
Bioturbation
Diagenesis
Magnetic susceptibility
0 (SI) 90
Density
0 (g/cm3) 2.5
Structure
Fossils
Disturbance
~SMI
Zone of Potential Gas Hydrate Occurrence
Lithostratigraphic Unit I
Drilled Interval (4m)
Total Depth of Drilled Interval 190mbsf
~BSR
NGHP Expedition 01
Cored Interval Site 18 - Hole A
Seafloor 1386 (m)
Key
Cored & Recovered:
APC Core Recovery
XCB Core Recovery
Cored Interval No Recovery
Lithology:
Clay
Foraminifera Bearing Clay
Foraminifera Rich Clay
Nannofossil Bearing Clay
Nannofossil Rich Foram Bearing Clay
Volcanic Glass Bearing Clay
Volcanic Glass Rich Clay
Nannofossil & Volcanic Glass Bearing Clay
Nannofossil & Volcanic Glass Rich Clay
Nannofossil, Diatom, & Volcanic Glass Bearing Clay
Biosiliceous Bearing Clay
Biosiliceous Rich Clay
Foraminifera Bearing Nannofossil Ooze
Biosiliceous Bearing Nannofossil Ooze
Catwalk Sampled Core
Bioturbation:
Rare
Moderate
Common
Abundant
Diagenesis:
Pyrite
FeS
FeS Nodule
Authigenic Carbonate Micro-Nodule
Structures:
Fining Upward Bedding
Planar Lamination
Fossils:
Shell Fragments
Foraminifera
Woody Debris
Mollusk
Disturbance:
Moussey
Expansion Cracks
Moderately Disturbed
Very Disturbed
Biscuit & Slurry

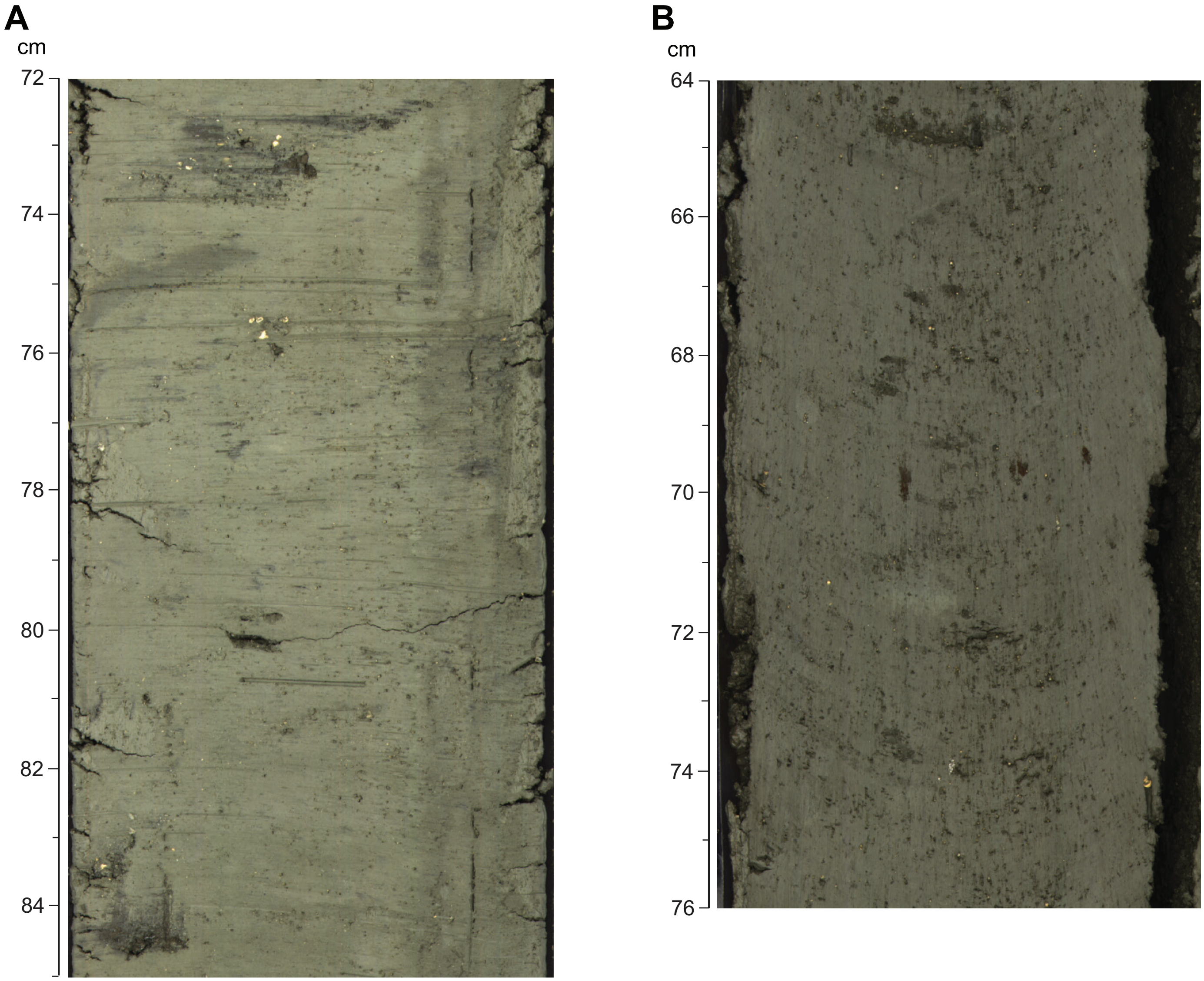

Figure 8. Visible foraminifera and shell fragments observed throughout Unit I. A, Section NGHP-01-18A-11H-4, 72–85 cm. B, Section NGHP-01-18A-15X-1, 64–76 cm. Also note the black iron sulfide precipitates in both A and B.

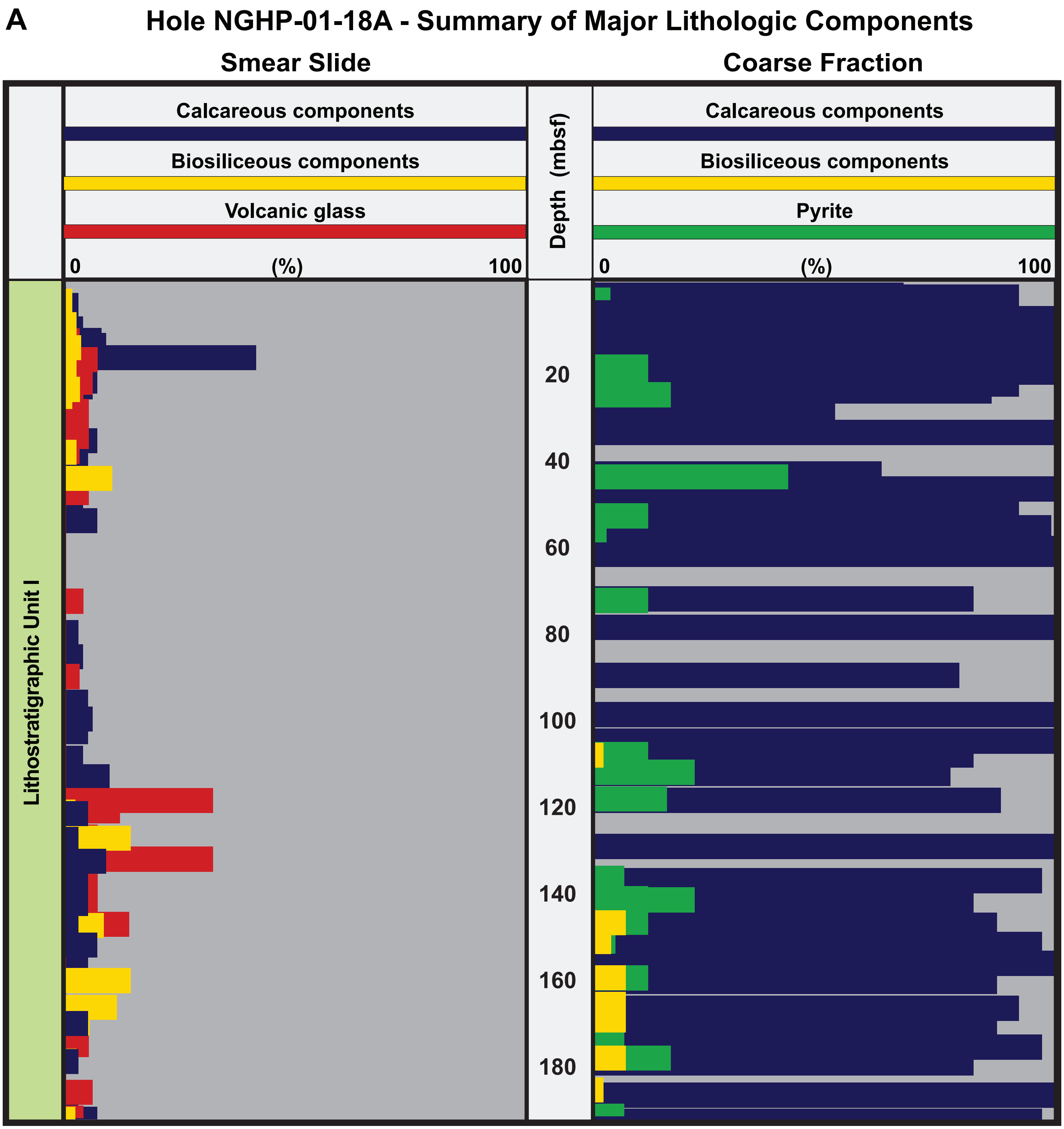

Figure 9. A, Major lithologic components in smear slides (see table 1) and coarse fraction (see table 2) plotted from percent visual estimation. B, Major lithologic components in coarse fraction and smear slides; shown for clarity as individual abundance plots.

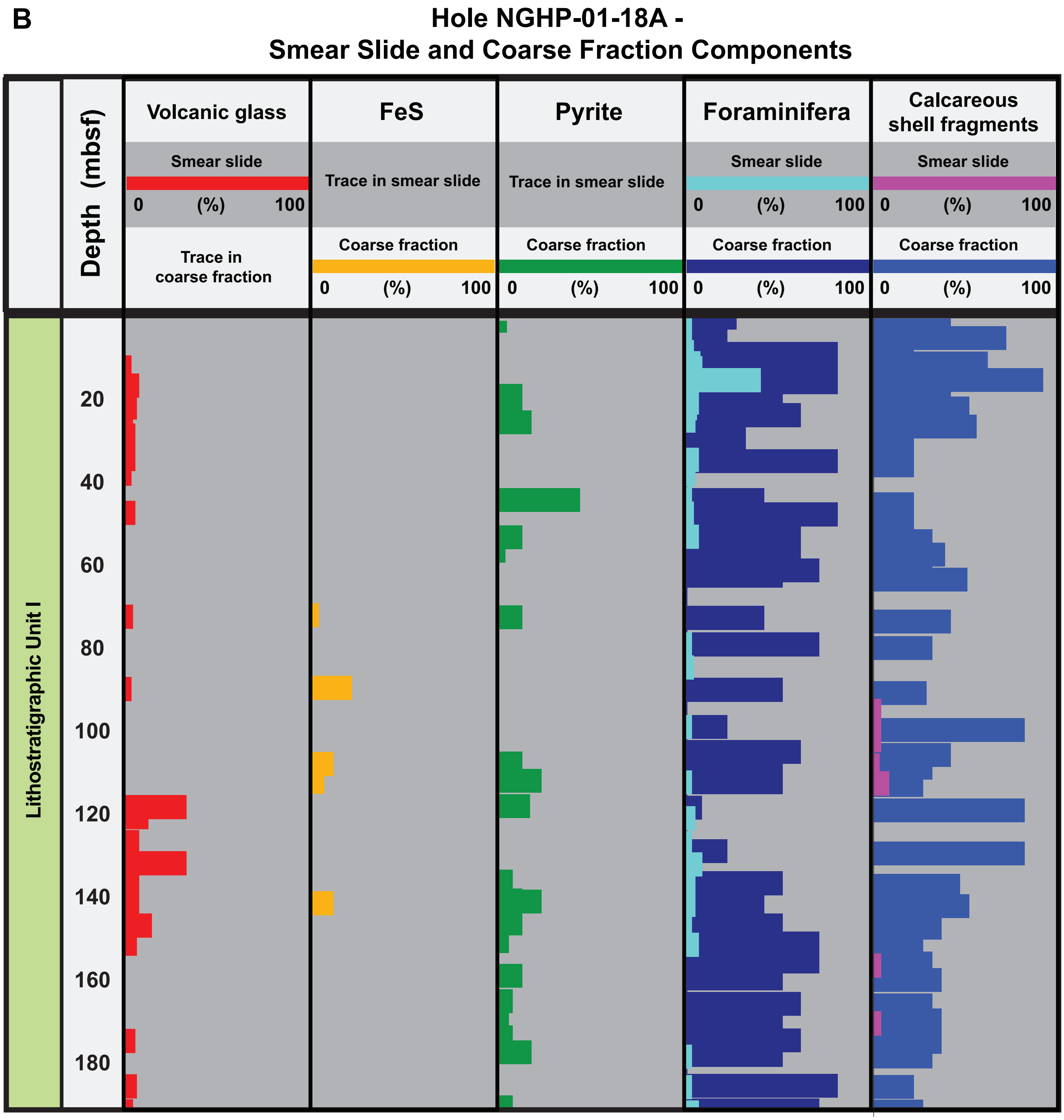

Figure 9. A, Major lithologic components in smear slides (see table 1) and coarse fraction (see table 2) plotted from percent visual estimation. B, Major lithologic components in coarse fraction and smear slides; shown for clarity as individual abundance plots.—Continued

Figure 10. Authigenic carbonate occurrence. Recovered in Section NGHP-01-18A-11H-2, 85–95 cm.

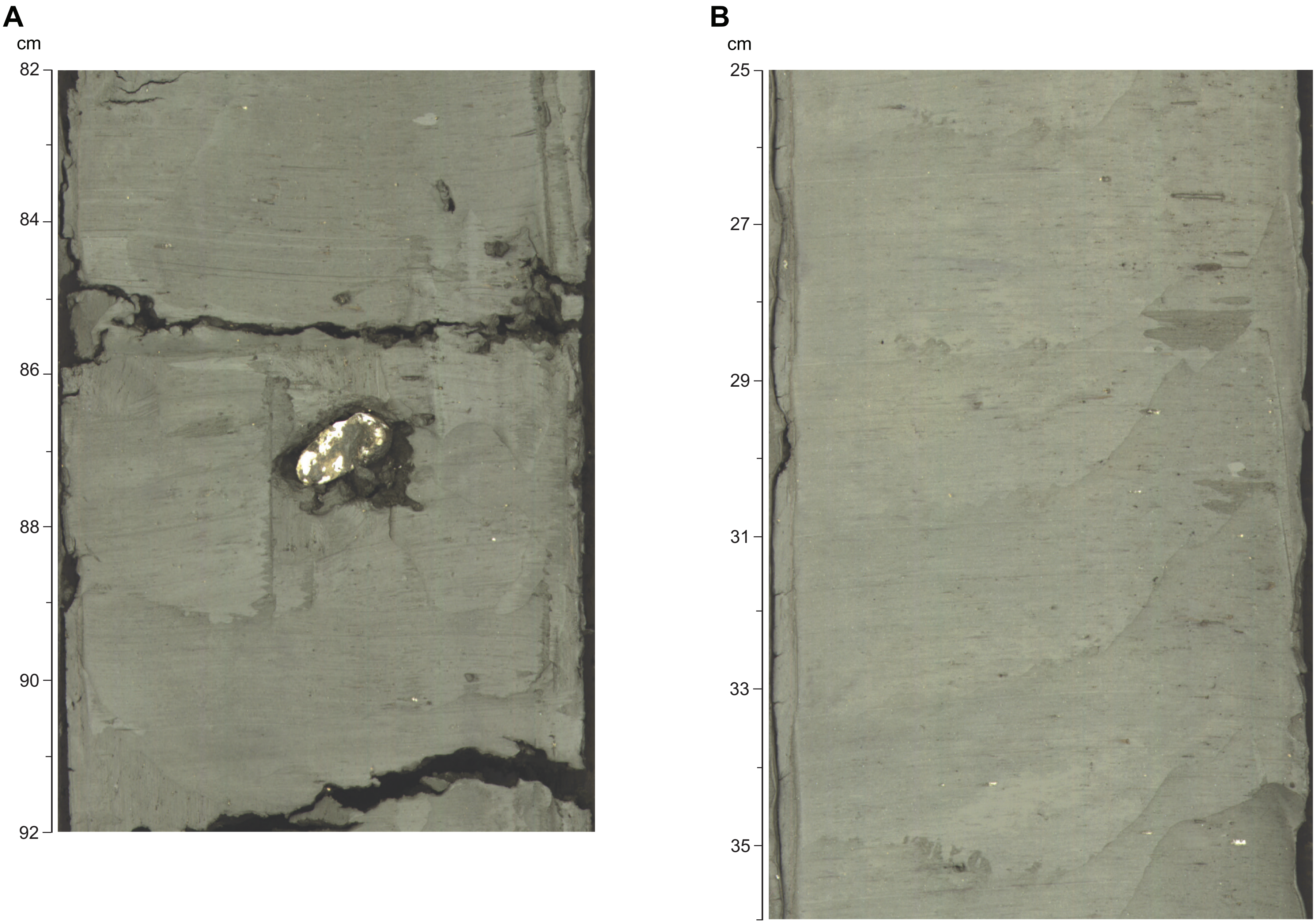

Figure 11. Volcanic glass fragment/pumice; A, Section NGHP-01-18A-07H-2, 82–92 cm and small (>1 mm) ash filled burrows (white); B, Section NGHP-01-18A-07H-5, 25–36 cm.

The chloride concentration depth profile (fig. 12A) shows two distinct zones. From the seafloor to ~100 mbsf, chlorinity values do not change with depth. In the deeper section, from ~100 mbsf to total depth (TD), a slight freshening trend with depth is observed, from approximately 559 to a minimum of 534 mM (table 4), which equates to ~95 percent of the seawater concentration. The depth distribution of IR temperatures (see "Infrared Imaging" in "Physical Properties") also shows a minor but distinct shift to colder values below ~115 mbsf. These two observations may reflect the presence of minor quantities of disseminated gas hydrate throughout this depth interval. A fault intersects the sediment section drilled at approximately 110 mbsf, suggesting that this structural feature may act as a boundary between the section above that is devoid of gas hydrate, most likely because of methane concentrations that are too low for gas-hydrate formation, and the section below having small amounts of disseminated gas hydrate. Some of the sediments below 100 mbsf show moussey textures that may be suggestive of gas-hydrate dissociation in preferred sediment intervals (see "Lithostratigraphy").

In order to explain the origin of the moussey textures, two moussey sediment intervals, from Sections NGHP-01-18-15X-6 and NGHP-01-18-17X-4 located at about 140 and 160 mbsf, were subsampled and analyzed for salinity, Cl^-, and SO_4^{2-} concentrations. The salinity was somewhat higher, ~32.5, than in the adjacent IW samples with ~30.5 salinity, and the sulfate concentrations were ~12.9 and 10.6 mM, respectively (table 3), equal to about 45 percent and 37 percent seawater sulfate value, whereas the adjacent IW samples have zero sulfate. This indicates that these moussey sample intervals are to a large extent contaminated with drill-water. This implies that instead of gas-hydrate dissociation, the strong heave prevailing at the time of drilling caused sediment disturbance that was responsible for the moussey textures in these samples.

Sulfate and Alkalinity Concentrations: Characterization of the SMI

The primary objectives of the higher resolution sampling in the upper 25 m of the sediment section were to delineate and characterize the SMI for future geochemical modeling of methane fluxes and to provide supporting data and samples for studies on the microbial dynamics of the SMI. At Site NGHP-01-18, the sulfate-methane interface is located at 21 mbsf, as illustrated in figure 13B. Alkalinity shows a broad maximum from 20 to 40 mbsf, where it reaches 24.8 mM (fig. 14). These depth-concentration profiles are controlled by the combined reactions of organic matter fueled sulfate reduction, anaerobic methane oxidation, and methanogenesis. The alkalinity concentration is significantly lower than predicted by organic fueled sulfate reduction or anaerobic methane oxidation, indicating a significant loss of alkalinity by authigenic carbonate formation. A second zone of authigenic carbonate formation occurs in the broad zone of minimum alkalinity between about 50 to ~110 mbsf in the alkalinity depth profile. In this zone, foraminiferal abundance also increases (see "Lithostratigraphy"). Below the fault at ~100 mbsf, the increase in alkalinity values with depth corresponds with an increase in CO_2 concentrations (see "Organic Geochemistry"). The Ca^{2+} and Mg^{2+} concentration profiles will be used to calculate total alkalinity loss by authigenic carbonate formation in the three distinct alkalinity concentration depth intervals.

The sulfate profile will be utilized to compute the vertical component of the methane flux at this site. Below the SMI, sulfate concentrations remain zero throughout the drilled section; the few slightly higher than 0.10 mM sulfate values, reported in table 3, most likely indicate contamination by drill-water. The most difficult samples to clean from drill-water contamination were the XCB cores, which were highly disturbed due to high swell conditions during drilling. The sulfate concentrations in these samples were used to calculate the amount of drill-water contamination, and the salinity, alkalinity, Cl^-, and Br^- concentrations were corrected for the contamination. The corrected concentrations are listed in table 4.

Bromide Concentrations

Pore water samples were analyzed for dissolved Br^- by ion chromatography. Bromide concentrations are primarily influenced by marine organic matter diagenesis, such that the Br^- concentration increases with organic matter decomposition. At Site NGHP-01-18A there is only a slight increase in dissolved bromide to a maximum value of 1.2 mM (fig. 14). The maximum Br^- value of 1.2 mM is somewhat less than the value of 1.6 mM in the upper 200 mbsf at Site NGHP-01-17 in the Andaman Sea. This difference probably suggests a larger amount of primarily marine organic matter in the Andaman Basin sediments as compared with the sediment at this site, with more terrestrial organic matter input via the Mahanadi River system.

Organic Geochemistry

Shipboard organic geochemical studies at Site NGHP-01-18 (MHGH-05) included analysis of the composition of volatile hydrocarbons including methane, ethane, and propane (C_1–C_3) and fixed natural gases (that is, O_2, CO_2, and N_2+Ar) from headspace and void gas. No pressure core sampler (PCS) degassing experiments were performed. In general, these analyses indicate that methane and carbon dioxide are the predominant gases found in the cores at Site NGHP-01-18. However, ethane was present near detection limits (<30 ppmv) in headspace and at moderate level concentrations (<440 ppmv) in void gas samples collected below 48 mbsf. The headspace samples above the SMI were dominated by air and slightly depleted in carbon dioxide. Methane was enriched below the SMI and above the seismically-inferred BSR.

Table 1. Smear-slide data for Hole NGHP-01-18A

Sample reference			Texture			Mineral										
Core, section, depth (cm, in section)	MBSF	Lithology	Sand	Silt	Clay	Quartz	Feld-spar	Mica	Heavy minerals	Clay minerals	Volcanic glass	Glau-conite	Fram-boidal pyrite	Iron sulfides	Rock framents	Authigenic carbonates
								NGHP-01-18A								
1H-1,40	0.4	D		3	97	20		trace		72						
1H-3,7	3.07	D		3	97	15		1		71				1		
2H-1,130	8.7	D		5	95	2	2	1		84				trace		4
2H-3,100	11.4	D		3	97	2				86	trace			1		
2H-3,51	10.91	M		20	80	trace										trace
2H-4,65	12.55	D		3	97	1				86	1			trace		
2H-5,50	13.9	D		2	98	2	1	trace		87				trace	trace	2
2H-6,47	15.37	M		40	60	2		trace		55	trace					trace
2H-7,55	16.95	D		10	90	1	trace			85	5			trace		1
3H-2,75	19.15	D		12	88	2	1			85	4		1			
3H-3,83	20.73	M		10	90	3				87	1			trace		
3H-4,81.5	22.215	M		30	70	14	3	3	1	67	4			1	trace	
3H-5,62	23.52	D		12	88	2	trace			86	2			2		
3H-6,75	25.15	D		10	90	8	1			83	1			trace		
4H-2,101	28.91	D		5	95	10				86	3					
4H-6,71	34.61	D		6	94					90	3		1			
5H-2,70	38.1	D		10	90	8	1			64	1			1		
5H-6,70	44.1	D		10	90	4	trace			81	trace			1		
6H-2,70	47.52	D		1	99	5				83	3					
6H-6,30	53.12	D		10	90	5				40	trace					
7H-2,35	56.33	D		1	99	10				74	trace					
7H-6,60	62.31	D			100	2				81	trace					
8H-2,90	66.77	D		25	75	20				64	trace					
8H-6,75	72.58	D		5	95	20				77	2					
9H-1,110	79	D		5	95	8		1		75	trace		trace	1		
9H-1,120	79.1	D		2	98	3		trace	1	87				1		
9H-5,60	84.5	D		7	93	4		1		70			2	1		
10H-2,100	89.9	D		1	99	3				74	1			1		
10H-6,10	94.98	D		2	98	2				70						
11H-2,62	99.02	D		1	99	1				74						
11H-4,62	102.02	D		3	97	2				75						
12H-2,100	108.06	D		3	97	2				71						
12H-5,80	112.36	D		7	93	2				59						
13X-2,100	118.4	D		5	95	2	trace			63	30			trace		
13X-4,40	120.8	D		5	95	3	trace			67	10			1		
14X-2,60	126.8	D		3	97	2	trace			74	5			trace		
14X-5,130	132	D		15	85	2	trace			28	30			2		
15X-2,80	136.81	D		5	95	2				75	5			1		
15X-6,60	141.63	D		5	95	2				53	5			1		
16X-2,70	146.95	D		2	98	2				73	12			1		
16X-5,60	151.35	D		7	93	3				25	4			1		
17X-2,87	155.67	D		1	99	2	1			81						
17X-5,40	159.7	D		5	95	2	trace			82						
18X-2,80	165.83	D		5	95	1	2			83						
18X-5,50	169.42	D		2	98	1				92	trace			trace		
19X-2,60	174.65	D		1	99	1				80	3					trace
19X-5,50	178.27	D		4	96	1				90	trace					
20X-6,61	191.61	D		10	90					87	2			3		
20X-2,61	185.61	D		2	98	2				86	4			1		

Table 1. Smear-slide data for Hole NGHP-01-18A—Continued

Sample reference			Biogenic								
Core, section, depth (cm, in section)	MBSF	Lithology	Fora-minifera	Nanno-fossils	Carbonate shell fragments	Dia-toms	Radio-larians	Silico-flagellates	Sponge spicules	Plant debris	Comments
NGHP-01-18A—Continued											
1H-1,40	0.4	D	trace	7		trace		trace	trace	1	
1H-3,7	3.07	D	1	10		trace	trace	trace		1	
2H-1,130	8.7	D	2	2		trace			1	2	
2H-3,100	11.4	D	6	3					1	1	
2H-3,51	10.91	M	trace	2						98	from burrow, poorly constructed slide
2H-4,65	12.55	D	7	3					1	1	very fine grained
2H-5,50	13.9	D	2	3		1	trace		1	1	from light green clay
2H-6,47	15.37	M	40	2		trace			trace	1	from possible turbidite
2H-7,55	16.95	D	3	3					1	1	from dark green clay
3H-2,75	19.15	D	3	3		1			trace	trace	
3H-3,83	20.73	M	5	2		trace			1	1	fine grained
3H-4,81.5	22.215	M	4	3							heay mineral is amphibole
3H-5,62	23.52	D	3	3		1			1		from light green clay
3H-6,75	25.15	D	3	3		trace			trace	1	
4H-2,101	28.91	D	trace	trace						1	
4H-6,71	34.61	D	5	trace						1	from light green clay
5H-2,70	38.1	D	3	20		trace			1	1	
5H-6,70	44.1	D	1	3		6		1	2	1	trace amphibole, pyritized diatoms
6H-2,70	47.52	D	2	5						2	
6H-6,30	53.12	D	5	40						10	
7H-2,35	56.33	D	trace	15						1	
7H-6,60	62.31	D	trace	15						2	
8H-2,90	66.77	D	trace	15						1	
8H-6,75	72.58	D								1	
9H-1,110	79	D	1	13						1	from dark green clay
9H-1,120	79.1	D	trace	7					trace	1	from light green clay
9H-5,60	84.5	D	2	20					trace		
10H-2,100	89.9	D	trace	20						1	
10H-6,10	94.98	D	trace	25	3						
11H-2,62	99.02	D	1	20	3					1	
11H-4,62	102.02	D	trace	20	3						
12H-2,100	108.06	D	trace	25	2						
12H-5,80	112.36	D	1	30	7					1	
13X-2,100	118.4	D	trace	5					trace		very fine grained volcanic glass with larger shards and fibrous pieces
13X-4,40	120.8	D	3	15					1		
14X-2,60	126.8	D	1	5		8		1	4		
14X-5,130	132	D	7	30					1		volcanic glass various degrees of dentrification and morphologies
15X-2,80	136.81	D	3	12					1	1	sutured quartz grains
15X-6,60	141.63	D	3	35					1		
16X-2,70	146.95	D	1	3		5		trace	2	1	
16X-5,60	151.35	D	5	60					1	1	
17X-2,87	155.67	D		13	3						
17X-5,40	159.7	D		3		7		1	5		
18X-2,80	165.83	D		4	trace	7		1	2		
18X-5,50	169.42	D			3	3		1			
19X-2,60	174.65	D	trace	12						4	
19X-5,50	178.27	D	1	5		1			trace	2	
20X-6,61	191.61	D	5	2		1					
20X-2,61	185.61	D	1	5						1	

Note: M = minor lithology, D = dominant lithology

Table 2. Coarse fraction (>63 µm) sieve data for Hole NGHP-01-18A.

Sample reference		Mineral											
Core, section, depth (cm, in section)	MBSF	Quartz	Feldspar	Mica	Heavy minerals	Volcanic glass	Pyrite	Iron sulfides	Fram-boidal pyrite	Rock fragments	Pumice	Other minerals	Authigenic carbonates
NGHP-01-18A													
1H-1,40	0.4			12	1		2						
1H-3,70	3.7			2									
2H-1,130	8.7												
2H-2,90	9.8												
2H-3,100	11.4				trace								
2H-5,50	13.9												
2H-6,65	15.55												
2H-6,67	15.57												
3H-2,25	18.65						10						
3H-3,83	20.73			trace	trace	trace							
3H-5,62	23.52						10						
3H-6,75	25.15	trace			1		15						
3H-6,81.5	25.215	90				2	trace						
4H-6,71	34.61						trace						
4H-2,101	28.91						trace					50	
5H-6,70	44.1						40						
6H-6,30	53.12						10						
6H-2,70	47.52						trace						
7H-5,60	60.98												
7H-6,60	62.31				1	Trace							
7H-2,35	56.33				1	1	1						
8H-6,75	72.58				6	2	10	2					
9H-1,110	79				Trace		trace						
10H-2,100	89.9	2						20					
11H-6,62	105												
11H-2,62	99.02	trace			Trace		trace						
12H-2,100	108.06	trace					10	10					
12H-5,80	112.36	trace					20	5					
13X-2,100	118.4	trace					14						
14X-3,130	129						trace						
15X-2,80	136.81						5						
15X-6,40	141.43	trace					10	10					
15X-6,60	141.63						20						
16X-2,70	146.95	trace			trace		10						
16X-5,60	151.35						3						
17X-2,87	155.67					trace	trace						
17X-5,40	159.7						10						
18X-2,80	165.83	trace			trace	trace	5						
18X-5,50	169.42	7					3						
19X-2,60	174.65	trace					5						
19X-5,50	178.27						15						
20X-2,61	185.61				trace	trace	trace						
20X-6,61	191.61						5						

Table 2. Coarse fraction (>63 µm) sieve data for Hole NGHP-01-18A.—Continued

Sample reference		Biogenic										
Core, section, depth (cm, in section)	MBSF	Fora-minifera	Carbonate shell fragments	Diatoms	Radio-larians	Silico-flagellates	Siliceous shell fragments	Sponge spicules	Fish remains	Other biogenic	Plant debris	Comments
NGHP-01-18A—Continued												
1H-1,40	0.4	25	40							20		Other biogenic is fecal pellets
1H-3,70	3.7	20	70							8	trace	Other biogenic is fecal pellets
2H-1,130	8.7	80	20									
2H-2,90	9.8	40	60									Trace of black organic matter light streaks
2H-3,100	11.4	80	18						2			
2H-5,50	13.9	10	90		trace							
2H-6,65	15.55	80	20									
2H-6,67	15.57	80	18							2		Other biogenic is micro gastropods
3H-2,25	18.65	50	40									
3H-3,83	20.73	50	50									Trace micro gastropods
3H-5,62	23.52	60	30									Silvery luster on pyrite
3H-6,75	25.15	30	54									
3H-6,81.5	25.215	8										
4H-6,71	34.61	80	20									G. Ruben forams
4H-2,101	28.91	30	20									Other minerals—greasy black, black streak, hardness of 2, marks paper
5H-6,70	44.1	40	20									
6H-6,30	53.12	60	30									
6H-2,70	47.52	80	20									G. Ruben forams
7H-5,60	60.98	70	30									
7H-6,60	62.31	50	49									(Pyrite) burrows kept out of total
7H-2,35	56.33	60	37									
8H-6,75	72.58	40	40									
9H-1,110	79	70	30									
10H-2,100	89.9	50	27				1					Glitter iron sulphides
11H-6,62	105	60	40									
11H-2,62	99.02	20	80									
12H-2,100	108.06	50	30		trace			trace				
12H-5,80	112.36	50	25									
13X-2,100	118.4	6	80									
14X-3,130	129	20	80									
15X-2,80	136.81	50	45									
15X-6,40	141.43	40	40									Silvery luster iron sulphides
15X-6,60	141.63	30	50		trace							
16X-2,70	146.95	50	35		5							
16X-5,60	151.35	70	25		2							
17X-2,87	155.67	70	30									
17X-5,40	159.7	50	35		5						trace	
18X-2,80	165.83	60	30		5							
18X-5,50	169.42	50	35		5							
19X-2,60	174.65	60	35		trace							
19X-5,50	178.27	50	30		3			2				
20X-2,61	185.61	80	20		trace			trace				
20X-6,61	191.61	70	25					trace				

Table 3. Interstitial-water data for Hole NGHP-01-18A. Note that a dash indicates the value was not determined. The samples that were corrected for drill-water contamination are marked by bold data in the sulfate concentration column. The Special Samples are those collected from the open cores to assist sedimentologists with their interpretation of mousey textures in the cores.

Sample name	Depth (mbsf)	Vol. (mL)	pH	Alk (mM)	Salinity	Titr Cl^- (mM)	Br^- (mM)	SO_4^{2-} (mM)	Comments
1H-1 140-150	1.4	40.0	7.7	5.88	34.5	557	0.87	24.41	Dark clay
1H-2 140-150	2.9	20.0	7.3	7.69	34.5	558	0.71	21.26	Dark-green fine clay
1H-3 140-150	4.4	40.0	7.4	10.97	34.5	558	0.70	18.04	Dark-green fine clay
1H-4 140-150	5.9	40.0	7.3	11.71	34.5	557	0.74	16.82	Green fine clay
1H-5 115-125	7.05	40.0	7.3	12.70	34.5	559	0.84	14.78	Green fine clay
2H-1 140-150	8.8	42.0	7.3	15.12	34.0	557	0.81	12.94	Green fine clay
2H-2 140-150	10.3	40.0	7.3	15.50	34.0	559	0.83	11.52	Green fine clay
2H-3 140-150	11.8	40.0	7.3	16.41	34.0	560	0.83	9.83	Dark-green clay. Forams
2H-4 140-150	13.3	40.0	7.3	15.86	34.0	559	1.00	8.07	Dark-green clay. Forams and shells
2H-5 140-150	14.8	40.0	7.3	16.74	33.5	555	0.83	6.04	Dark-green clay. Forams and shells
2H-6 140-150	16.3	40.0	7.3	19.62	33.5	558	0.85	4.89	Dark-green clay. Forams and shells
3H-1 1401-50	18.3	40.0	7.5	21.53	33.0	560	1.00	1.91	Core 3H-2 has first presence of methane. Dark clay with shells and piece of wood
3H-3 140-150	21.3	40.0	7.6	23.60	34.0	560	0.85	0.09	Clay with shells. Sulfide smell and black sulfides
3H-5 140-150	24.3	40.0	7.5	21.63	33.0	555	1.01	0.06	Core 3H-6 has methane present. Very dark gray fine clay with black sulfides. Sulfide smell. Sticky
3H-7 69-79	26.09	42.0	7.6	24.60	33.0	559	1.00	0.08	Very dark fine clay with sulfides
4H-1 140-150	27.8	40.0	7.7	24.81	34.0	559	0.95	0.13	Very dark fine clay with sulfides
4H-3 140-150	30.8	40.0	7.8	23.94	34.0	560	0.94	0.28	Very dark fine clay with sulfides. H2S smell
4H-5 140-150	33.8	40.0	7.6	23.49	33.5	559	0.94	0.08	Green clay with black sulfides mottling. No H2S smell
5H-2 140-150	38.8	40.0	7.6	21.88	33.0	557	0.95	0.35	Green clay with black sulfides mottling and shells. No H2S smell
5H-5 140-150	43.3	40.0	7.8	20.66	32.0	559	0.97	0.00	Green clay with black sulfides mottling and shells. No H2S smell
6H-2 135-150	48.17	40.0	7.6	18.04	32.0	556	0.96	0.15	Green clay with black sulfides mottling.
6H-5 135-150	52.67	41.0	7.9	16.23	32.0	557	0.86	0.00	Green clay with black sulfides mottling. Foram rich
7H-2 135-150	57.33	40.0	7.8	15.86	32.0	558	0.95	0.39	Green clay with black sulfides mottling. Foram rich
7H-5 118-133	61.56	40.0	7.9	15.51	32.0	558	0.95	0.00	Lots of voids in sample. Green clay with forams
8H-2 129-146	67.16	39.0	8.0	14.27	31.5	559	0.98	0.00	Green clay with forams. Stiff
8H-5 135-150	71.68	35.0	8.2	13.95	31.0	559	0.99	0.06	Green clay with forams. Stiff
9H-2 135-150	80.75	35.0	8.2	14.22	31.8	558	0.95	0.06	Dark, almost black clay and forams. Stiff
9H-4 130-150	83.7	18.0	8.0	14.63	31.5	556	1.01	0.00	Dark, almost black clay and forams. Stiff
10H-4 135-150	93.23	36.0	8.0	14.57	31.5	559	0.97	0.07	Dark, almost black clay and forams. Stiff. Some authigenic carbonate
11H-3 130-150	101.2	40.0	8.0	12.97	31.8	557	0.83	0.08	Dark, almost black clay and forams. Stiff
12H-5 130-150	112.86	29.0	7.9	13.39	31.5	554	1.15	0.16	Dark, almost black clay and forams. Stiff
13X-4 125-150	121.65	11.0	-	-	31.0	553	1.16	0.16	Very few undeveloped biscuits. Discarded most of the sample
14X-2 120-150	127.4	3.0	-	-	31.0	547	0.95	0.30	Very few undeveloped biscuits. Discarded most of the sample
15X-5 100-140	140.63	39.0	7.5	18.46	31.3	547	1.01	0.34	Very few undeveloped biscuits; only 2 good biscuits. Discarded most of the sample
15X-7 56-86	142.77	39.0	7.4	17.77	31.5	556	0.99	0.15	This sample seemed to be slightly "colder" then 15X-5 and the rest of this core.
16X-6 40-70	152.65	11.0	-	-	31.2	557	1.23	0.51	Same as previous cores with a few broken biscuits. No change in lithology
17X-5 110-140	160.4	21.0	7.3	20.28	31.5	551	1.21	0.10	Same as previous cores with a few broken biscuits. No change in lithology
18X-5 120-150	170.12	16.0	-	-	30.2	537	1.22	0.14	Same as previous cores with a few broken biscuits. No change in lithology
19X-2 88-118	174.93	4.5	-	-	30.5	551	1.01	0.38	This was the coldest interval seen in Hole 18A
19X-6 80-110	179.43	31.0	7.2	22.39	30.1	551	0.97	0.14	Not as "cold" as sample 19X-2 (based on IR)
20X-2 120-150	186.2	14.5	-	-	31.0	550	1.02	0.00	Same lithology as above. Few biscuits were highly broken
Special Samples									
15X-6 18-21	141.5	15.0	-	-	32.3	540	0.74	12.93	"Moussy" sample on sampling table
17X-4 18-26	159.2	18.0	-	-	32.8	544	0.92	10.56	"Moussy" sample on sampling table

Table 4. Interstitial-water data corrected for drill-water contamination based on sulfate concentration, for Hole NGHP-01-18A. Note that a dash indicates the value was not determined. The samples that were corrected for drill-water contamination are marked by bold data in the sulfate concentration column.

Sample name	Depth (mbsf)	V Samp (mL)	pH	Alk (mM)	Salinity	Titr Cl^- (mM)	Br^- (mM)	Br–/Cl–	SO_4^{2-} (mM)
1H-1 140-150	1.4	40.0	7.7	5.88	34.5	557	0.87	0.0016	24.41
1H-2 140-150	2.9	20.0	7.3	7.69	34.5	558	0.71	0.0013	21.26
1H-3 140-150	4.4	40.0	7.4	10.97	34.5	558	0.70	0.0013	18.04
1H-4 140-150	5.9	40.0	7.3	11.71	34.5	557	0.74	0.0013	16.82
1H-5 115-125	7.05	40.0	7.3	12.70	34.5	559	0.84	0.0015	14.78
2H-1 140-150	8.8	42.0	7.3	15.12	34.0	557	0.81	0.0015	12.94
2H-2 140-150	10.3	40.0	7.3	15.50	34.0	559	0.83	0.0015	11.52
2H-3 140-150	11.8	40.0	7.3	16.41	34.0	560	0.83	0.0015	9.83
2H-4 140-150	13.3	40.0	7.3	15.86	34.0	559	1.00	0.0018	8.07
2H-5 140-150	14.8	40.0	7.3	16.74	33.5	555	0.83	0.0015	6.04
2H-6 140-150	16.3	40.0	7.3	19.62	33.5	558	0.85	0.0015	4.89
3H-1 1401-50	18.3	40.0	7.5	21.53	33.0	560	1.00	0.0018	1.91
3H-3 140-150	21.3	40.0	7.6	23.60	34.0	560	0.85	0.0015	0.09
3H-5 140-150	24.3	40.0	7.5	21.63	33.0	555	1.01	0.0018	0.06
3H-7 69-79	26.09	42.0	7.6	24.60	33.0	559	1.00	0.0018	0.08
4H-1 140-150	27.8	40.0	7.7	24.80	33.8	557	0.94	0.0017	0.00
4H-3 140-150	30.8	40.0	7.8	23.92	33.7	555	0.93	0.0017	0.00
4H-5 140-150	33.8	40.0	7.6	23.49	33.5	559	0.94	0.0017	0.08
5H-2 140-150	38.8	40.0	7.6	21.85	32.6	550	0.94	0.0017	0.00
5H-5 140-150	43.3	40.0	7.8	20.66	32.0	559	0.97	0.0017	0.00
6H-2 135-150	48.17	40.0	7.6	18.03	31.8	553	0.95	0.0017	0.00
6H-5 135-150	52.67	41.0	7.9	16.23	32.0	557	0.86	0.0015	0.00
7H-2 135-150	57.33	40.0	7.8	15.83	31.5	550	0.94	0.00171	0.00
7H-5 118-133	61.56	40.0	7.9	15.51	32.0	558	0.95	0.00171	0.00
8H-2 129-146	67.16	39.0	8.0	14.27	31.5	559	0.98	0.00176	0.00
8H-5 135-150	71.68	35.0	8.2	13.95	31.0	559	0.99	0.00178	0.06
9H-2 135-150	80.75	35.0	8.2	14.22	31.8	558	0.95	0.00171	0.06
9H-4 130-150	83.7	18.0	8.0	14.63	31.5	556	1.01	0.00181	0.00
10H-4 135-150	93.23	36.0	8.0	14.57	31.5	559	0.97	0.00174	0.07
11H-3 130-150	101.2	40.0	8.0	12.97	31.8	557	0.83	0.00149	0.08
12H-5 130-150	112.86	29.0	7.9	13.38	31.3	551	1.14	0.00207	0.00
13X-4 125-150	121.65	11.0	-	-	30.8	550	1.16	0.00211	0.00
14X-2 120-150	127.4	3.0	-	-	30.6	541	0.94	0.00174	0.00
15X-5 100-140	140.63	39.0	7.5	18.43	30.9	540	1.00	0.00186	0.00
15X-7 56-86	142.77	39.0	7.4	17.76	31.3	553	0.99	0.00178	0.00
16X-6 40-70	152.65	11.0	-	-	30.6	547	1.22	0.00222	0.00
17X-5 110-140	160.4	21.0	7.3	20.28	31.5	551	1.21	0.00219	0.10
18X-5 120-150	170.12	16.0	-	-	30.0	534	1.22	0.00228	0.00
19X-2 88-118	174.93	4.5	-	-	30.0	544	1.00	0.00184	0.00
19X-6 80-110	179.43	31.0	7.2	22.38	29.9	548	0.97	0.00176	0.00
20X-2 120-150	186.2	14.5	-	-	31.0	550	1.02	0.00185	0.00

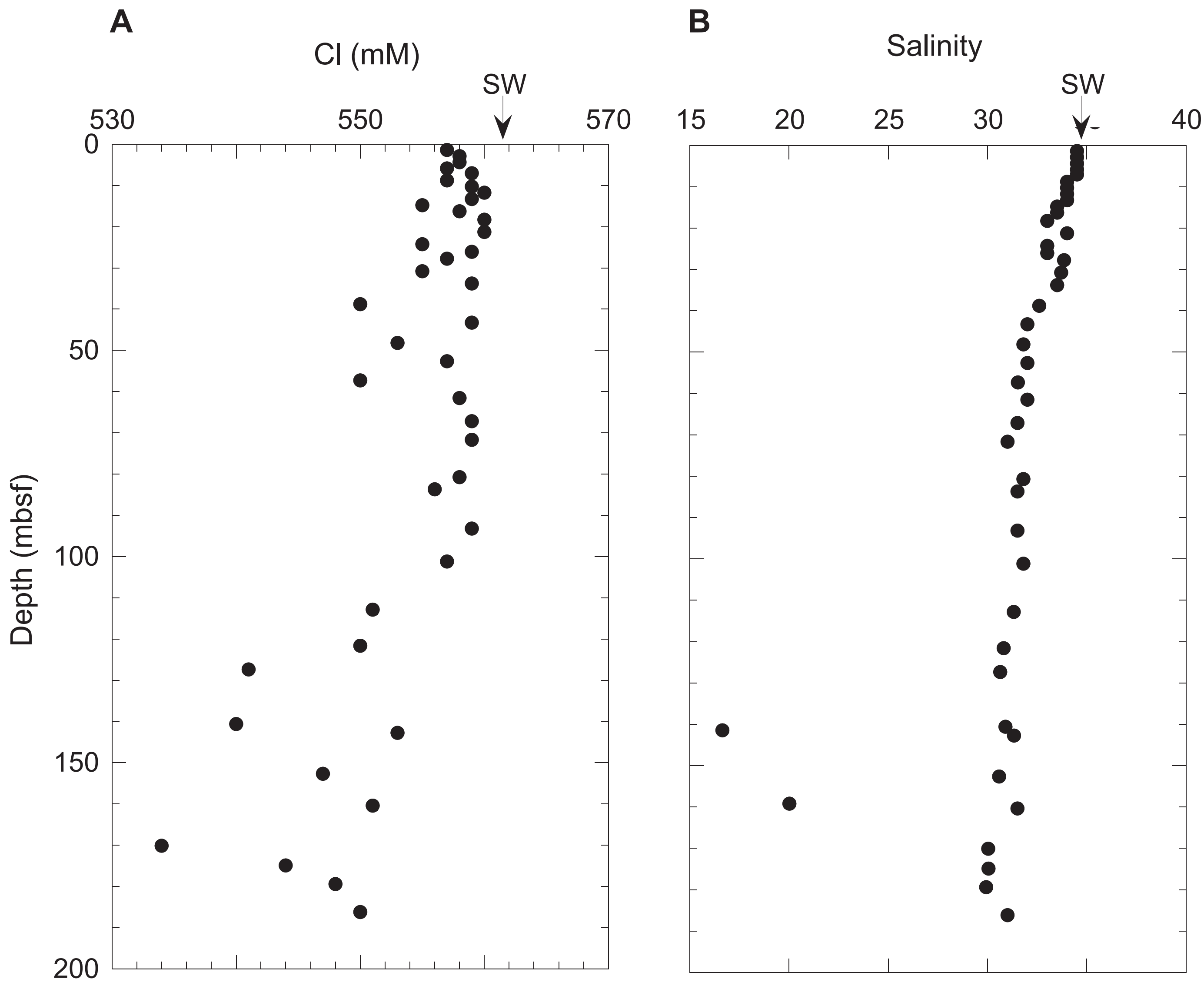

Figure 12. Concentration-depth profiles of A, chloride and B, salinity at Hole NGHP-01-18A. Seawater value is designated as “sw” in A and B.

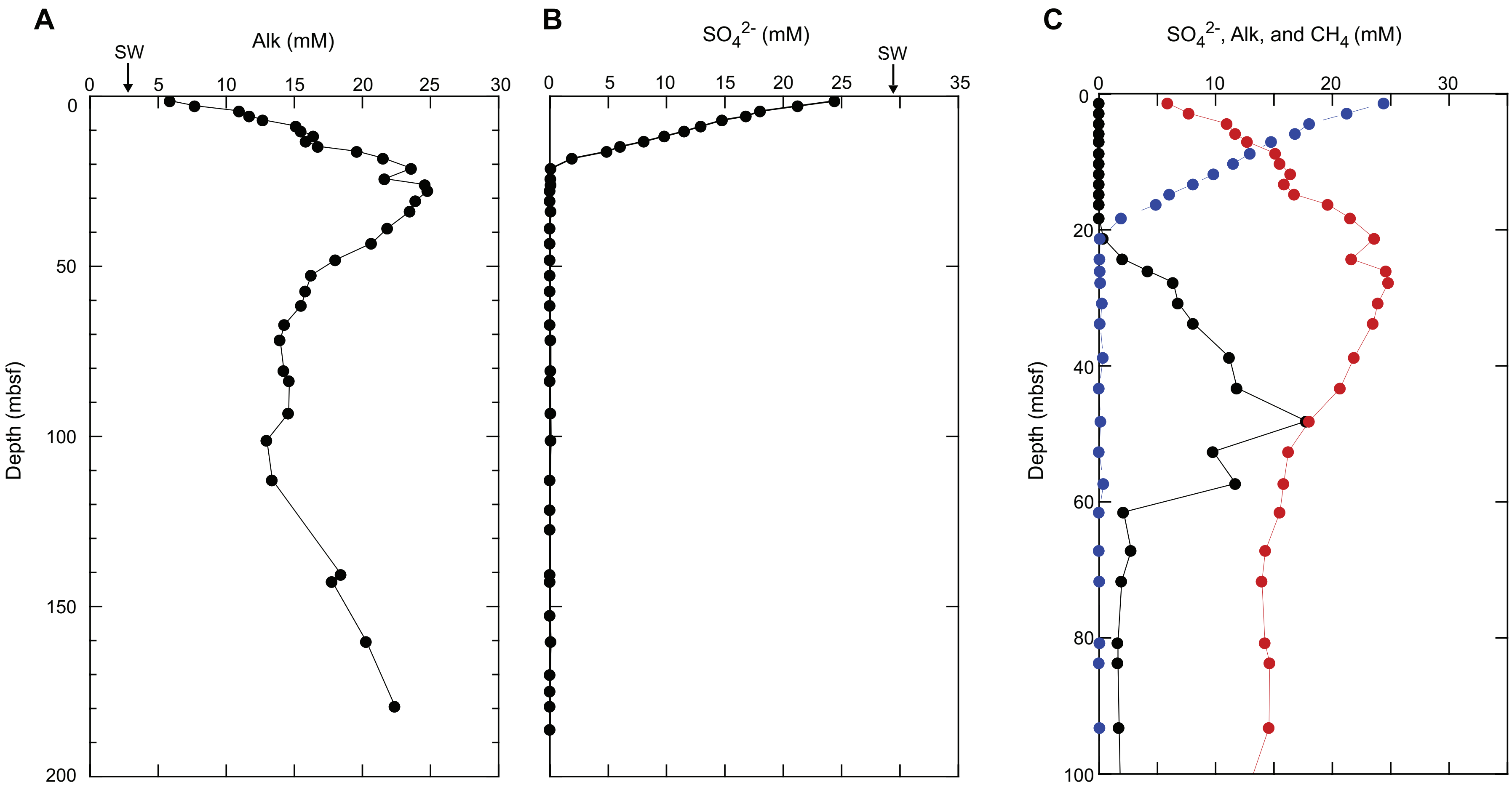

Figure 13. Concentration-depth profiles of A, alkalinity; B, sulfate; and C, sulfate, methane, and alkalinity at NGHP-01-18A. Note the alkalinity maximum at the SMI depth (21 mbsf) and the steep increase in methane concentration below the SMI. Seawater value is designated as “sw” in A and B. [SMI, sulfate-methane interface; mbsf, meters below sea floor]

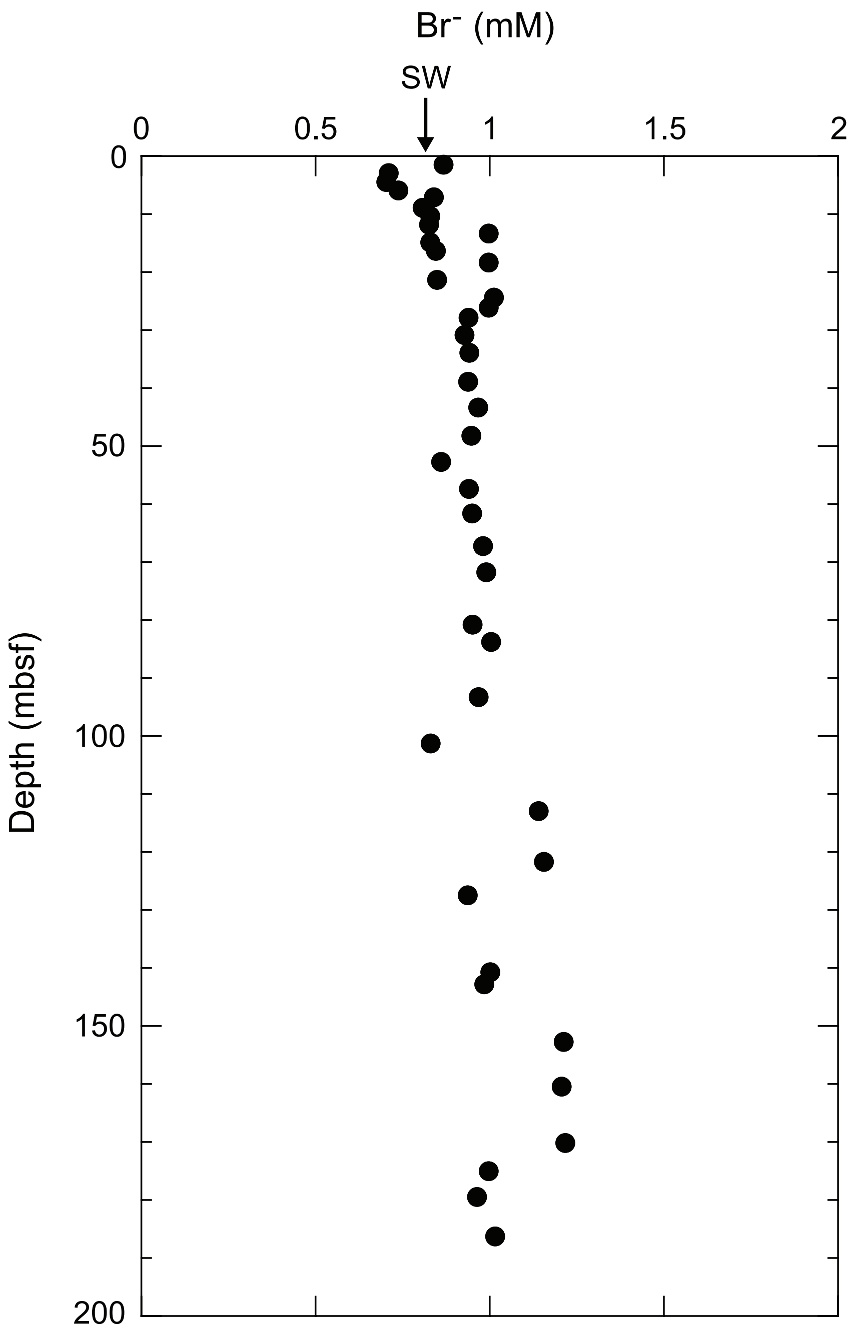

Figure 14. Concentration-depth profile of dissolved bromide at NGHP-01-18A. Seawater value is designated as “sw.”

Headspace gas analyses were performed on forty-four samples from Hole NGHP-01-18A ranging in depth from 1.35 to 185.8 meters below seafloor (mbsf). The concentrations given here represent minimum proxy measurements of the actual concentrations due to limitations of the gas headspace method (Kvenvolden and Lorenson, 2000). The sediment pore water contained methane at concentrations ranging from non-detectable near the surface to 15.7 mM at ~33.5 mbsf (table 5). Theoretical methane saturation in pore water under site-specific physical conditions, calculated using the Duan and others (1992) and Xu (2002, 2004) methodologies, increases from 54.1 mM at the seafloor to 134.3 mM near the borehole completion depth of 200 mbsf. Ethane was detected at very low concentrations of less than 30 ppmv, though not consistently, below 25.5 mbsf. No C_3 or higher molecular weight hydrocarbon gases were detected in headspace samples, suggesting a microbial source of methane; however post expedition isotopic analyses will further constrain the source of gas. Methane concentrations increase step-wise from non-detectable at 18.25 mbsf to 2 mM at ~21 mbsf placing the sulfate-methane interface (SMI) lies between this interval (fig. 15; see "Inorganic Geochemistry"). Methane concentrations in the upper hole peak below the SMI at approximately the same depth as the alkalinity maximum of ~25 mM (see "Inorganic Geochemistry"). Methane concentration is relatively uniform (~1.5 mM) from ~45 mbsf to the BSR, and may be associated with the presence of free gas or gas hydrate, as other IR anomaly measurements suggest that gas hydrate was present in this interval (see "Physical Properties"). There is a near 2-fold increase of methane concentration between 90 and 120 mbsf, a depth interval that corresponds to a low velocity reflector, likely a fault with a dip of approximately 30–35° through the borehole location (see "Physical Properties"). Methane concentration does not appear to decrease near the bottom simulating reflector (BSR). There was no apparent effect of coring type (APC vs. XCB) on methane concentrations. The methane concentrations were generally an order of magnitude below theoretical *in situ* saturation throughout the length of the borehole (fig. 15); however this is likely due to preferential losses of methane during sampling.

Carbon dioxide (CO_2) concentrations ranged from 0.6 to 4.6 mM in pore water contained within the sediment (table 5). CO_2 concentrations appear to increase slightly with depth, though this trend is not consistent (fig. 16). The lowest concentrations are found above the SMI at a depth ranging from 0 to 10 mbsf, with the exception of one extremely low value near 170 mbsf (fig. 16). Below the SMI, concentrations were highly variable from 0.4 to 7.6 mM. The highest variance in CO_2 concentrations were found in the entire interval below ~75 mbsf. The methane to carbon dioxide ratio indicated that methane may not be preferentially concentrated from ~110 mbsf to the BSR (fig. 17). Some portion of the variability observed for samples obtained at depths greater than 120 mbsf may be due to XCB coring agitation. The air gases (N_2+Ar), and O_2 were the balance gases, however the (N_2+Ar)/O_2 ratios were typically greater than air reflecting the ratio in pore fluids and also possibly indicating that some air was trapped in the headspace samples and some oxygen has likely dissolved preferentially compared to N_2. Air gases are present in all samples as the core plugs were degassed in an air headspace.

Void gas samples were collected from seventeen different void spaces ranging in depth from 48.2 to 177.8 mbsf. Methane concentrations within voids averaged nearly 904,500 ppm (±234,400 or 90.4 percent ± 23.4 percent). The void gases contained methane above 83 percent at all intervals except one, located at 115 mbsf, as noted in table 6. The anomalously low concentration in this interval is believed to be due to contamination during sampling and(or) core handling because the ratio of (N_2+Ar)/O_2 corresponds to the atmospheric value (~3.73). Ethane was detected at levels ranging from non-detectable to ~420 ppm; however higher molecular weight gases (C_{3+}) were not detected. Ethane concentrations increased with depth, but no obvious connection can be made as to whether the ethane is from a minor thermogenic source, or if the ethane is from dissociated gas hydrate. Carbon dioxide concentrations ranged from ~420 to 15,700 parts per million by volume (ppmv) and are tabulated with other gas data in table 6. The methane to carbon dioxide ratios are quite uniform with increasing depth between the SMI and the BSR (fig. 17). This appears inconsistent with the headspace C_1/CO_2 trend for depths below 110 mbsf, which is likely due to preferential loss of methane in headspace and XCB coring agitation. Void gas C_1/CO_2 is typically 2 orders of magnitude greater than headspace due to the preferential loss of volatile methane by the headspace sample method. Ratio values for C_1 to C_2 gases averaged ~5,000 and showed the typical decreasing trend with depth (fig. 18). The concentrations are focused in the center of the 'normal' occurrence interval as depicted in the graph. These high methane concentrations versus low concentrations of ethane (table 6) provide strong evidence for a microbially-dominated hydrocarbon gas source. The air gases (N_2+Ar), and O_2 composed the balance gases and reflect air contamination plus concentrations within the sediment.

Microbiology

Hole NGHP-01-18A

Analysis of all microbiological samples will be shore-based. Twenty samples were collected for cell enumeration (CEL) and a limited number of additional microbiological samples were taken. Lab code JUD, 23 samples; Lab code JAN, 20 samples (table 7).

Table 5. Headspace gas composition for Site NGHP-01-18.

Sample	Site	Hole	Core	Section	Interval (cm)	Sed wt. (g)	Sample depth (mbsf)	CO_2 (ppm-v)	C_1 (ppm-v)	C_2 (ppm-v)
18A-1H1-135-140	18	A	1	1	135–140	9.4	1.35	7,700	nd	nd
18A-1H2-105-110	18	A	1	2	105–110	7.3	2.55	9,100	nd	nd
18A-1H3-135-140	18	A	1	3	135–140	7.1	4.35	13,200	nd	nd
18A-1H4-100-105	18	A	1	4	100–105	8.6	5.50	4,400	nd	nd
18A-1H5-100-105	18	A	1	5	100–105	7.4	7.00	4,400	nd	nd
18A-2H1-135-140	18	A	2	1	135–140	7.7	8.75	8,100	nd	nd
18A-2H2-135-140	18	A	2	2	135–140	7.7	10.25	14,600	nd	nd
18A-2H3-105-110	18	A	2	3	105–110	8.8	11.45	17,900	nd	nd
18A-2H4-135-140	18	A	2	4	135–140	9.2	13.25	17,800	nd	nd
18A-2H5-100-105	18	A	2	5	100–105	8.5	14.40	14,800	nd	nd
18A-2H6-135-140	18	A	2	6	135–140	8.8	16.25	10,400	nd	nd
18A-3H1-135-140	18	A	3	1	135–140	7.9	18.25	9,800	nd	nd
18A-3H2-145-150	18	A	3	2	145–150	7.6	19.85	6,500	1,400	nd
18A-3H3-105-110	18	A	3	3	105–110	8.2	20.95	9,500	9,300	nd
18A-3H4-145-150	18	A	3	4	145–150	8.9	22.85	11,700	21,200	nd
18A-3H5-105-110	18	A	3	5	105–110	8.6	23.90	15,000	30,600	nd
18A-3H6-95-100	18	A	3	6	95–100	9.1	25.85	10,700	34,800	20
18A-3H7-64-69	18	A	3	7	64–69	7.9	26.04	14,800	34,300	10
18A-4H1-135-140	18	A	4	1	135–140	7.6	27.75	17,900	44,800	20
18A-4H3-125-130	18	A	4	3	125–130	7.5	30.65	19,900	45,900	10
18A-4H5-100-105	18	A	4	5	100–105	7.5	33.40	17,200	67,900	10
18A-5H2-125-130	18	A	5	2	125–130	7.1	38.65	14,500	34,100	10
18A-5H5-100-105	18	A	5	5	100–105	7.7	42.90	13,100	44,400	10
18A-6H2-120-125	18	A	6	2	120–125	8.0	48.02	11,200	8,200	nd
18A-6H5-95-100	18	A	6	5	95–100	8.6	52.27	6,500	11,600	nd
18A-7H2-120-125	18	A	7	2	120–125	8.0	57.18	6,100	7,300	nd
18A-7H5-78-83	18	A	7	5	78–83	7.4	61.16	7,400	5,500	nd
18A-8H2-114-119	18	A	8	2	114–119	9.2	67.01	11,300	7,200	nd
18A-8H5-95-100	18	A	8	5	95–100	9.6	71.28	11,500	7,900	nd
18A-9H2-120-25	18	A	9	2	120–125	7.2	80.60	5,600	5,700	nd
18A-9H4-95-100	18	A	9	4	95–100	8.5	83.30	5,500	4,500	nd
18A-10H4-95-100	18	A	10	4	95–100	7.4	92.83	11,300	11,400	nd
18A-11H3-90-95	18	A	11	3	90–95	8.8	100.80	10,600	12,600	nd
18A-12H5-90-95	18	A	12	5	90–95	9.0	112.46	29,700	15,100	10
18A-13X4-85-90	18	A	13	4	85–90	11.1	121.25	20,600	9,100	nd
18A-14X2-80-85	18	A	14	2	80–85	11.7	127.00	50,200	11,300	10
18A-15X5-60-65	18	A	15	5	60–65	11.4	140.23	11,300	6,800	nd
18A-15X7-51-56	18	A	15	7	51–56	13.4	142.72	57,400	17,500	20
18A-16X6-0-5	18	A	16	6	0–5	11.7	152.25	41,500	7,000	nd
18A-17X5-70-75	18	A	17	5	70–75	8.3	160.00	44,300	10,200	10
18A-18X5-80-85	18	A	18	5	80–85	12.9	169.72	3,900	3,500	nd
18A-19X2-83-88	18	A	19	2	83–88	13.7	174.88	49,100	11,200	nd
18A-19X6-40-45	18	A	19	6	40–45	11.8	179.03	14,800	600	nd
18A-20X2-80-85	18	A	20	2	80–85	9.6	185.80	39,800	8,400	nd

Table 5. Headspace gas composition for Site NGHP-01-18.—Continued

Sample	C_3 (ppm-v)	O_2 (ppm-v)	N_2+Ar (ppm-v)	H_2S (ppm-v)	C1 (µL/L WS)	C1 (mM PW)	CO_2 (µL/L WS)	CO_2 (mM PW)	C_1/CO_2
18A-1H1-135-140	nd	186,900	749,600	nd	nd	nd	18,100	0.9	-
18A-1H2-105-110	nd	187,000	751,500	nd	nd	nd	30,300	1.6	-
18A-1H3-135-140	nd	185,800	746,400	nd	nd	nd	45,200	2.1	-
18A-1H4-100-105	nd	181,200	721,900	nd	nd	nd	11,600	0.5	-
18A-1H5-100-105	nd	190,700	745,900	nd	nd	nd	14,400	0.8	-
18A-2H1-135-140	nd	183,300	716,700	nd	nd	nd	24,900	1.4	-
18A-2H2-135-140	nd	185,900	733,300	nd	nd	nd	45,000	2.8	-
18A-2H3-105-110	nd	184,400	728,400	nd	nd	nd	46,200	3.2	-
18A-2H4-135-140	nd	182,100	726,500	nd	nd	nd	43,000	3.2	-
18A-2H5-100-105	nd	187,500	737,200	nd	nd	nd	40,000	3.0	-
18A-2H6-135-140	nd	189,600	736,600	nd	nd	nd	26,700	2.2	-
18A-3H1-135-140	nd	186,200	732,200	nd	nd	nd	29,300	2.0	-
18A-3H2-145-150	nd	183,300	709,700	nd	4,500	0.4	20,500	1.6	0.2
18A-3H3-105-110	nd	183,600	723,600	nd	26,500	2.0	27,100	2.1	1.0
18A-3H4-145-150	nd	181,200	726,800	nd	53,900	3.6	29,600	2.0	1.8
18A-3H5-105-110	nd	174,000	719,100	nd	81,500	5.5	40,000	2.7	2.0
18A-3H6-95-100	nd	182,400	716,900	nd	85,600	5.1	26,300	1.6	3.3
18A-3H7-64-69	nd	175,400	721,200	nd	102,600	6.2	44,200	2.7	2.3
18A-4H1-135-140	nd	165,500	705,900	nd	140,800	8.7	56,300	3.5	2.5
18A-4H3-125-130	nd	158,700	716,700	nd	146,800	10.6	63,600	4.6	2.3
18A-4H5-100-105	nd	162,700	702,100	nd	217,200	15.7	55,000	4.0	3.9
18A-5H2-125-130	nd	175,500	717,300	nd	117,100	8.0	49,900	3.4	2.4
18A-5H5-100-105	nd	173,400	707,100	nd	137,300	8.5	40,400	2.5	3.4
18A-6H2-120-125	nd	195,900	796,000	nd	23,900	1.7	32,800	2.3	0.7
18A-6H5-95-100	nd	183,200	738,300	nd	30,800	2.5	17,200	1.4	1.8
18A-7H2-120-125	nd	190,900	747,500	nd	21,500	1.4	18,000	1.2	1.2
18A-7H5-78-83	nd	184,600	728,700	nd	17,800	1.3	24,100	1.8	0.7
18A-8H2-114-119	nd	184,400	739,200	nd	17,500	1.4	27,500	2.2	0.6
18A-8H5-95-100	nd	181,900	735,200	nd	18,000	1.6	26,200	2.3	0.7
18A-9H2-120-25	nd	186,400	746,800	nd	19,200	1.4	18,900	1.4	1.0
18A-9H4-95-100	nd	188,300	759,400	nd	12,100	0.9	14,900	1.1	0.8
18A-10H4-95-100	nd	181,200	739,300	nd	37,100	3.4	36,900	3.3	1.0
18A-11H3-90-95	nd	184,400	733,900	nd	32,400	2.8	27,300	2.3	1.2
18A-12H5-90-95	nd	161,500	753,700	nd	37,800	3.0	74,200	5.9	0.5
18A-13X4-85-90	nd	154,600	754,200	nd	16,800	1.3	37,900	3.0	0.4
18A-14X2-80-85	nd	70,500	845,400	nd	19,100	1.3	84,900	5.7	0.2
18A-15X5-60-65	nd	143,900	771,800	nd	11,900	0.9	19,900	1.5	0.6
18A-15X7-51-56	nd	67,200	821,500	nd	23,600	1.6	77,600	5.3	0.3
18A-16X6-0-5	nd	115,600	789,400	nd	11,800	0.9	70,200	5.3	0.2
18A-17X5-70-75	nd	109,400	784,500	nd	28,400	1.7	123,700	7.6	0.2
18A-18X5-80-85	nd	167,100	737,800	nd	5,000	0.4	5,600	0.4	0.9
18A-19X2-83-88	nd	86,100	784,200	nd	14,500	1.1	63,700	4.7	0.2
18A-19X6-40-45	nd	171,800	729,200	nd	1,000	0.1	24,700	1.6	0.0
18A-20X2-80-85	nd	139,700	759,800	nd	19,200	1.6	90,800	7.6	0.2

Notes: nd= not detected. WS= Wet sediment. PW= porewater. Approximate detection limits are about 15 ppmv for methane, 30 ppmv for ethane, 50 ppmv for propane, and 20 ppmv for hydrogen sulfide.

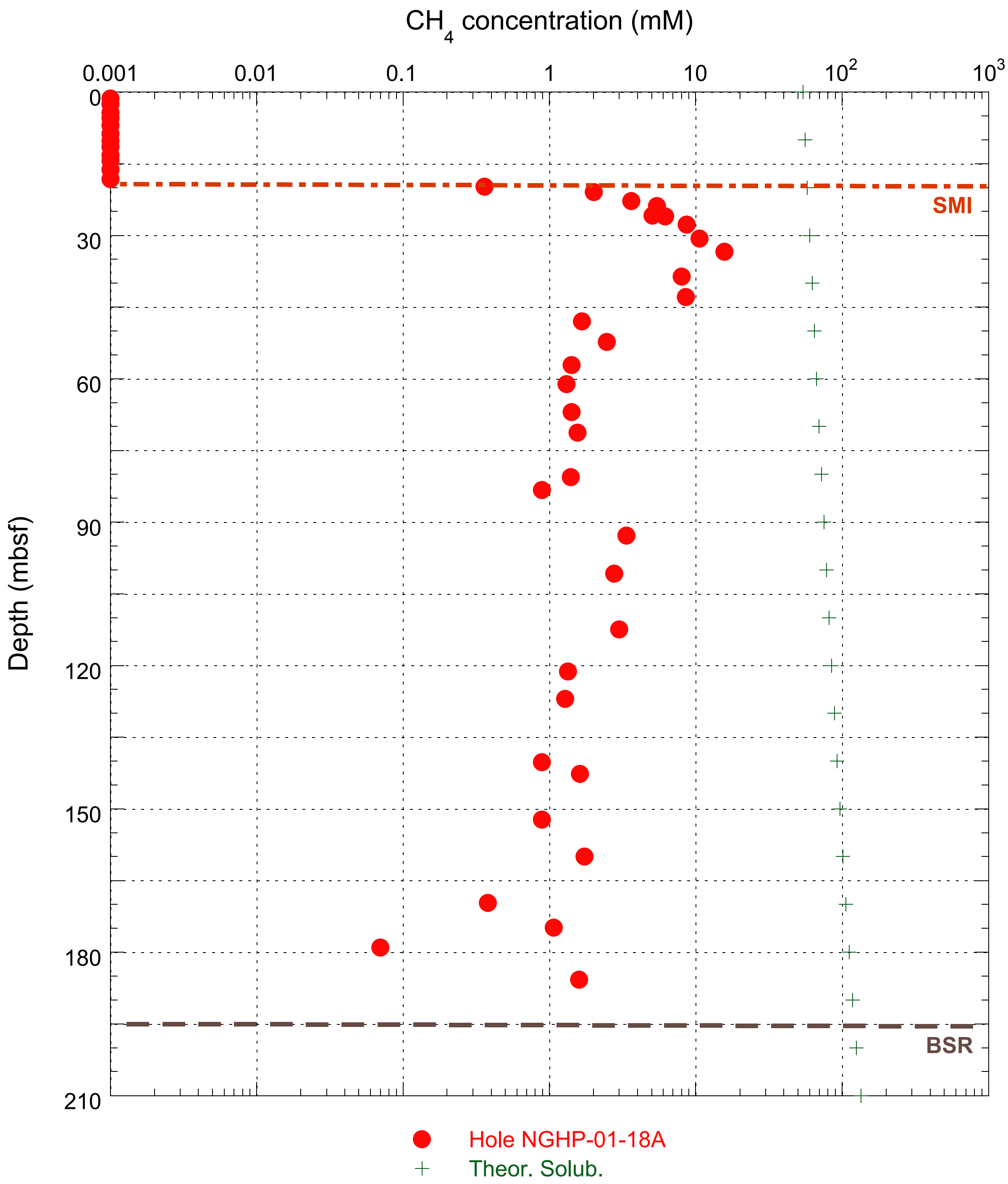

Figure 15. Plot of headspace methane gas concentration (mM) with depth for Hole NGHP-01-18A. Note the methane gradient between 18 and 24 mbsf indicating that the SMI occurs in this interval. Also note the slight enrichment from 90 to 120 mbsf. Values less than 0.003 mM are below instrument detection limits but are plotted for reference. Text inside a symbol denotes special coring tool (E, HRC; P, PCS; Y, FPC). Theoretical solubility of methane calculated using the Duan and others (1992) and Xu (2002, 2004) methodologies. [mbsf, meters below sea floor; SMI, sulfate-methane interface]

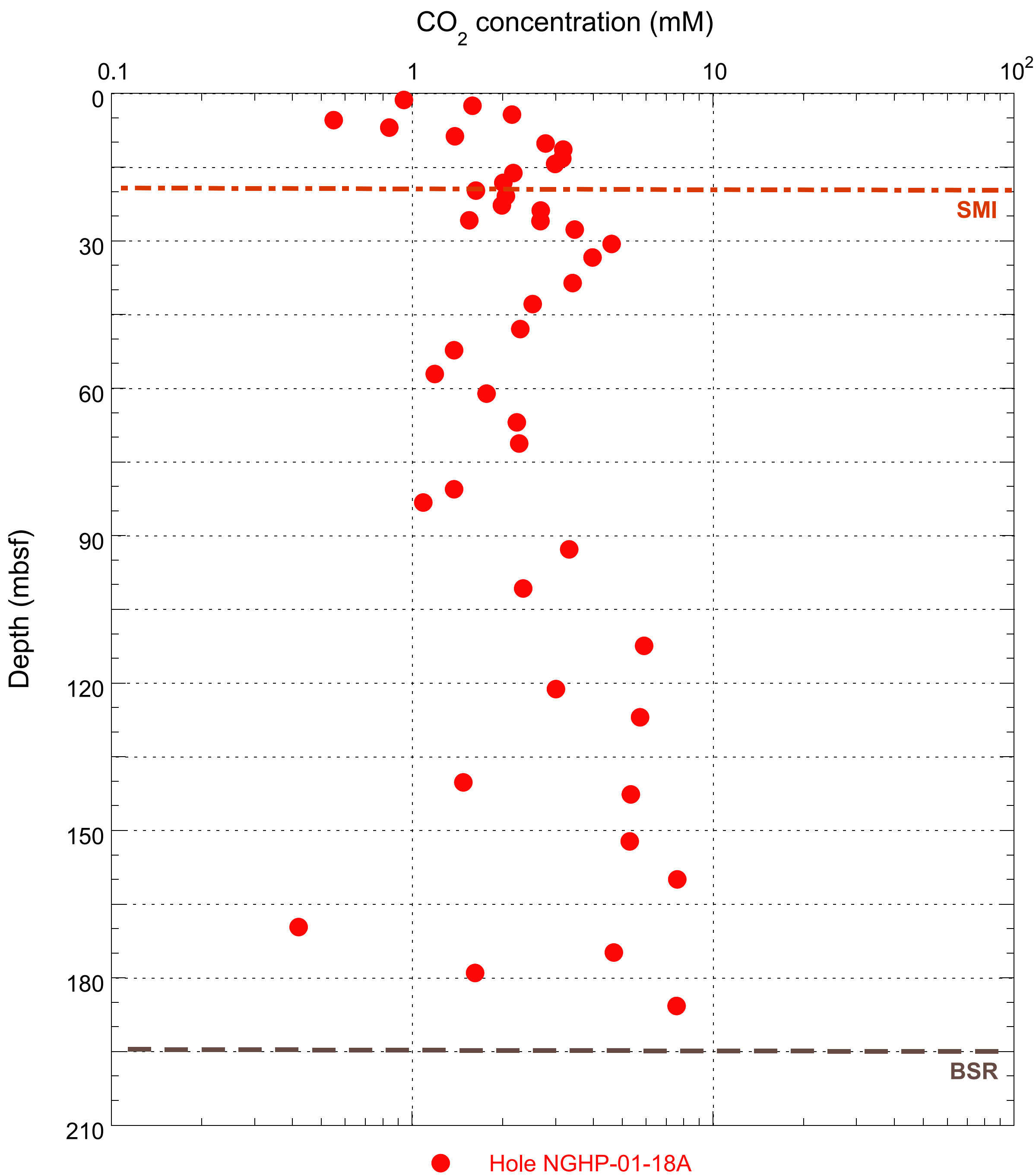

Figure 16. Plot of headspace carbon dioxide gas concentration (mM) with depth for Hole NGHP-01-18A.

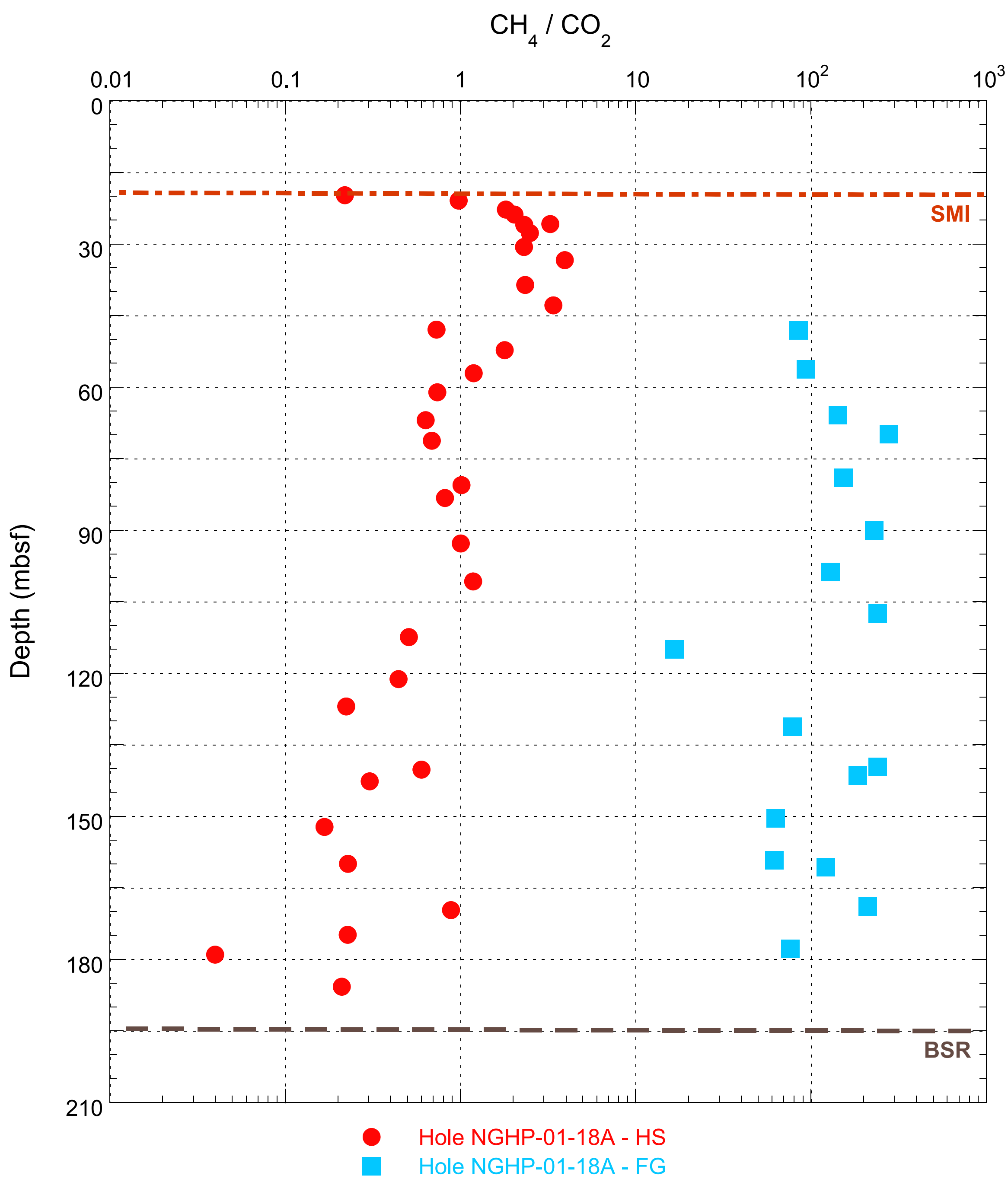

Figure 17. Plot of methane to carbon dioxide gas ratio with depth for headspace, void gas, and PCS gas for Hole NGHP-01-18A. Preferential losses of methane during core handling and by sample procedures result in the order of magnitude difference in ratio magnitude. [PCS, pressure core sampler]

Table 6. Void gas composition for Site NGHP-01-18.

Sample	Site	Hole	Core	Section	Interval (cm)	Sample depth (mbsf)	CO_2	C_1	C_2	C_3	O_2	N_2+Ar	H_2S	C_1/CO_2	C_1/C_2
							(ppmv) normalized to nitrogen+argon								
18A-6H2-132	18	A	6	2	132	48.14	11,000	938,500	140	nd	2,100	48,200	nd	90	6,700
18A-7H2-35	18	A	7	2	35	56.33	10,300	968,100	140	nd	1,500	20,000	nd	90	6,900
18A-8H2-1	18	A	8	2	1	65.88	6,900	981,300	150	nd	1,600	10,100	nd	140	6,500
18A-8H4-104	18	A	8	4	104	69.87	3,600	986,300	180	nd	900	9,100	nd	270	5,500
18A-9H1-118	18	A	9	1	118	79.08	6,400	976,400	170	nd	1,200	15,800	nd	150	5,700
18A-10H2-125	18	A	10	2	125	90.15	4,300	985,300	170	nd	1,000	9,300	nd	230	5,800
18A-11H2-37	18	A	11	2	37	98.77	7,600	978,400	160	nd	900	13,000	nd	130	6,100
18A-12H2-51	18	A	12	2	51	107.57	4,100	985,000	160	nd	1,500	9,300	nd	240	6,200
18A-12H7-51	18	A	12	7	51	115.06	400	7,000	nd	nd	199,600	792,900	nd	20	-
18A-14X5-57	18	A	14	5	57	131.27	12,300	970,700	210	nd	5,600	11,200	nd	80	4,600
18A-15X5-1	18	A	15	5	1	139.64	4,000	965,500	200	nd	4,900	25,400	nd	240	4,800
18A-15X6-47	18	A	15	6	47	141.5	5,000	931,500	230	nd	14,000	49,200	nd	190	4,100
18A-16X4-123	18	A	16	4	123	150.48	15,500	974,300	260	nd	2,200	7,700	nd	60	3,700
18A-17X4-142	18	A	17	4	142	159.22	15,700	971,400	240	nd	1,800	10,900	nd	60	4,000
18A-17X6-1	18	A	17	6	1	160.71	6,800	828,100	100	nd	33,300	131,700	nd	120	8,300
18A-18X5-1	18	A	18	5	1	168.93	4,700	988,500	420	nd	1,300	5,100	nd	210	2,400
18A-19X5-1	18	A	19	5	1	177.78	12,300	939,300	240	nd	13,300	34,800	nd	80	3,900

Notes: nd = not detected. nr = not recorded. Approximate detection limits are about 15 ppmv for methane, 30 ppmv for ethane, 50 ppmv for propane, and 20 ppmv for hydrogen sulfide.

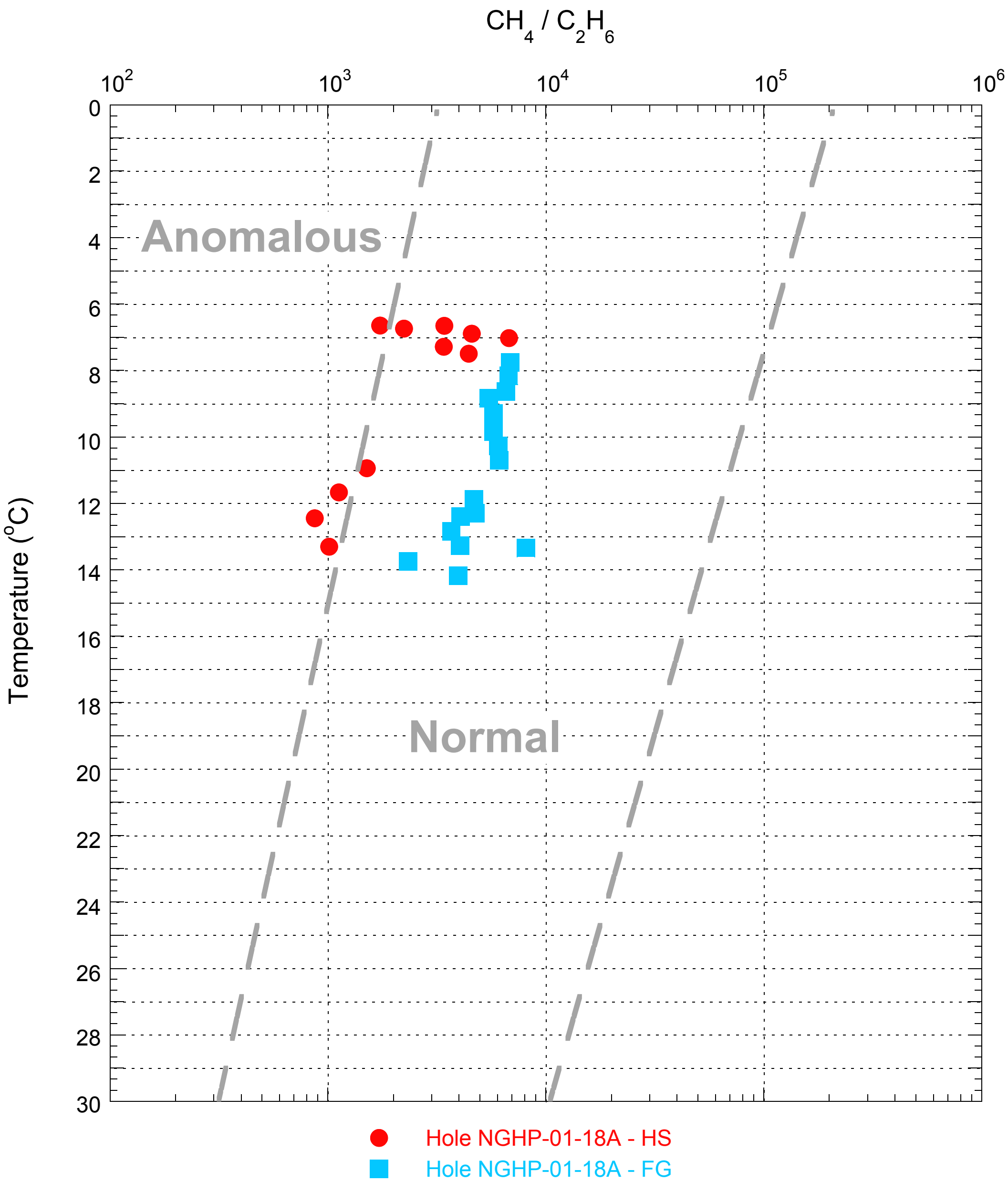

Figure 18. Plot of free/void gas and PCS methane to ethane gas ratio with depth for Hole NGHP-01-18A. Ethane levels were near detection limits for all headspace samples (table 5). Note that the hydrocarbon gas occurrences fall along the typical range. [PCS, pressure core sampler]

Table 7. List of microbiological samples taken for Site NGHP-01-18.

Sample reference						Comments
Core, section	Sample code	Top (cm)	Bottom (cm)	Depth (mbsf)	Volume (cc)	
NGHP-01-18A						
1H-4	CEL	100	105	5.5	5	
2H-5	CEL	100	105	14.4	5	
3H-5	CEL	100	105	23.9	5	
4H-5	CEL	100	105	33.4	5	
5H-5	CEL	100	105	42.9	5	
6H-5	CEL	95	100	52.27	5	
7H-5	CEL	78	83	61.16	5	
8H-5	CEL	95	100	71.28	5	
9H-4	CEL	90	95	83.3	5	
10H-4	CEL	95	100	92.83	5	
11H-3	CEL	90	95	100.8	5	
12H-5	CEL	90	95	112.46	5	
13X-4	CEL	85	90	121.25	5	
14X-2	CEL	80	85	127	5	
15X-5	CEL	60	65	140.23	5	
16X-6	CEL	0	5	152.25	5	SAMPLE CUT OUT
17X-5	CEL	70	75	160	5	
18X-5	CEL	80	85	169.72	5	
19X-6	CEL	40	45	179.03	5	
20X-2	CEL	80	85	185.8	5	
1H-4	JAN	105	110	5.55	187	
2H-5	JAN	105	110	14.45	187	
3H-5	JAN	105	110	23.95	187	
4H-5	JAN	105	110	33.45	187	
5H-5	JAN	105	110	42.95	187	
6H-5	JAN	100	105	52.32	187	
7H-5	JAN	83	88	61.21	187	
8H-5	JAN	100	105	71.33	187	
9H-4	JAN	95	100	83.35	187	
10H-4	JAN	100	105	92.88	187	
11H-3	JAN	95	100	100.85	187	
12H-5	JAN	95	100	112.51	187	
13X-4	JAN	90	95	121.3	187	
14X-2	JAN	85	90	127.05	187	
15X-5	JAN	65	70	140.28	187	
16X-6	JAN	5	10	152.3	187	
17X-5	JAN	75	80	160.05	187	
18X-5	JAN	85	90	169.77	187	
19X-6	JAN	45	50	179.08	187	
20X-2	JAN	85	90	185.85	187	
1H-2	JUD	120	130	2.7	374	
1H-4	JUD	120	130	5.7	374	
2H-3	JUD	120	130	11.6	374	
2H-5	JUD	120	130	14.6	374	
3H-3	JUD	120	130	21.1	374	
3H-5	JUD	120	130	24.1	374	
4H-5	JUD	120	130	33.6	374	
5H-5	JUD	120	130	43.1	374	
6H-5	JUD	115	125	52.47	374	
7H-5	JUD	98	108	61.36	374	
8H-5	JUD	115	125	71.48	374	
9H-4	JUD	110	120	83.5	374	
10H-4	JUD	115	125	93.03	374	
11H-3	JUD	110	120	101	374	
12H-5	JUD	110	120	112.66	374	
13X-4	JUD	105	115	121.45	374	
14X-2	JUD	100	110	127.2	374	
15X-5	JUD	80	90	140.43	374	
16X-6	JUD	20	30	152.45	374	
17X-5	JUD	90	100	160.2	374	
18X-5	JUD	100	110	169.92	374	
19X-6	JUD	60	70	179.23	374	
20X-2	JUD	100	110	186	374	

Physical Properties

Whole-round cores at NGHP Expedition 01, Site 18 were imaged using an IR camera on the catwalk to determine the location of temperature anomalies on the surface of core liners and enable sections containing potential gas hydrate to be quickly removed, preserved, and studied. After IR imaging was finished, non-destructive measurements were conducted on temperature-equilibrated whole-round core sections with the MSCL. Thermal conductivity measurements were also conducted on whole-round cores. Various tests were performed on split cores including: electrical resistivity (ER) by use of a Wenner array, *P*-wave velocity by inserted spades, and shear strength by mini-vane and Pocket Penetrometer. Core subsamples were placed in 10-mL beakers and dried at 105 °C for at least 24-hours to determine water content. Subsequently, the dried samples were analyzed for grain density using gas pycnometers and other sediment parameters were then calculated. See the "Physical Properties" section of the "Methods " chapter for more details.

The physical properties program at Site NGHP-01-18 focused primarily on Hole NGHP-01-18A located within the Mahanadi Basin off the East coast of India in ~1374 m of water. Hole NGHP-01-18A was continuously cored to 190 mbsf and had an overall core recovery of 97.6 percent. IR images indicated that gas hydrate may have been present in disseminated form from approximately 115 mbsf to the bottom of the hole at 190 mbsf.

Infrared Imaging

Environmental Conditions

Catwalk environment was monitored during the entire drilling operation at Site NGHP-01-18. Temperature on the catwalk averaged ~27 °C, ranging from 26 to 28 °C during the drilling operation (a relatively narrow range and cooler average compared to earlier drilling sites; fig. 19). Relative humidity ranged from 84 to 96 percent (fig. 19), which is consistent with a marine environmental setting in the northwestern Bay of Bengal, but notably higher than previous sites. While temperature and relative humidity conditions were mostly constant during drilling, adverse environmental conditions (mainly rough seas and high winds) persisted during drilling operations at this site. While these conditions were severe enough to prevent both geophysical logging and pressure coring at the site, they did not appear to impact the IR images, particularly since ambient temperature remained relatively consistent during drilling.

Infrared Images

All APC and XCB cores from Site NGHP-01-18 were systematically scanned upon arrival on the catwalk using the track-mounted IR camera described in the "Physical Properties" section of the "Methods" chapter. IR anomalies, commonly referred to as "cold spots," indicate gas-hydrate dissociation during core recovery, which subsequently provides guidance to catwalk sampling. Summary digital maps of the scans of all cores are available on the data DVD that accompanies this report and listings of the image files are presented in tables 8 and 9. Temperature arrays in text-formatted files were exported from the IR camera software and then concatenated for each core. The arrays were then further concatenated for all available cores at Site NGHP-01-18. Downcore temperatures were averaged for each pixel row in the array, excluding pixels ~1 cm from the edge of the image and 2 cm along the midline of the image. Exclusion of these pixels minimized the effects caused by major thermal artifacts in the images. This processing enabled us to measure the average amplitude of the cold anomalies and identify warm anomalies due to voids from the background temperature field.

Infrared track imaging at Site NGHP-01-18A consisted of 20 scans for a total scanned core length of ~185 m. The complete set of IR images collected for borehole NGHP-01-18A is presented in figure 20 along with the corresponding downcore temperatures. The core liner surface temperature extracted from the IR images for Hole NGHP-01-18A ranged from a high of ~25 °C on void sections of the core liner throughout the hole, to a low of ~20 °C at a few locations in the lower part of the borehole (~115 to 195 mbsf). As shown in figure 20, there is a subtle shift in IR temperature to overall cooler cores in this range. No strong IR anomalies occurred in cores from Hole NGHP-01-18A. Instead, the deeper zone is shifted to temperatures ~1 °C cooler than temperatures higher in the hole with superimposed minor zones of still cooler temperature, for example at ~145 mbsf. The shift to lower temperature coincides with a slight decrease in chlorinity (see "Inorganic Geochemistry"), indicating that the temperature shift is likely caused by disseminated gas hydrate. This conclusion is supported by core-end IR images from the coolest part of the deeper zone (Section NGHP-01-18A-13X-3) which is slightly cooler than Section NGHP-01-18A-19X-3 (fig. 21). It is noteworthy that the slightly cooler zone in the lower third of Hole NGHP-01-18A is below a possible fault indicated from seismic reflection profiles and the fault may control the distribution of small amounts of disseminated gas hydrate in this area. It is also observed that the temperature shift coincides with the switch from APC to XCB coring. This change is not typically associated with consistent core temperature shifts, but should be evaluated further during post-cruise research on the IR data.

A slight cold anomaly also occurs at a shallower depth (~58 to 64 mbsf, Core NGHP-01-18A-07H, see fig. 20). This slightly cooler zone does not correlate with a significant chlorinity shift. Post-cruise analysis will compare the depths of IR temperature shifts with chlorinity data from this zone.

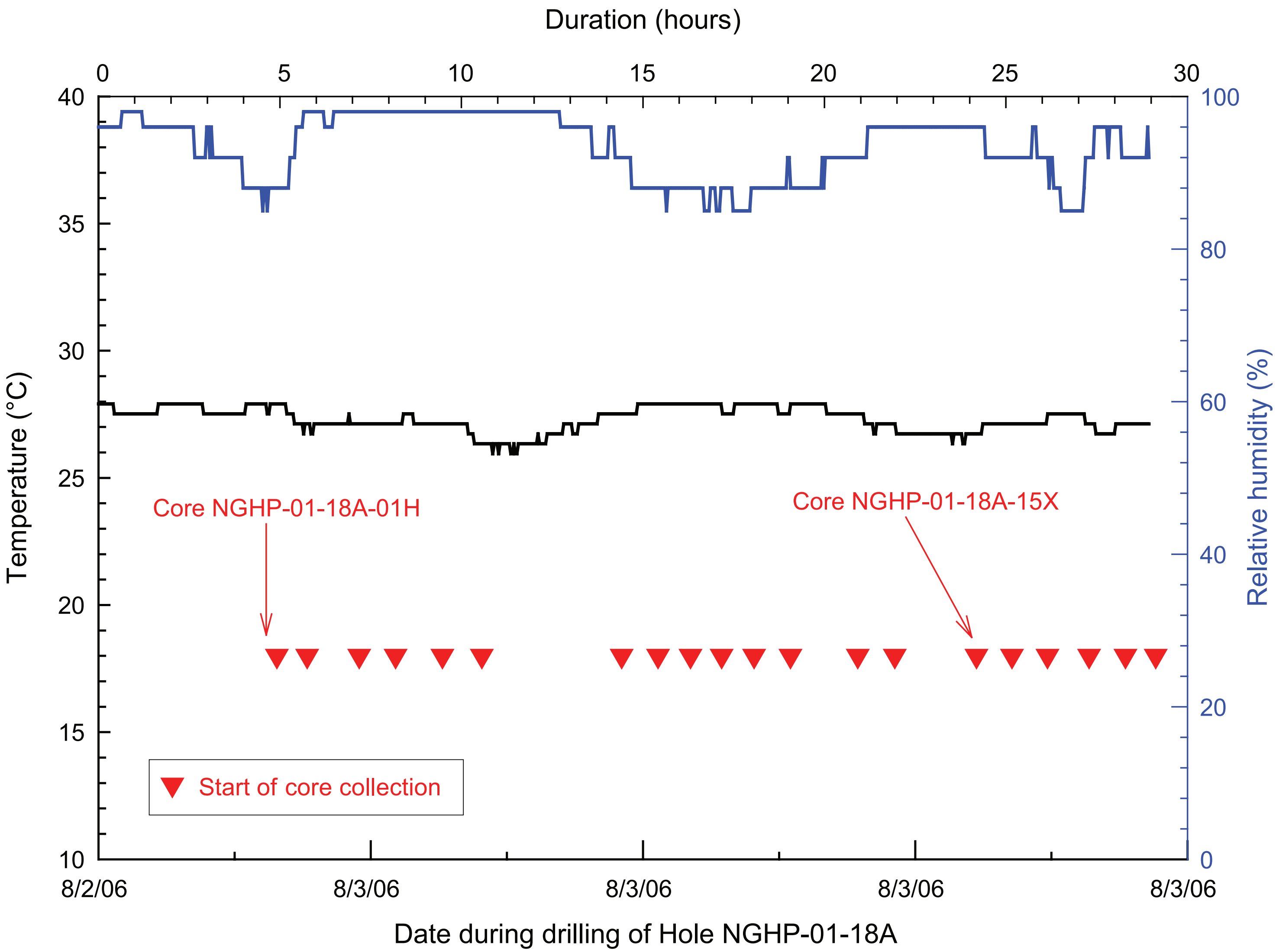

Figure 19. Catwalk temperature and humidity measurements as a function of time during drilling operations at Site NGHP-01-18.

Table 8. List of infrared images collected from Hole NGHP-01-18A.

Core	Imaging length (cm)	First run	Date	Start time	Temperature (start/end) (°C)	Comments
1H	720	x	8/3	0:56	27.9/27.9	
2H	970	x	8/3	1:36	27.9/27.9	
3H	930	x	8/3	2:45	27.1/27.1	
4H	910	x	8/3	3:33	27.1/27.1	
5H	970	x	8/3	4:35	27.1/27.1	
6H	970	x	8/3	5:27	27.1/27.1	
7H	970	x	8/3	8:32	27.5/27.50	
8H	970	x	8/3	9:20	27.5/27.50	
9H	970	x	8/3	10:03	27.9/27.9	
10H	970	x	8/3	10:44	27.9/27.9	
11H	970	x	8/3	11:27	27.5/27.50	
12H	970	x	8/3	12:15	27.9/27.9	
13X	900	x	8/3	13:44	27.5/27.50	
14X	950	x	8/3	14:33	26.5/26.7	Rain (accounts for T drop)
15X	950	x	8/3	16:21	26.7/26.7	
16X	950	x	8/3	17:08	27.1/27.1	
17X	950	x	8/3	17:55	27.1/27.1	
18X	950	x	8/3	18:50	27.5/27.5	IW in coolest spot, likely drilling impact, poor recovery
19X	950	x	8/3	19:38	26.7/26.7	One slightly cool spot (IW)
20X	840	x	8/3	20:18	27.1/27.1	EOH no could spot

Table 9. List of infrared image files collected on section ends from Hole NGHP-01-18A.

Core	Section	Top	Bottom	Date	Time	Image #	Comments
1H	3	x		8/3	1:15	G0803-01, 02	IMG file odd numbers, BMP even #'s
2H	3	x		8/3	1:48	G0803-03, 04	
3H	3	x		8/3	3:00	G0803-05, 06	
4H	3	x		8/3	3:43	G0803-07, 08	
5H	3	x		8/3	4:47	G0803-09, 10	
6H	3	x		8/3	5:45	G0803-11, 12	
7H	3	x		8/3	8:56	G0803-13, 14	
8H	3	x		8/3	9:40	G0803-15, 16	
9H	3	x		8/3	10:20	G0803-17, 18	
10H	3	x		8/3	11:00	G0803-19, 20	
11H	3	x		8/3	11:45	G0803-21, 22	
12H	3	x		8/3	12:40	G0803-23, 24	Fresh trim of end
13X	3		x	8/3	13:52	G0803-25, 26	
14X	3		x	8/3	14:43	G0803 27, 28	End cut is rough
15X	3		x	8/3	16:32	G0803 29, 30	Fresh cut
16X	2		x	8/3	15:18	G0803 31 32	Fresh cut
17X	3		x	8/3	18:07	G0803 33, 34	Fresh cut
18X	2	x		8/3	19:02	G0803 35, 36	Cool spot is hole
19X	3		x	8/3	19:42	G0803 37, 38	Fresh cut. Time is approximate
20X	3		x	8/3	20:18	G0803 39, 40	Fresh cut but with slash (hole)

Moussey textures in split cores were observed at five depths in Hole NGHP-01-18A (fig. 22, see "Lithostratigraphy"). Such textures are typically associated with dissociation of lenses or layers of gas hydrate. However, in core from Hole NGHP-01-18A there was no definitive spatial association between moussey texture and subtle IR anomalies within the temperature-shifted zone. In fact, the shallowest zone is slightly above the temperature-shifted zone. Geochemistry on two moussey samples indicates significant presence of seawater, suggesting that the heave conditions were lifting the bit and core off bottom and allowing seawater to penetrate the core during the drilling process.

Core-End Temperature Readings

Core-end-temperature readings were taken on most cores immediately following the IR track imaging (table 10). Typically four temperature probes were inserted approximately 8 cm into the end of each core and allowed to remain there until the core was completely processed and removed from the catwalk. Temperatures from the center position probes are typically 5 to 10 °C less than the IR temperatures as expected since the IR images measure the liner temperature which has warmed closer to ambient temperatures that the center of the core, except where significant gas hydrate is present.

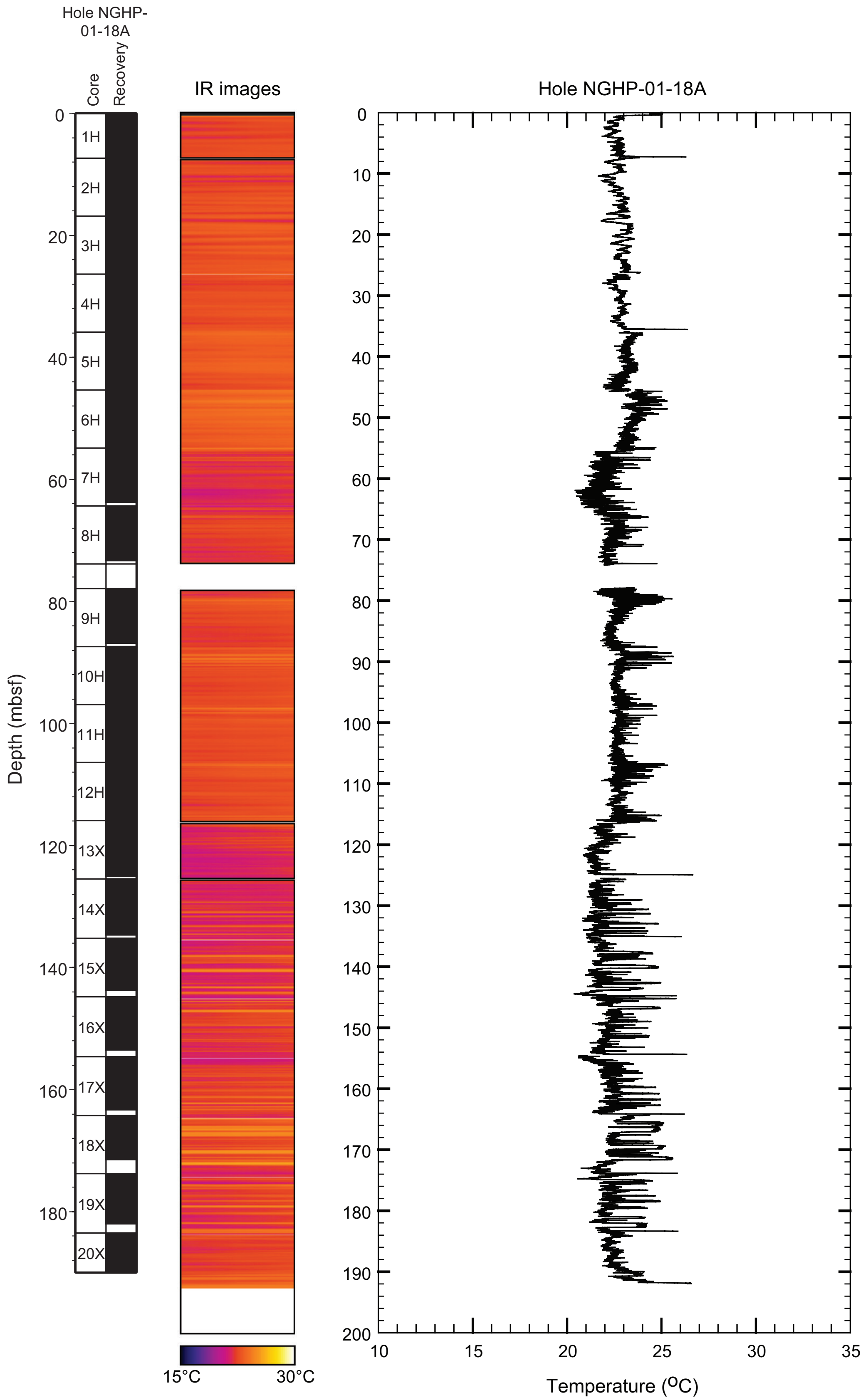

Figure 20. Infrared imaging and the derived downhole temperature profile for Hole NGHP-01-18A.

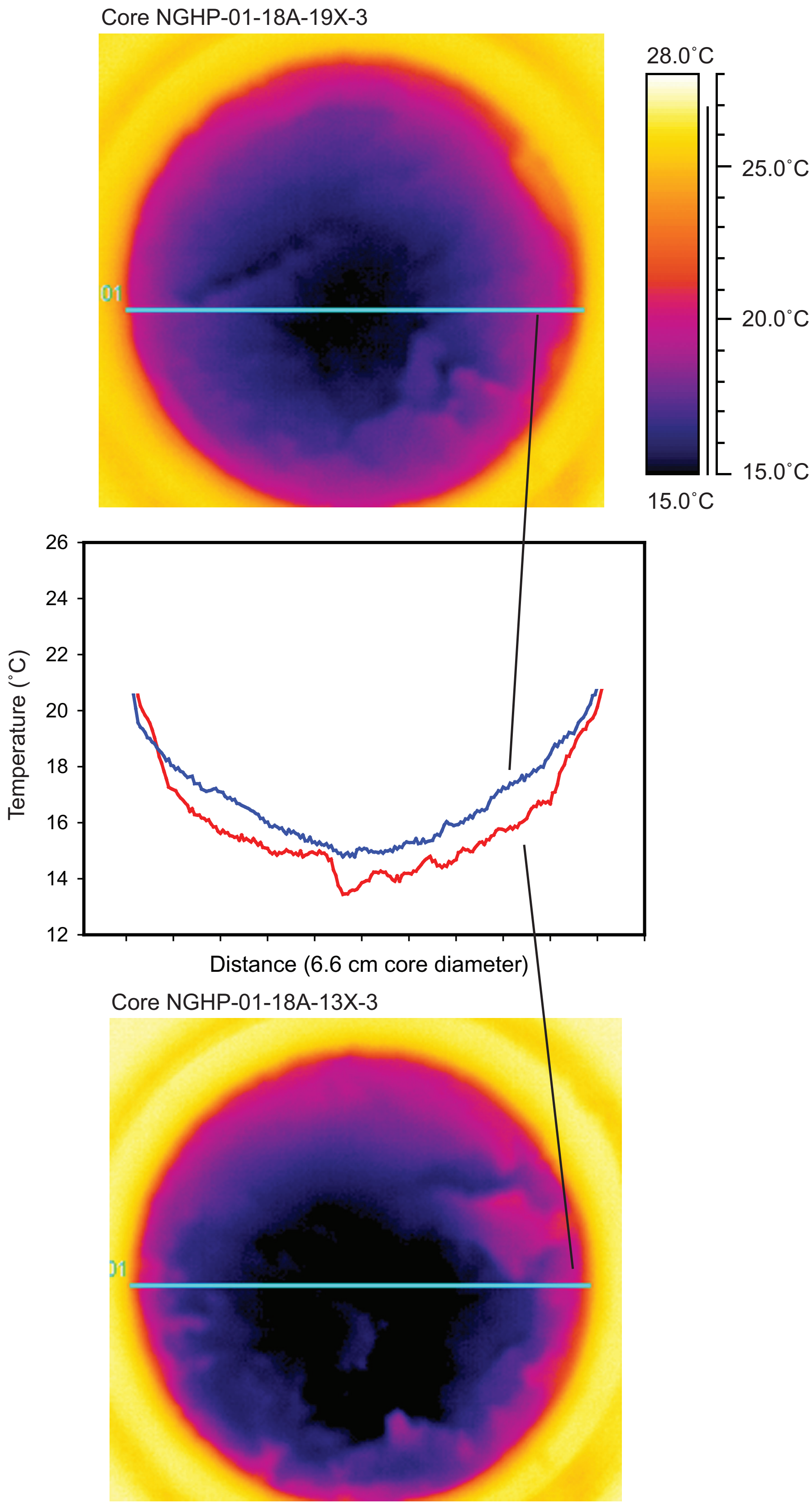

Figure 21. Comparison of core-end infrared images and cross-core T profiles from two different parts of Hole NGHP-01-18A.

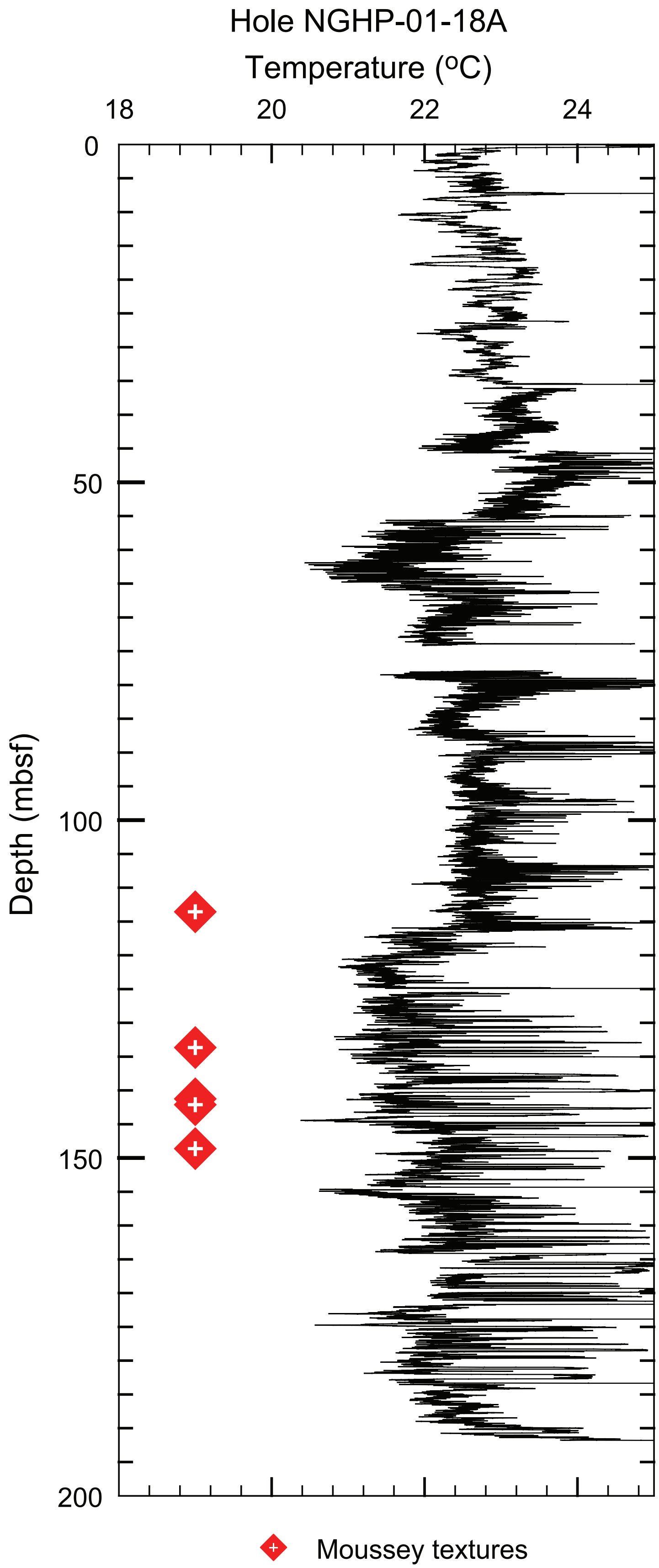

Figure 22. Downcore temperature profile for Hole NGHP-01-18A with location of moussey textures (see "Lithostratigraphy").

Table 10. List of temperature probe data collected at bottom of cores from Hole NGHP-01-18A.

Core	Section	Bottom	Date	In time	Out time	Temperature probe #	Comments
1H	last	x	8/3	0:57	1:14	F-1, F-2, F-3, F-4	Alternate pattern to core 18X, probe 2 center, 1 up, 3 down 4 side.
2H	last	x	8/3	1:38	1:48	F-1, F-2, F-3, F-4	
3H	last	x	8/3	2:46	3:00	F-1, F-2, F-3, F-4	
4H	last	x	8/3	3:34	3:43	F-1, F-2, F-3, F-4	
5H	last	x	8/3	4:37	4:47	F-1, F-2, F-3, F-4	
6H	last	x	8/3	5:27	5:45	F-1, F-2, F-3, F-4	
7H	last	x	8/3	8:33	8:54	F-1, F-2, F-3, F-4	
8H	last	x	8/3	9:21	NA	F-1, F-2, F-3, F-4	
9H	last	x	8/3	10:04	10:19	F-1, F-2, F-3, F-4	
10H	last	x	8/3	10:45	11:00	F-1, F-2, F-3, F-4	
11H	last	x	8/3	11:28	11:45	F-1, F-2, F-3, F-4	
12H	last	x	8/3	12:19	12:36	F-1, F-2, F-3, F-4	Used standard pattern(1, 4 on edge 90 deg apart, 3 center, 2 between 1 and 3 (until core 20X)
13H	last	x	8/3	13:48	13:52	F-1, F-2, F-3, F-4	Inserted only halfway
14X	last	x	8/3	14:38	14:47	F-1, F-2, F-3, F-4	Probe 1 and 4 initially switched
15X	last	x	8/3	16:25	16:39	F-1, F-2, F-3, F-4	Solid, good insertion
16X	last	x	8/3	17:11	17:22	F-1, F-2, F-3, F-4	Good, solid insertion for probes 2 and 3
17X	last	x	8/3	18:00	18:10	F-1, F-2, F-3, F-4	Good, solid insertion
18X	last	x	8/3	18:52	19:06	F-1, F-2, F-3, F-4	Good, solid insertion but bumped after insertion
19X	last	x	8/3	19:43	19:55	F-1, F-2, F-3, F-4	Good insertion
20X	last	x	8/3	20:21	20:21	F-1, F-2, F-3, F-4	Poor insertion, cracked, core undersized, partial insertion only

Index Properties

Numerous index properties were performed on split core from Hole NGHP-01-18A (figs. 23 and 24). They define a near-seafloor (0 to 13 mbsf) layer that is common in recent depositional marine settings in which initially high water content and porosity values decrease at a rapid rate with depth. The layer is also characterized by a corresponding increase in bulk density. The water content (related to solids) in this layer (table 11 and fig. 23) decreases from 114 to 68 percent, and then to about 52 percent near the bottom of the hole. Porosity varies from about 75 percent at the top of the hole to 63 percent at 13 mbsf and then to a low of about 58 percent at the bottom of the hole. Grain density was slightly lower than the core average (2.69 g/cm^3) at the top of the hole, but not as low as at the sites in the Krishna-Godavari (KG) basin. Because of poor weather conditions, wire-line logging was not conducted at this site.

Strength

Shear strength increases to about 20 mbsf, decreases and remains constant to 55 mbsf then increases to the boundary between APC and XCB coring at 115 mbsf (tables 12, 13, and fig. 23). Strength stays essentially constant to the bottom of the hole; however, accurate strength measurements are more difficult to obtain in XCB cores because of disturbance caused by rotary coring on sediment. Although testing was to be restricted to intact biscuits, it was occasionally difficult to differentiate between biscuits and adjacent disturbed sediment.

The measured shear strengths were normalized to the effective vertical stress (σ'_v; fig. 25) to provide qualitative information on the stress history of the sediment. The strength/effective vertical stress ranges from approximately 0.5 at the top of the hole to an average of about 0.075 below 50 m. Almost all of these values are in agreement with a number of other normally consolidated clays (Holtz and Kovacs, 1981). Hunt (1984) states that the strength/effective vertical stress ratio typically is between 0.4 and 0.16. The wide scatter in the results at the top of the hole reflect the dependency of this ratio on the stress path as well as the test method (Bjerrum, 1972; Ladd, and others, 1977). Because almost all of the values are below 0.4, the implication is that these sediments have not experienced a vertical effective stress greater than what is now being applied *in situ*. They have not been overconsolidated by erosional or other geologic processes.

The peak (Sv) and remolded (Srem) vane shear strengths clearly increase with sub-bottom depth (fig. 26) and the sensitivity (St), which equals Sv/Srem, varies between 1.5 and 4. Sensitivity values represent the amount of strength loss after remolding and in extreme examples can reach values of 500 (Lambe and Whitman, 1969). This sediment has low to medium sensitivity (Holtz and Kovacs, 1981). High values of sensitivity are indicative of good quality core recovery because the sediment has not been highly disturbed.

Electrical Resistivity

Strong agreement exists between ER values produced by the MSCL and the Wenner array except between 20 and 80 mbsf (fig. 24). The resistivity values determined using the Wenner array on split cores (table 14) are on the low side of the MSCL data, in part because the Wenner measurements are conducted on intact core material, rather than a wider portion of core that may contain voids or small expansion cracks. Lower MSCL values are more representative of undisturbed sediment as they are less impacted by the presence of such micro voids caused by gas expansion.

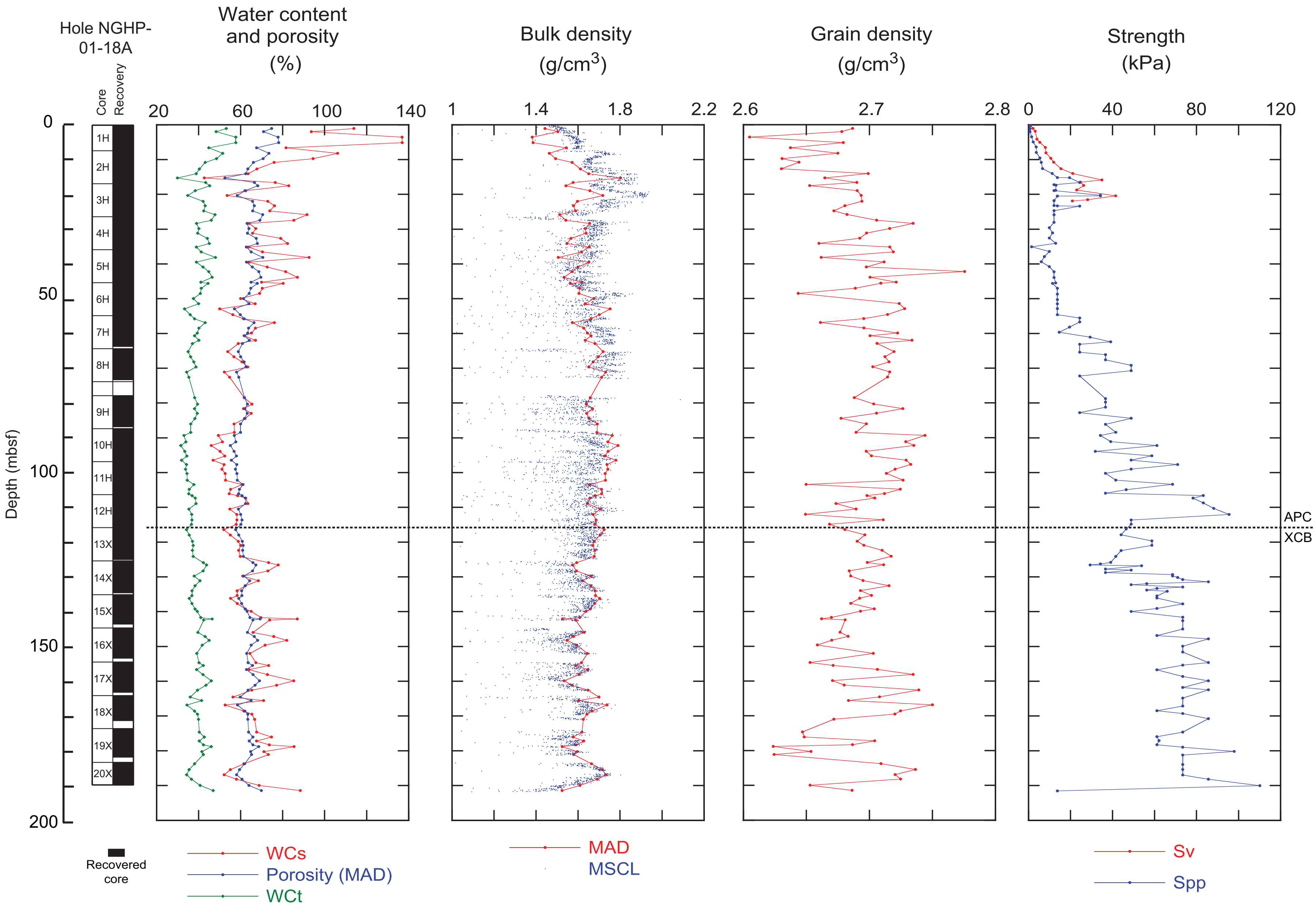

Figure 23. Profiles of core recovery, index, and strength properties for Hole NGHP-01-18A.

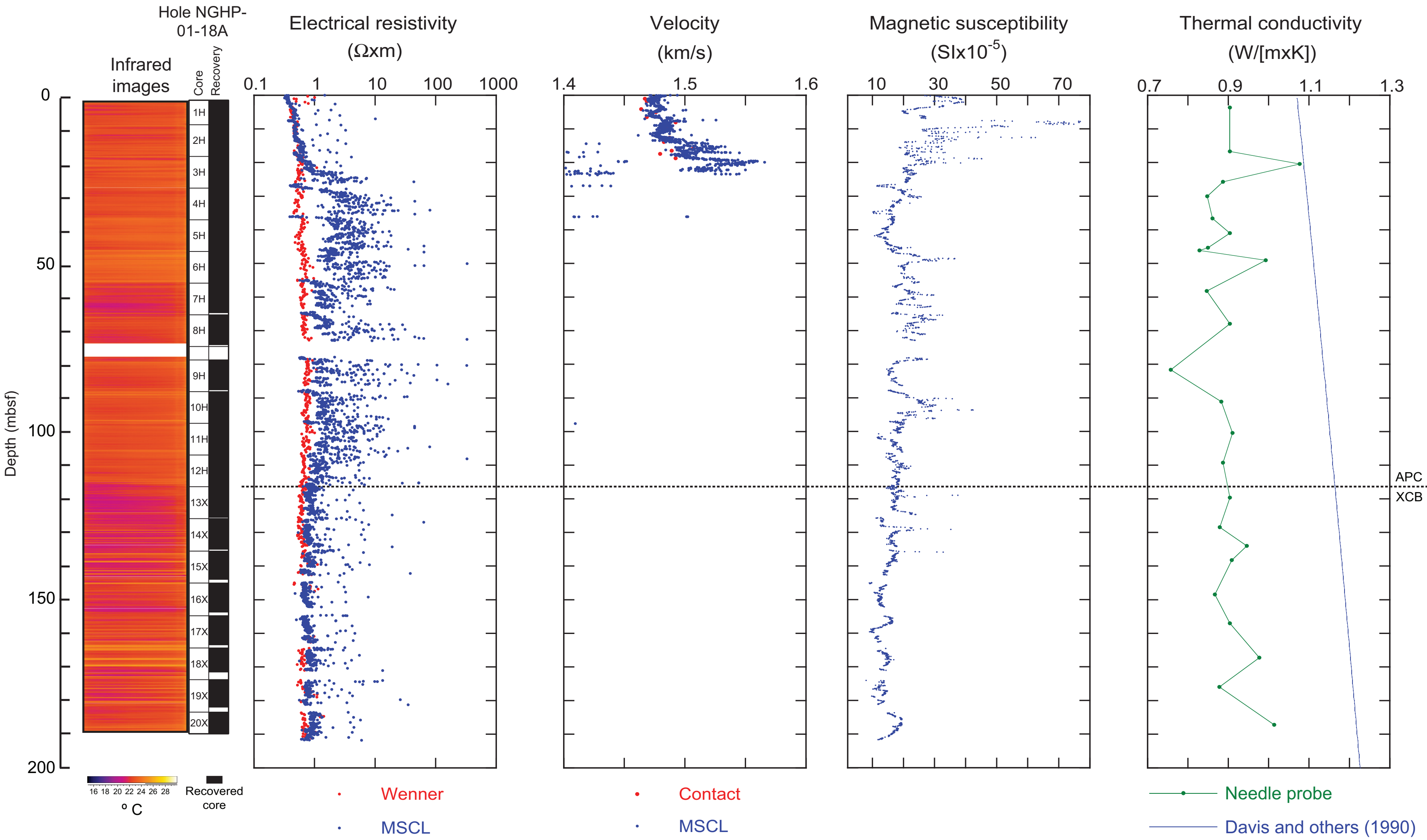

Figure 24. Profiles of infrared images, core recovery, electrical resistivity, acoustic *P*-wave velocity, magnetic susceptibility, and thermal conductivity for Hole NGHP-01-18A.

Table 11. Moisture and density physical properties for Hole NGHP-01-18A.

Core, section	Sample code	Depth, int, from (cm)	Depth, int, to (cm)	Depth (mbsf)	WCt (%)	WCs (%)	Grain density (g/cm³)	Bulk density (g/cm³)	Dry bulk density (g/cm³)	Porosity (%)	Void ratio	Unit weight (kN/m³)
						NGHP-01-18A						
1H-1	MAD	110	114	1.11	53.26	113.94	2.69	1.44	0.67	74.90	2.98	14.15
1H-2	MAD	52	56	2.03	48.38	93.74	2.68	1.51	0.78	70.98	2.45	14.76
1H-3	MAD	60	64	3.61	57.78	136.88	2.61	1.38	0.58	77.85	3.52	13.56
1H-4	MAD	68	72	5.19	57.81	137.00	2.68	1.39	0.59	78.15	3.58	13.60
1H-5	MAD	62	66	6.63	44.94	81.63	2.64	1.55	0.85	67.69	2.09	15.15
2H-1	MAD	79	83	8.20	51.50	106.20	2.68	1.46	0.71	73.48	2.77	14.35
2H-2	MAD	82	87	9.74	48.61	94.57	2.63	1.49	0.77	70.79	2.42	14.65
2H-3	MAD	44	49	10.85	43.18	75.98	2.64	1.57	0.89	66.20	1.96	15.43
2H-4	MAD	82	84	12.72	40.40	67.79	2.63	1.61	0.96	63.48	1.74	15.81
2H-5	MAD	69	74	14.11	38.87	63.58	2.70	1.65	1.01	62.55	1.67	16.19
2H-6	MAD	38	43	15.30	29.96	42.77	2.66	1.80	1.26	52.62	1.11	17.67
2H-7	MAD	23	28	16.65	43.36	76.56	2.69	1.58	0.89	66.67	2.00	15.47
3H-1	MAD	62	64	17.52	45.37	83.04	2.65	1.54	0.84	68.22	2.15	15.13
3H-2	MAD	57	59	18.97	38.47	62.53	2.69	1.66	1.02	62.12	1.64	16.24
3H-3	MAD	47	49	20.37	34.91	53.64	2.69	1.72	1.12	58.48	1.41	16.85
3H-4	MAD	62	64	22.02	42.19	72.99	2.69	1.60	0.92	65.71	1.92	15.67
3H-5	MAD	40	42	23.30	43.24	76.18	2.68	1.58	0.90	66.56	1.99	15.49
3H-6	MAD	38	40	24.78	42.51	73.94	2.67	1.59	0.91	65.82	1.93	15.58
3H-7	MAD	43	45	25.83	47.82	91.64	2.68	1.51	0.79	70.55	2.40	14.84
4H-1	MAD	107	109	27.47	46.07	85.42	2.71	1.54	0.83	69.26	2.25	15.13
4H-2	MAD	49	50	28.39	39.09	64.18	2.73	1.66	1.01	63.11	1.71	16.24
4H-3	MAD	49	50	29.89	40.20	67.23	2.72	1.63	0.98	64.03	1.78	16.02
4H-4	MAD	29	31	31.19	39.65	65.70	2.70	1.64	0.99	63.34	1.73	16.07
4H-5	MAD	29	31	32.69	44.18	79.13	2.69	1.57	0.88	67.50	2.08	15.37
4H-6	MAD	27	29	34.17	45.15	82.33	2.66	1.55	0.85	68.10	2.13	15.17
4H-7	MAD	27	29	35.17	38.96	63.84	2.72	1.65	1.01	62.83	1.69	16.22
5H-1	MAD	70	72	36.60	41.34	70.47	2.72	1.62	0.95	65.13	1.87	15.85
5H-2	MAD	75	77	38.15	48.10	92.68	2.66	1.51	0.78	70.63	2.40	14.77
5H-3	MAD	60	62	39.50	39.03	64.01	2.71	1.65	1.01	62.85	1.69	16.20
5H-4	MAD	51	53	40.91	42.10	72.71	2.70	1.60	0.93	65.66	1.91	15.69
5H-5	MAD	36	38	42.26	44.91	81.50	2.78	1.57	0.87	68.80	2.20	15.41
5H-6	MAD	50	52	43.90	46.55	87.10	2.70	1.53	0.82	69.63	2.29	15.05
5H-7	MAD	38	40	45.28	41.19	70.04	2.72	1.62	0.95	65.01	1.86	15.88
6H-1	MAD	23	25	45.63	44.54	80.30	2.71	1.56	0.87	68.00	2.13	15.33
6H-2	MAD	23	25	47.05	41.31	70.38	2.69	1.61	0.94	64.90	1.85	15.77
6H-3	MAD	19	21	48.51	40.89	69.16	2.64	1.61	0.95	64.11	1.79	15.74
6H-5	MAD	15	17	51.47	40.11	66.97	2.72	1.63	0.98	64.05	1.78	16.03
6H-6	MAD	10	12	52.92	33.37	50.09	2.73	1.75	1.17	57.17	1.33	17.20
6H-7	MAD	81	83	54.63	36.04	56.35	2.71	1.70	1.09	59.91	1.49	16.69
7H-1	MAD	91	93	55.81	38.06	61.45	2.70	1.66	1.03	61.81	1.62	16.30
7H-2	MAD	95	97	56.93	43.22	76.12	2.66	1.57	0.89	66.43	1.98	15.43
7H-3	MAD	99	101	58.47	40.14	67.06	2.70	1.63	0.97	63.85	1.77	15.97
7H-4	MAD	99	101	59.93	39.48	65.22	2.72	1.64	1.00	63.43	1.73	16.13
7H-5	MAD	30	32	60.68	38.15	61.67	2.70	1.66	1.03	61.93	1.63	16.30
7H-6	MAD	29	31	62.00	40.18	67.18	2.73	1.64	0.98	64.21	1.79	16.04
7H-7	MAD	27	29	62.92	37.08	58.94	2.71	1.68	1.06	60.91	1.56	16.49
8H-1	MAD	89	91	65.29	35.05	53.98	2.72	1.72	1.12	58.92	1.43	16.87
8H-2	MAD	89	91	66.76	36.26	56.90	2.71	1.70	1.08	60.12	1.51	16.64
8H-3	MAD	88	90	68.21	37.78	60.71	2.72	1.67	1.04	61.70	1.61	16.39
8H-4	MAD	82	84	69.65	38.79	63.38	2.70	1.65	1.01	62.59	1.67	16.20
8H-5	MAD	78	80	71.11	34.36	52.36	2.72	1.73	1.14	58.15	1.39	16.99
8H-6	MAD	78	80	72.61	35.41	54.82	2.71	1.71	1.11	59.24	1.45	16.80
9H-1	MAD	60	62	78.50	38.20	61.82	2.69	1.66	1.02	61.88	1.62	16.26
9H-2	MAD	95	97	80.35	39.55	65.44	2.70	1.64	0.99	63.35	1.73	16.08
9H-3	MAD	74	76	81.64	38.07	61.46	2.73	1.67	1.03	62.08	1.64	16.37
9H-4	MAD	60	62	83.00	39.43	65.10	2.71	1.64	0.99	63.24	1.72	16.10
9H-5	MAD	59	61	84.49	38.33	62.15	2.68	1.65	1.02	61.91	1.63	16.22
9H-6	MAD	75	77	86.02	36.31	57.02	2.70	1.69	1.08	60.04	1.50	16.60

Table 11. Moisture and density physical properties for Hole NGHP-01-18A.—Continued

Core, section	Sample code	Depth, int, from (cm)	Depth, int, to (cm)	Depth (mbsf)	WCt (%)	WCs (%)	Grain density (g/cm³)	Bulk density (g/cm³)	Dry bulk density (g/cm³)	Porosity (%)	Void ratio	Unit weight (kN/m³)
					NGHP-01-18A—Continued							
10H-1	MAD	111	113	88.51	36.32	57.02	2.69	1.69	1.08	59.97	1.50	16.58
10H-2	MAD	47	49	89.37	33.11	49.49	2.74	1.76	1.18	57.02	1.33	17.29
10H-3	MAD	78	80	91.18	33.96	51.43	2.73	1.74	1.15	57.82	1.37	17.09
10H-4	MAD	40	42	92.28	31.56	46.11	2.74	1.79	1.23	55.20	1.23	17.56
10H-5	MAD	57	59	93.95	33.44	50.24	2.70	1.74	1.16	56.97	1.32	17.10
10H-6	MAD	38	40	95.26	34.43	52.50	2.70	1.73	1.13	58.08	1.39	16.94
10H-7	MAD	18	20	96.49	31.95	46.96	2.73	1.78	1.21	55.59	1.25	17.47
11H-1	MAD	81	83	97.71	34.29	52.17	2.73	1.74	1.14	58.21	1.39	17.04
11H-2	MAD	68	70	99.08	33.83	51.14	2.72	1.74	1.15	57.61	1.36	17.09
11H-3	MAD	40	42	100.30	34.50	52.68	2.71	1.73	1.13	58.27	1.40	16.95
11H-4	MAD	82	84	102.22	34.59	52.88	2.73	1.73	1.13	58.48	1.41	16.97
11H-5	MAD	57	59	103.45	37.80	60.77	2.65	1.66	1.03	61.14	1.57	16.24
11H-6	MAD	48	50	104.86	35.58	55.24	2.72	1.71	1.10	59.52	1.47	16.79
11H-7	MAD	60	62	106.12	35.34	54.65	2.71	1.71	1.11	59.15	1.45	16.80
12H-1	MAD	29	31	106.69	36.95	58.60	2.70	1.68	1.06	60.70	1.54	16.49
12H-2	MAD	30	32	107.36	38.48	62.55	2.70	1.66	1.02	62.30	1.65	16.25
12H-3	MAD	40	42	108.96	38.84	63.52	2.67	1.64	1.01	62.39	1.66	16.12
12H-4	MAD	49	51	110.55	35.44	54.89	2.69	1.71	1.10	59.05	1.44	16.73
12H-5	MAD	52	54	112.08	36.78	58.19	2.65	1.67	1.06	60.10	1.51	16.40
12H-6	MAD	61	63	113.67	36.85	58.35	2.71	1.69	1.07	60.71	1.55	16.54
12H-7	MAD	40	42	114.90	36.68	57.93	2.67	1.68	1.06	60.16	1.51	16.46
13H-1	MAD	57	59	116.47	34.24	52.08	2.68	1.72	1.13	57.70	1.36	16.91
13H-2	MAD	57	59	117.97	35.56	55.19	2.70	1.71	1.10	59.25	1.45	16.72
13H-3	MAD	92	94	119.82	37.09	58.97	2.69	1.68	1.06	60.78	1.55	16.45
13H-4	MAD	57	59	120.97	37.52	60.06	2.70	1.67	1.04	61.27	1.58	16.39
13H-5	MAD	49	51	122.39	37.16	59.13	2.71	1.68	1.06	61.03	1.57	16.49
13H-6	MAD	75	77	124.15	37.45	59.88	2.72	1.68	1.05	61.38	1.59	16.45
14H-1	MAD	40	42	125.90	42.31	73.34	2.70	1.59	0.92	65.91	1.93	15.64
14H-2	MAD	41	43	126.61	43.81	77.98	2.71	1.57	0.88	67.38	2.07	15.44
14H-3	MAD	61	63	128.31	42.23	73.11	2.68	1.59	0.92	65.72	1.92	15.62
14H-4	MAD	61	63	129.81	37.91	61.05	2.69	1.66	1.03	61.56	1.60	16.30
14H-5	MAD	41	43	131.11	40.67	68.55	2.70	1.62	0.96	64.39	1.81	15.89
14H-6	MAD	42	44	132.62	38.35	62.21	2.72	1.66	1.02	62.27	1.65	16.30
14H-7	MAD	32	34	134.02	36.86	58.38	2.69	1.68	1.06	60.57	1.54	16.49
15X-1	MAD	19	21	135.39	36.88	58.43	2.70	1.68	1.06	60.66	1.54	16.51
15X-2	MAD	19	21	136.20	35.60	55.28	2.69	1.70	1.10	59.25	1.45	16.71
15X-3	MAD	19	21	137.70	36.90	58.47	2.69	1.68	1.06	60.54	1.53	16.47
15X-4	MAD	26	28	139.27	38.41	62.37	2.70	1.66	1.02	62.23	1.65	16.26
15X-5	MAD	29	31	139.92	39.43	65.11	2.69	1.64	0.99	63.14	1.71	16.07
15X-6	MAD	70	72	141.73	41.05	69.64	2.67	1.61	0.95	64.50	1.82	15.77
15X-6	MAD	108	110	142.11	46.53	87.01	2.66	1.53	0.82	69.35	2.26	14.96
15X-7	MAD	19	21	142.40	42.48	73.87	2.68	1.59	0.91	65.92	1.93	15.58
16X-1	MAD	118	120	145.98	39.75	65.97	2.68	1.63	0.98	63.30	1.73	15.99
16X-2	MAD	89	91	147.14	43.14	75.87	2.68	1.58	0.90	66.54	1.99	15.48
16X-3	MAD	54	56	148.29	45.06	82.02	2.67	1.55	0.85	68.15	2.14	15.18
16X-4	MAD	43	45	149.68	41.77	71.74	2.66	1.59	0.93	65.08	1.86	15.64
16X-5	MAD	128	130	152.03	39.21	64.49	2.70	1.65	1.00	63.01	1.70	16.13
17X-1	MAD	8	10	154.68	40.25	67.37	2.65	1.62	0.97	63.58	1.75	15.86
17X-2	MAD	70	72	155.50	42.33	73.41	2.67	1.59	0.92	65.70	1.92	15.58
17X-3	MAD	40	42	156.70	39.05	64.07	2.71	1.65	1.00	62.88	1.69	16.16

Table 11. Moisture and density physical properties for Hole NGHP-01-18A.—Continued

Core, section	Sample code	Depth, int, from (cm)	Depth, int, to (cm)	Depth (mbsf)	WCt (%)	WCs (%)	Grain density (g/cm³)	Bulk density (g/cm³)	Dry bulk density (g/cm³)	Porosity (%)	Void ratio	Unit weight (kN/m³)
NGHP-01-18A—Continued												
17X-4	MAD	32	34	158.12	42.12	72.77	2.73	1.60	0.93	66.03	1.94	15.74
17X-5	MAD	58	60	159.88	46.04	85.31	2.67	1.53	0.83	69.00	2.23	15.05
17X-6	MAD	49	51	161.19	43.55	77.16	2.68	1.57	0.89	66.89	2.02	15.42
17X-7	MAD	39	41	162.59	39.53	65.37	2.74	1.65	1.00	63.63	1.75	16.16
18X-1	MAD	27	29	164.57	36.07	56.42	2.71	1.70	1.09	59.88	1.49	16.67
18X-2	MAD	56	58	165.59	41.53	71.02	2.68	1.60	0.94	65.06	1.86	15.73
18X-3	MAD	36	38	166.89	34.50	52.67	2.75	1.74	1.14	58.59	1.42	17.05
18X-4	MAD	55	57	168.58	38.11	61.58	2.72	1.67	1.03	62.11	1.64	16.36
18X-5	MAD	58	60	169.50	39.58	65.50	2.72	1.64	0.99	63.51	1.74	16.11
18X-6	MAD	56	58	170.98	40.00	66.68	2.67	1.63	0.98	63.52	1.74	15.94
19X-2	MAD	59	61	174.64	40.36	67.68	2.65	1.62	0.97	63.85	1.77	15.88
19X-3	MAD	88	90	176.11	42.79	74.80	2.65	1.58	0.90	65.93	1.94	15.47
19X-4	MAD	46	48	177.19	40.34	67.61	2.70	1.63	0.97	64.11	1.79	15.95
19X-5	MAD	58	60	178.35	42.42	73.66	2.69	1.59	0.92	65.91	1.93	15.60
19X-6	MAD	21	23	178.84	46.08	85.47	2.62	1.53	0.82	68.66	2.19	14.96
19X-7	MAD	56	58	180.29	41.58	71.18	2.65	1.60	0.93	64.85	1.85	15.66
19X-8	MAD	43	45	181.11	42.28	73.26	2.62	1.58	0.91	65.26	1.88	15.49
20X-1	MAD	29	31	183.79	38.12	61.60	2.71	1.66	1.03	61.98	1.63	16.32
20X-2	MAD	46	48	185.46	35.55	55.15	2.74	1.72	1.11	59.59	1.47	16.83
20X-3	MAD	46	48	186.96	34.32	52.25	2.72	1.73	1.14	58.14	1.39	17.01
20X-4	MAD	23	25	188.23	36.72	58.02	2.72	1.69	1.07	60.70	1.54	16.60
20X-5	MAD	51	53	190.01	40.77	68.82	2.65	1.61	0.95	64.08	1.78	15.78
20X-6	MAD	47	49	191.47	46.94	88.48	2.69	1.52	0.81	69.90	2.32	14.95

Table 12. Vane shear strength results for Hole NGHP-01-18A.

Core, section	Sample	Top (cm)	Depth (mbsf)	Sv (kPa)	Sres (kPa)	Srem (kPa)	St
NGHP-01-18A							
1H-1	VS	33	0.33	1.0	0.8	0.6	1.7
1H-1	VS	103	1.03	2.2	1.6	0.7	3.4
1H-2	VS	36	1.86	3.3	2.5	1.5	2.2
1H-3	VS	115	4.15	4.0	2.3	1.6	2.6
1H-4	VS	55	5.05	5.4	3.5	1.7	3.1
1H-5	VS	55	6.55	8.1	4.9	2.3	3.5
2H-1	VS	65	8.05	8.4	6.6	2.4	3.5
2H-2	VS	75	9.65	10.7	7.0	3.5	3.1
2H-3	VS	35	10.75	12.0	8.2	4.6	2.6
2H-4	VS	75	12.65	15.5	8.6	4.1	3.8
2H-5	VS	63	14.03	21.1	13.2	7.4	2.9
2H-6	VS	98	15.88	35.0	19.7	10.7	3.3
2H-7	VS	15	16.55	24.9	14.8	7.6	3.3
3H-1	VS	55	17.45	26.3	11.5	7.1	3.7
3H-2	VS	35	18.75	23.0	11.5	7.1	3.3
3H-3	VS	55	20.45	41.6	25.1	13.0	3.2
3H-4	VS	15	21.55	28.2	16.5	8.2	3.4
3H-4	VS	55	21.95	21.0	9.9	5.3	3.9

Table 13. Pocket Penetrometer strength results for Hole NGHP-01-18A.

Core, section	Sample	Top (cm)	Depth (mbsf)	Spp (kPa)	Core, section	Sample	Top (cm)	Depth (mbsf)	Spp (kPa)
				NGHP-01-18A					
1H-1	PP	31	0.31	0.8	5H-5	PP	40	42.30	12.3
1H-1	PP	116	1.16	0.8	5H-6	PP	54	43.94	12.3
1H-2	PP	49	1.99	0.8	5H-7	PP	60	45.50	13.0
1H-3	PP	48	3.48	1.5	6H-1	PP	19	45.59	11.5
1H-4	PP	48	4.98	2.3	6H-2	PP	22	47.04	13.8
1H-5	PP	40	6.40	3.7	6H-3	PP	39	48.71	13.8
2H-1	PP	56	7.96	3.8	6H-4	PP	48	50.30	13.8
2H-2	PP	67	9.57	5.5	6H-5	PP	18	51.50	13.8
2H-3	PP	41	10.81	6.1	6H-6	PP	5	52.87	13.8
2H-4	PP	68	12.58	6.7	6H-7	PP	80	54.62	13.8
2H-5	PP	65	14.05	11.3	7H-1	PP	69	55.59	24.5
2H-6	PP	32	15.22	13.8	7H-2	PP	74	56.72	24.5
2H-6	PP	35	15.25	19.6	7H-3	PP	70	58.18	19.6
2H-7	PP	22	16.62	24.5	7H-4	PP	70	59.64	14.7
3H-1	PP	33	17.23	12.3	7H-5	PP	70	61.08	29.4
3H-1	PP	47	17.37	13.2	7H-6	PP	70	62.41	39.2
3H-2	PP	46	18.86	13.0	7H-7	PP	50	63.15	24.5
3H-2	PP	53	18.93	12.3	8H-1	PP	102	65.42	24.5
3H-3	PP	37	20.27	34.3	8H-2	PP	25	66.12	36.8
3H-3	PP	54	20.44	34.3	8H-3	PP	30	67.63	36.8
3H-3	PP	61	20.51	13.8	8H-4	PP	35	69.18	49.0
3H-4	PP	40	21.80	12.3	8H-5	PP	40	70.73	49.0
3H-4	PP	47	21.87	12.3	8H-6	PP	40	72.23	24.5
3H-5	PP	37	23.27	12.3	9H-1	PP	85	78.75	36.8
3H-5	PP	45	23.35	13.8	9H-2	PP	40	79.80	36.8
3H-5	PP	48	23.38	24.5	9H-3	PP	30	81.20	36.8
3H-6	PP	34	24.74	12.3	9H-4	PP	40	82.80	24.5
3H-7	PP	48	25.88	12.3	9H-5	PP	50	84.40	49.0
4H-2	PP	20	28.10	12.3	9H-6	PP	90	86.17	36.8
4H-3	PP	20	29.60	10.0	10H-1	PP	106	88.46	41.7
4H-4	PP	20	31.10	11.5	10H-2	PP	44	89.34	34.3
4H-5	PP	18	32.58	10.0	10H-3	PP	73	91.13	39.2
4H-6	PP	21	34.11	13.0	10H-4	PP	37	92.25	61.3
5H-1	PP	54	36.44	10.0	10H-5	PP	54	93.92	31.9
5H-2	PP	54	37.94	7.7	10H-6	PP	35	95.23	58.8
5H-3	PP	50	39.40	6.1	10H-7	PP	13	96.44	49.0
5H-4	PP	40	40.80	10.0	11H-1	PP	79	97.69	71.1

Table 13. Pocket Penetrometer strength results for Hole NGHP-01-18A.—Continued

Core, section	Sample	Top (cm)	Depth (mbsf)	Spp (kPa)	Core, section	Sample	Top (cm)	Depth (mbsf)	Spp (kPa)
				NGHP-01-18A—Continued					
11H-2	PP	65	99.05	49.0	15X-1	PP	30	135.50	61.3
11H-3	PP	37	100.27	36.8	15X-2	PP	10	136.11	61.3
11H-4	PP	77	102.17	41.7	15X-3	PP	30	137.81	73.5
11H-5	PP	54	103.42	68.6	15X-4	PP	12	139.13	61.3
11H-6	PP	54	104.92	46.6	15X-5	PP	33	139.96	49.0
11H-7	PP	46	105.98	36.8	15X-6	PP	56	141.59	73.5
12H-1	PP	20	106.60	83.3	15X-7	PP	41	142.62	73.5
12H-2	PP	33	107.39	78.4	16X-1	PP	20	145.00	73.5
12H-3	PP	20	108.76	83.3	16X-2	PP	64	146.89	61.3
12H-4	PP	30	110.36	88.2	16X-3	PP	9	147.84	85.8
12H-5	PP	49	112.05	95.6	16X-4	PP	73	149.98	73.5
12H-6	PP	59	113.65	49.0	16X-5	PP	90	151.65	73.5
12H-7	PP	37	114.87	49.0	17X-1	PP	7	154.67	85.8
13H-1	PP	36	116.26	46.6	17X-2	PP	60	155.40	73.5
13H-2	PP	53	117.93	44.1	17X-3	PP	43	156.73	61.3
13H-3	PP	74	119.64	58.8	17X-4	PP	85	158.65	73.5
13H-4	PP	54	120.94	58.8	17X-5	PP	60	159.90	85.8
13H-5	PP	56	122.46	44.1	17X-6	PP	115	161.85	73.5
13H-6	PP	74	124.14	41.7	17X-7	PP	30	162.50	85.8
14H-1	PP	38	125.88	39.2	18X-1	PP	60	164.90	73.5
14H-2	PP	8	126.28	34.3	18X-3	PP	63	167.16	73.5
14H-2	PP	37	126.57	29.4	18X-4	PP	47	168.50	61.3
14H-2	PP	63	126.83	53.9	18X-5	PP	40	169.32	73.5
14H-3	PP	8	127.78	36.8	18X-6	PP	39	170.81	85.8
14H-3	PP	38	128.08	49.0	19X-2	PP	59	174.64	73.5
14H-3	PP	110	128.80	36.8	19X-3	PP	75	175.98	61.3
14H-4	PP	12	129.32	68.6	19X-4	PP	38	177.11	62.2
14H-4	PP	53	129.73	68.6	19X-5	PP	50	178.27	61.3
14H-4	PP	100	130.20	71.1	19X-6	PP	35	178.98	73.5
14H-5	PP	10	130.80	73.5	19X-7	PP	48	180.21	98.0
14H-5	PP	70	131.40	85.8	19X-8	PP	54	181.22	73.5
14H-5	PP	130	132.00	56.4	20X-1	PP	50	184.00	73.5
14H-6	PP	10	132.30	49.0	20X-2	PP	40	185.40	73.5
14H-6	PP	77	132.97	73.5	20X-3	PP	50	187.00	73.5
14H-6	PP	114	133.34	61.3	20X-4	PP	20	188.20	85.8
14H-7	PP	11	133.81	56.4	20X-5	PP	55	190.05	110.3
14H-7	PP	45	134.15	66.2	20X-6	PP	57	191.57	13.8

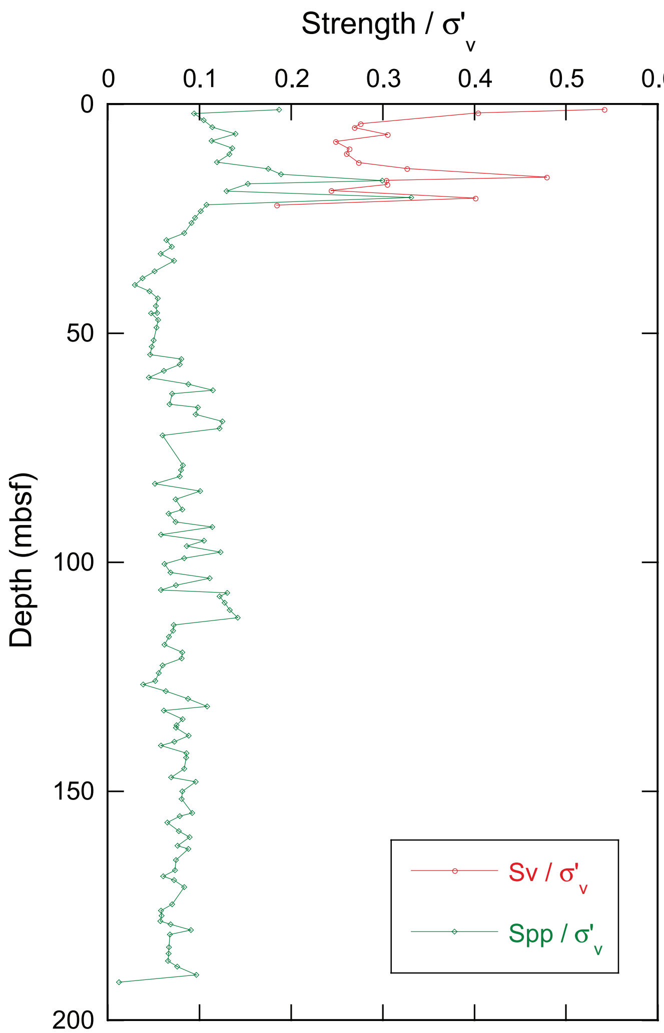

Figure 25. Shear strengths normalized to the effective vertical stress versus sub-bottom depth for Hole NGHP-01-18A.

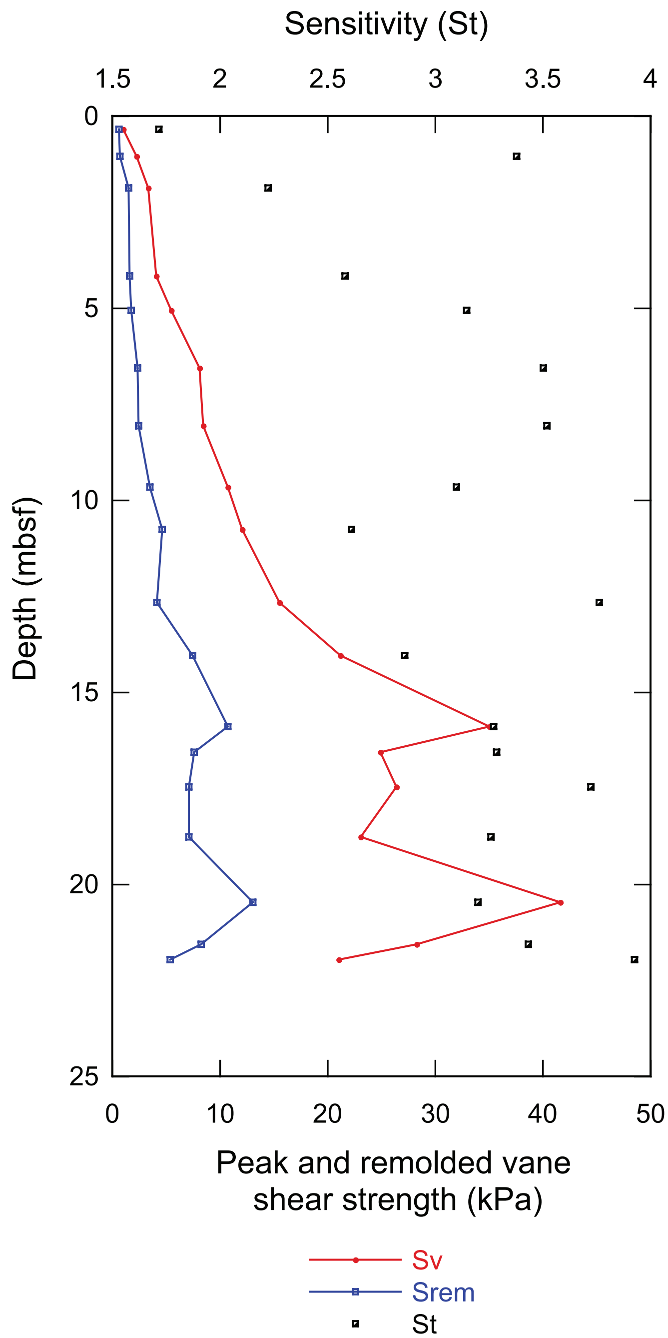

Figure 26. Peak and remolded vane shear strengths and sensitivity for Hole NGHP-01-18A.

Table 14. Wenner array electrical resistivity and formation factor results for Hole NGHP-01-18A. (To view the complete table, please see the ASCII files.)

Core, section	Sample	Top (cm)	Depth (mbsf)	Electrical resistivity (W×m)	Apparent formation factor	Core, section	Sample	Top (cm)	Depth (mbsf)	Electrical resistivity (W×m)	Apparent formation factor
					NGHP-01-18A						
1H-1	ER	33	0.33	0.778	3.89	2H-7	ER	15	16.55	0.465	2.33
1H-1	ER	67	0.67	1.009	5.05	2H-7	ER	44	16.84	0.586	2.93
1H-1	ER	103	1.03	0.459	2.30	2H-7	ER	59	16.99	0.592	2.96
1H-1	ER	116	1.16	0.502	2.51	3H-1	ER	15	17.05	0.496	2.48
1H-2	ER	35	1.85	0.501	2.51	3H-1	ER	35	17.25	0.511	2.56
1H-2	ER	55	2.05	0.699	3.50	3H-1	ER	55	17.45	0.512	2.56
1H-2	ER	97	2.47	0.791	3.96	3H-1	ER	75	17.65	0.52	2.60
1H-3	ER	15	3.15	0.405	2.03	3H-1	ER	95	17.85	0.524	2.62
1H-3	ER	35	3.35	0.406	2.03	3H-1	ER	115	18.05	0.518	2.59
1H-3	ER	55	3.55	0.432	2.16	3H-1	ER	126	18.16	0.524	2.62
1H-3	ER	75	3.75	0.424	2.12	3H-2	ER	15	18.55	0.644	3.22
1H-3	ER	95	3.95	0.426	2.13	3H-2	ER	35	18.75	0.549	2.75
1H-3	ER	115	4.15	0.418	2.09	3H-2	ER	55	18.95	0.572	2.86
1H-3	ER	130	4.30	0.398	1.99	3H-2	ER	75	19.15	0.555	2.78
1H-4	ER	15	4.65	0.407	2.04	3H-2	ER	95	19.35	0.589	2.95
1H-4	ER	35	4.85	0.41	2.05	3H-2	ER	115	19.55	0.649	3.25
1H-4	ER	55	5.05	0.413	2.07	3H-2	ER	135	19.75	0.579	2.90
1H-4	ER	75	5.25	0.426	2.13	3H-3	ER	15	20.05	0.62	3.10
1H-4	ER	95	5.45	0.423	2.12	3H-3	ER	35	20.25	0.636	3.18
1H-5	ER	15	6.15	0.444	2.22	3H-3	ER	55	20.45	0.6	3.00
1H-5	ER	35	6.35	0.437	2.19	3H-3	ER	75	20.65	0.63	3.15
1H-5	ER	55	6.55	0.401	2.01	3H-3	ER	95	20.85	0.548	2.74
1H-5	ER	75	6.75	0.439	2.20	3H-4	ER	15	21.55	1.096	5.48
2H-1	ER	45	7.85	0.526	2.63	3H-4	ER	35	21.75	0.677	3.39
2H-1	ER	65	8.05	0.501	2.51	3H-4	ER	55	21.95	0.533	2.67
2H-1	ER	85	8.25	0.517	2.59	3H-4	ER	75	22.15	0.607	3.04
2H-1	ER	105	8.45	0.515	2.58	3H-4	ER	95	22.35	0.523	2.62
2H-1	ER	125	8.65	0.533	2.67	3H-4	ER	115	22.55	0.575	2.88
2H-2	ER	15	9.05	0.457	2.29	3H-4	ER	135	22.75	0.623	3.12
2H-2	ER	35	9.25	0.513	2.57	3H-5	ER	17	23.07	0.541	2.71
2H-2	ER	55	9.45	0.482	2.41	3H-5	ER	35	23.25	0.58	2.90
2H-2	ER	75	9.65	0.476	2.38	3H-5	ER	51	23.41	0.547	2.74
2H-2	ER	95	9.85	0.462	2.31	3H-5	ER	75	23.65	0.647	3.24
2H-2	ER	115	10.05	0.461	2.31	3H-5	ER	95	23.85	0.558	2.79
2H-3	ER	15	10.55	0.465	2.33	3H-6	ER	4	24.44	0.54	2.70
2H-3	ER	35	10.75	0.461	2.31	3H-6	ER	36	24.76	0.547	2.74
2H-3	ER	55	10.95	0.507	2.54	3H-6	ER	52	24.92	0.526	2.63
2H-3	ER	75	11.15	0.469	2.35	3H-6	ER	83	25.23	0.571	2.86
2H-3	ER	95	11.35	0.461	2.31	3H-7	ER	6	25.46	0.693	3.47
2H-4	ER	15	12.05	0.473	2.37	3H-7	ER	25	25.65	0.49	2.45
2H-4	ER	35	12.25	0.46	2.30	3H-7	ER	46	25.86	0.485	2.43
2H-4	ER	55	12.45	0.499	2.50	4H-1	ER	84	27.24	0.485	2.43
2H-4	ER	75	12.65	0.49	2.45	4H-1	ER	99	27.39	0.569	2.85
2H-4	ER	95	12.85	0.495	2.48	4H-1	ER	119	27.59	0.624	3.12
2H-4	ER	115	13.05	0.536	2.68	4H-2	ER	20	28.10	0.53	2.65
2H-5	ER	15	13.55	0.495	2.48	4H-2	ER	40	28.30	0.526	2.63
2H-5	ER	35	13.75	0.556	2.78	4H-2	ER	60	28.50	0.505	2.53
2H-5	ER	55	13.95	0.54	2.70	4H-2	ER	80	28.70	0.662	3.31
2H-5	ER	75	14.15	0.573	2.87	4H-2	ER	109	28.99	0.566	2.83
2H-5	ER	95	14.35	0.61	3.05	4H-2	ER	129	29.19	0.542	2.71
2H-6	ER	10	15.00	0.534	2.67	4H-3	ER	18	29.58	0.589	2.95
2H-6	ER	30	15.20	0.589	2.95	4H-3	ER	47	29.87	0.625	3.13
2H-6	ER	50	15.40	0.63	3.15	4H-3	ER	70	30.10	0.596	2.98
2H-6	ER	70	15.60	0.527	2.64	4H-3	ER	94	30.34	0.637	3.19
2H-6	ER	90	15.80	0.579	2.90	4H-3	ER	111	30.51	0.618	3.09
2H-6	ER	110	16.00	0.57	2.85	4H-4	ER	17	31.07	0.489	2.45
2H-6	ER	130	16.20	0.573	2.87	4H-4	ER	37	31.27	0.544	2.72

Table 14. Wenner array electrical resistivity and formation factor results for Hole NGHP-01-18A. (To view the complete table, please see the ASCII files.)—Continued

Core, section	Sample	Top (cm)	Depth (mbsf)	Electrical resistivity (W×m)	Apparent formation factor	Core, section	Sample	Top (cm)	Depth (mbsf)	Electrical resistivity (W×m)	Apparent formation factor
NGHP-01-18A—Continued											
4H-4	ER	57	31.47	0.522	2.61	6H-2	ER	20	47.02	0.641	3.21
4H-4	ER	77	31.67	0.501	2.51	6H-2	ER	40	47.22	0.614	3.07
4H-4	ER	97	31.87	0.524	2.62	6H-2	ER	60	47.42	0.72	3.60
4H-4	ER	117	32.07	0.473	2.37	6H-2	ER	80	47.62	0.649	3.25
4H-5	ER	20	32.60	0.543	2.72	6H-2	ER	100	47.82	0.69	3.45
4H-5	ER	40	32.80	0.542	2.71	6H-3	ER	20	48.52	0.796	3.98
4H-5	ER	60	33.00	0.53	2.65	6H-3	ER	44	48.76	0.672	3.36
4H-5	ER	81	33.21	0.558	2.79	6H-3	ER	60	48.92	0.7	3.50
4H-6	ER	18	34.08	0.51	2.55	6H-3	ER	80	49.12	0.63	3.15
4H-6	ER	39	34.29	0.479	2.40	6H-3	ER	100	49.32	0.736	3.68
4H-6	ER	59	34.49	0.507	2.54	6H-3	ER	125	49.57	0.77	3.85
4H-6	ER	79	34.69	0.462	2.31	6H-3	ER	142	49.74	0.719	3.60
4H-7	ER	15	35.05	0.457	2.29	6H-4	ER	22	50.04	0.627	3.14
4H-7	ER	42	35.32	0.647	3.24	6H-4	ER	40	50.22	0.627	3.14
5H-1	ER	38	36.28	0.573	2.87	6H-4	ER	61	50.43	0.698	3.49
5H-1	ER	58	36.48	0.611	3.06	6H-4	ER	80	50.62	0.705	3.53
5H-1	ER	81	36.71	0.644	3.22	6H-4	ER	100	50.82	0.84	4.20
5H-1	ER	100	36.90	0.633	3.17	6H-4	ER	123	51.05	0.682	3.41
5H-1	ER	121	37.11	0.683	3.42	6H-4	ER	140	51.22	0.944	4.72
5H-2	ER	20	37.60	0.631	3.16	6H-5	ER	21	51.53	0.594	2.97
5H-2	ER	40	37.80	0.773	3.87	6H-5	ER	41	51.73	0.666	3.33
5H-2	ER	60	38.00	0.661	3.31	6H-5	ER	61	51.93	0.699	3.50
5H-2	ER	82	38.22	0.674	3.37	6H-5	ER	81	52.13	0.738	3.69
5H-2	ER	100	38.40	0.627	3.14	6H-6	ER	20	53.02	0.712	3.56
5H-2	ER	118	38.58	0.611	3.06	6H-6	ER	41	53.23	0.711	3.56
5H-3	ER	20	39.10	0.605	3.03	6H-7	ER	20	54.02	0.723	3.62
5H-3	ER	40	39.30	0.69	3.45	6H-7	ER	41	54.23	0.748	3.74
5H-3	ER	60	39.50	0.633	3.17	6H-7	ER	66	54.48	0.972	4.86
5H-3	ER	80	39.70	0.664	3.32	6H-7	ER	85	54.67	0.636	3.18
5H-3	ER	100	39.90	0.595	2.98	7H-1	ER	10	55.00	0.525	2.63
5H-4	ER	19	40.59	0.622	3.11	7H-1	ER	25	55.15	0.525	2.63
5H-4	ER	38	40.78	0.553	2.77	7H-1	ER	55	55.45	0.635	3.18
5H-4	ER	60	41.00	0.577	2.89	7H-1	ER	75	55.65	0.63	3.15
5H-4	ER	80	41.20	0.569	2.85	7H-1	ER	95	55.85	0.658	3.29
5H-4	ER	100	41.40	0.562	2.81	7H-2	ER	20	56.18	0.603	3.02
5H-4	ER	120	41.60	0.517	2.59	7H-2	ER	40	56.38	0.638	3.19
5H-4	ER	140	41.80	0.584	2.92	7H-2	ER	60	56.58	0.595	2.98
5H-5	ER	20	42.10	0.486	2.43	7H-2	ER	80	56.78	0.614	3.07
5H-5	ER	44	42.34	0.546	2.73	7H-2	ER	100	56.98	0.622	3.11
5H-5	ER	60	42.50	0.551	2.76	7H-3	ER	21	57.69	0.685	3.43
5H-5	ER	82	42.72	0.554	2.77	7H-3	ER	41	57.89	0.654	3.27
5H-6	ER	20	43.60	0.622	3.11	7H-3	ER	61	58.09	0.907	4.54
5H-6	ER	40	43.80	0.481	2.41	7H-3	ER	81	58.29	0.677	3.39
5H-6	ER	60	44.00	0.554	2.77	7H-3	ER	102	58.50	0.641	3.21
5H-6	ER	80	44.20	0.535	2.68	7H-3	ER	122	58.70	0.684	3.42
5H-6	ER	100	44.40	0.652	3.26	7H-4	ER	20	59.14	0.757	3.79
5H-6	ER	120	44.60	0.609	3.05	7H-4	ER	40	59.34	0.71	3.55
5H-7	ER	20	45.10	0.633	3.17	7H-4	ER	60	59.54	0.662	3.31
5H-7	ER	38	45.28	0.612	3.06	7H-4	ER	80	59.74	0.676	3.38
5H-7	ER	58	45.48	0.658	3.29	7H-4	ER	105	59.99	0.649	3.25
5H-7	ER	78	45.68	0.701	3.51	7H-4	ER	125	60.19	0.583	2.92
6H-1	ER	20	45.60	0.618	3.09	7H-5	ER	20	60.58	0.621	3.11
6H-1	ER	40	45.80	0.537	2.69	7H-5	ER	40	60.78	0.602	3.01
6H-1	ER	58	45.98	0.6	3.00	7H-5	ER	60	60.98	0.597	2.99
6H-1	ER	80	46.20	0.573	2.87	7H-6	ER	20	61.91	0.606	3.03
6H-1	ER	100	46.40	0.682	3.41	7H-6	ER	40	62.11	0.675	3.38
6H-1	ER	120	46.60	0.652	3.26	7H-6	ER	63	62.34	0.612	3.06

Table 14. Wenner array electrical resistivity and formation factor results for Hole NGHP-01-18A. (To view the complete table, please see the ASCII files.)—Continued

Core, section	Sample	Top (cm)	Depth (mbsf)	Electrical resistivity (W×m)	Apparent formation factor	Core, section	Sample	Top (cm)	Depth (mbsf)	Electrical resistivity (W×m)	Apparent formation factor
NGHP-01-18A—Continued											
7H-6	ER	83	62.54	0.635	3.18	9H-5	ER	40	84.30	0.686	3.43
7H-7	ER	20	62.85	0.631	3.16	9H-5	ER	63	84.53	0.812	4.06
7H-7	ER	40	63.05	0.648	3.24	9H-5	ER	85	84.75	0.781	3.91
7H-7	ER	60	63.25	0.654	3.27	9H-5	ER	105	84.95	0.855	4.28
8H-1	ER	87	65.27	0.629	3.15	9H-5	ER	125	85.15	0.71	3.55
8H-1	ER	107	65.47	0.766	3.83	9H-6	ER	20	85.47	0.665	3.33
8H-1	ER	127	65.67	0.689	3.45	9H-6	ER	41	85.68	0.749	3.75
8H-2	ER	20	66.07	0.631	3.16	9H-6	ER	57	85.84	0.789	3.95
8H-2	ER	40	66.27	0.691	3.46	9H-6	ER	74	86.01	0.731	3.66
8H-2	ER	60	66.47	0.654	3.27	9H-6	ER	94	86.21	0.698	3.49
8H-2	ER	80	66.67	0.684	3.42	10H-1	ER	65	88.05	0.594	2.97
8H-2	ER	100	66.87	0.728	3.64	10H-1	ER	85	88.25	0.637	3.19
8H-3	ER	20	67.53	0.664	3.32	10H-1	ER	105	88.45	0.721	3.61
8H-3	ER	40	67.73	0.667	3.34	10H-1	ER	125	88.65	0.788	3.94
8H-3	ER	60	67.93	0.686	3.43	10H-1	ER	145	88.85	0.697	3.49
8H-3	ER	79	68.12	0.684	3.42	10H-2	ER	15	89.05	0.733	3.67
8H-3	ER	100	68.33	0.713	3.57	10H-2	ER	35	89.25	0.733	3.67
8H-3	ER	120	68.53	0.646	3.23	10H-2	ER	46	89.36	0.773	3.87
8H-3	ER	140	68.73	0.614	3.07	10H-2	ER	84	89.74	0.833	4.17
8H-4	ER	20	69.03	0.657	3.29	10H-2	ER	101	89.91	0.729	3.65
8H-4	ER	40	69.23	0.645	3.23	10H-2	ER	123	90.13	0.731	3.66
8H-4	ER	60	69.43	0.691	3.46	10H-2	ER	139	90.29	0.84	4.20
8H-4	ER	79	69.62	0.759	3.80	10H-3	ER	15	90.55	0.714	3.57
8H-4	ER	100	69.83	0.63	3.15	10H-3	ER	35	90.75	0.709	3.55
8H-4	ER	120	70.03	0.689	3.45	10H-3	ER	55	90.95	0.818	4.09
8H-5	ER	20	70.53	0.714	3.57	10H-3	ER	75	91.15	0.782	3.91
8H-5	ER	39	70.72	0.674	3.37	10H-3	ER	95	91.35	0.771	3.86
8H-5	ER	60	70.93	0.66	3.30	10H-3	ER	116	91.56	0.849	4.25
8H-5	ER	83	71.16	0.654	3.27	10H-3	ER	136	91.76	0.728	3.64
8H-6	ER	20	72.03	0.693	3.47	10H-4	ER	15	92.03	0.718	3.59
8H-6	ER	40	72.23	0.892	4.46	10H-4	ER	35	92.23	0.773	3.87
8H-6	ER	58	72.41	0.779	3.90	10H-4	ER	55	92.43	0.723	3.62
8H-6	ER	80	72.63	0.808	4.04	10H-4	ER	75	92.63	0.741	3.71
8H-6	ER	100	72.83	0.816	4.08	10H-4	ER	89	92.77	0.762	3.81
9H-1	ER	27	78.17	0.616	3.08	10H-5	ER	15	93.53	0.756	3.78
9H-1	ER	63	78.53	0.763	3.82	10H-5	ER	35	93.73	0.676	3.38
9H-1	ER	83	78.73	0.785	3.93	10H-5	ER	55	93.93	0.71	3.55
9H-1	ER	103	78.93	0.926	4.63	10H-5	ER	75	94.13	0.671	3.36
9H-1	ER	123	79.13	0.794	3.97	10H-5	ER	95	94.33	0.719	3.60
9H-1	ER	143	79.33	0.732	3.66	10H-5	ER	116	94.54	0.618	3.09
9H-2	ER	20	79.60	0.755	3.78	10H-5	ER	133	94.71	0.642	3.21
9H-2	ER	40	79.80	0.762	3.81	10H-6	ER	15	95.03	0.64	3.20
9H-2	ER	58	79.98	0.795	3.98	10H-6	ER	35	95.23	0.672	3.36
9H-2	ER	78	80.18	0.759	3.80	10H-6	ER	55	95.43	0.795	3.98
9H-2	ER	100	80.40	0.797	3.99	10H-6	ER	87	95.75	0.789	3.95
9H-2	ER	116	80.56	0.759	3.80	10H-6	ER	105	95.93	0.749	3.75
9H-3	ER	20	81.10	0.797	3.99	10H-6	ER	125	96.13	0.718	3.59
9H-3	ER	40	81.30	0.745	3.73	10H-7	ER	15	96.46	0.765	3.83
9H-3	ER	65	81.55	1.081	5.41	10H-7	ER	35	96.66	0.731	3.66
9H-3	ER	93	81.83	0.824	4.12	11H-1	ER	35	97.25	0.722	3.61
9H-3	ER	112	82.02	0.89	4.45	11H-1	ER	58	97.48	0.695	3.48
9H-3	ER	132	82.22	0.738	3.69	11H-1	ER	80	97.70	0.766	3.83
9H-4	ER	20	82.60	0.812	4.06	11H-1	ER	104	97.94	0.751	3.76
9H-4	ER	40	82.80	0.703	3.52	11H-1	ER	122	98.12	0.771	3.86
9H-4	ER	64	83.04	0.799	4.00	11H-2	ER	24	98.64	0.865	4.33
9H-4	ER	84	83.24	0.747	3.74	11H-2	ER	37	98.77	0.741	3.71
9H-5	ER	20	84.10	0.705	3.53	11H-2	ER	67	99.07	0.776	3.88

Table 14. Wenner array electrical resistivity and formation factor results for Hole NGHP-01-18A. (To view the complete table, please see the ASCII files.)—Continued

Core, section	Sample	Top (cm)	Depth (mbsf)	Electrical resistivity (W×m)	Apparent formation factor	Core, section	Sample	Top (cm)	Depth (mbsf)	Electrical resistivity (W×m)	Apparent formation factor
					NGHP-01-18A—Continued						
11H-2	ER	85	99.25	0.751	3.76	12H-5	ER	55	112.11	0.625	3.13
11H-2	ER	105	99.45	0.763	3.82	12H-5	ER	81	112.37	0.676	3.38
11H-2	ER	128	99.68	0.919	4.60	12H-6	ER	17	113.23	0.686	3.43
11H-3	ER	8	99.98	0.744	3.72	12H-6	ER	37	113.43	0.712	3.56
11H-3	ER	25	100.15	0.917	4.59	12H-6	ER	59	113.65	0.805	4.03
11H-3	ER	38	100.28	0.838	4.19	12H-6	ER	87	113.93	0.735	3.68
11H-3	ER	52	100.42	1.004	5.02	12H-6	ER	108	114.14	0.676	3.38
11H-3	ER	86	100.76	0.62	3.10	12H-6	ER	129	114.35	0.66	3.30
11H-4	ER	15	101.55	0.734	3.67	12H-7	ER	15	114.65	0.624	3.12
11H-4	ER	34	101.74	0.737	3.69	12H-7	ER	35	114.85	0.643	3.22
11H-4	ER	60	102.00	0.658	3.29	12H-7	ER	51	115.01	0.592	2.96
11H-4	ER	78	102.18	0.668	3.34	12H-7	ER	71	115.21	0.736	3.68
11H-4	ER	108	102.48	0.76	3.80	12H-7	ER	103	115.53	0.623	3.12
11H-4	ER	126	102.66	0.82	4.10	12H-7	ER	128	115.78	0.629	3.15
11H-4	ER	143	102.83	0.726	3.63	13X-1	ER	15	116.05	0.598	2.99
11H-5	ER	15	103.03	0.635	3.18	13X-1	ER	35	116.25	0.566	2.83
11H-5	ER	35	103.23	0.802	4.01	13X-1	ER	55	116.45	0.621	3.11
11H-5	ER	55	103.43	0.667	3.34	13X-1	ER	75	116.65	0.809	4.05
11H-5	ER	75	103.63	0.669	3.35	13X-1	ER	95	116.85	0.702	3.51
11H-5	ER	95	103.83	0.668	3.34	13X-1	ER	115	117.05	0.654	3.27
11H-5	ER	115	104.03	0.642	3.21	13X-1	ER	135	117.25	0.717	3.59
11H-5	ER	135	104.23	0.687	3.44	13X-2	ER	15	117.55	0.629	3.15
11H-6	ER	6	104.44	0.669	3.35	13X-2	ER	35	117.75	0.658	3.29
11H-6	ER	19	104.57	0.803	4.02	13X-2	ER	55	117.95	0.658	3.29
11H-6	ER	40	104.78	0.849	4.25	13X-2	ER	76	118.16	0.717	3.59
11H-6	ER	57	104.95	0.767	3.84	13X-2	ER	95	118.35	0.639	3.20
11H-6	ER	70	105.08	0.768	3.84	13X-2	ER	115	118.55	0.636	3.18
11H-6	ER	85	105.23	0.843	4.22	13X-2	ER	135	118.75	0.644	3.22
11H-6	ER	108	105.46	0.713	3.57	13X-3	ER	15	119.05	0.568	2.84
11H-7	ER	10	105.62	0.703	3.52	13X-3	ER	35	119.25	0.556	2.78
11H-7	ER	58	106.10	0.727	3.64	13X-3	ER	53	119.43	0.602	3.01
12H-1	ER	10	106.50	0.61	3.05	13X-3	ER	75	119.65	0.59	2.95
12H-1	ER	32	106.72	0.608	3.04	13X-3	ER	95	119.85	0.609	3.05
12H-2	ER	15	107.21	0.67	3.35	13X-3	ER	115	120.05	0.594	2.97
12H-2	ER	35	107.41	0.629	3.15	13X-3	ER	135	120.25	0.622	3.11
12H-2	ER	60	107.66	0.666	3.33	13X-4	ER	15	120.55	0.605	3.03
12H-2	ER	88	107.94	0.657	3.29	13X-4	ER	35	120.75	0.58	2.90
12H-2	ER	98	108.04	0.693	3.47	13X-4	ER	55	120.95	0.633	3.17
12H-2	ER	123	108.29	0.682	3.41	13X-4	ER	75	121.15	0.66	3.30
12H-2	ER	142	108.48	0.688	3.44	13X-5	ER	15	122.05	0.614	3.07
12H-3	ER	8	108.64	0.658	3.29	13X-5	ER	35	122.25	0.594	2.97
12H-3	ER	22	108.78	0.667	3.34	13X-5	ER	55	122.45	0.562	2.81
12H-3	ER	42	108.98	0.65	3.25	13X-5	ER	75	122.65	0.629	3.15
12H-3	ER	62	109.18	0.652	3.26	13X-5	ER	95	122.85	0.629	3.15
12H-3	ER	94	109.50	0.676	3.38	13X-5	ER	115	123.05	0.605	3.03
12H-3	ER	113	109.69	0.662	3.31	13X-5	ER	135	123.25	0.605	3.03
12H-3	ER	141	109.97	0.668	3.34	13X-6	ER	15	123.55	0.652	3.26
12H-4	ER	15	110.21	0.69	3.45	13X-6	ER	33	123.73	0.611	3.06
12H-4	ER	32	110.38	0.693	3.47	13X-6	ER	55	123.95	0.62	3.10
12H-4	ER	52	110.58	0.7	3.50	13X-6	ER	75	124.15	0.603	3.02
12H-4	ER	71	110.77	0.688	3.44	13X-6	ER	95	124.35	0.587	2.94
12H-4	ER	91	110.97	0.808	4.04	13X-6	ER	114	124.54	0.639	3.20
12H-4	ER	110	111.16	0.831	4.16	13X-6	ER	132	124.72	0.618	3.09
12H-4	ER	120	111.26	0.657	3.29	14X-1	ER	7	125.57	0.544	2.72
12H-5	ER	15	111.71	0.64	3.20	14X-1	ER	18	125.68	0.562	2.81
12H-5	ER	35	111.91	0.66	3.30	14X-1	ER	36	125.86	0.569	2.85

Table 14. Wenner array electrical resistivity and formation factor results for Hole NGHP-01-18A. (To view the complete table, please see the ASCII files.)—Continued

Core, section	Sample	Top (cm)	Depth (mbsf)	Electrical resistivity (W×m)	Apparent formation factor	Core, section	Sample	Top (cm)	Depth (mbsf)	Electrical resistivity (W×m)	Apparent formation factor
NGHP-01-18A—Continued											
14X-1	ER	56	126.06	0.602	3.01	15X-4	ER	57	139.58	1.121	5.61
14X-2	ER	7	126.27	0.553	2.77	15X-5	ER	20	139.83	0.593	2.97
14X-2	ER	41	126.61	0.623	3.12	15X-5	ER	40	140.03	0.604	3.02
14X-2	ER	61	126.81	0.586	2.93	15X-6	ER	31	141.34	0.615	3.08
14X-2	ER	67	126.87	0.541	2.71	15X-6	ER	51	141.54	0.619	3.10
14X-3	ER	12	127.82	0.655	3.28	15X-6	ER	71	141.74	0.57	2.85
14X-3	ER	35	128.05	0.539	2.70	15X-6	ER	92	141.95	0.54	2.70
14X-3	ER	55	128.25	0.56	2.80	15X-7	ER	20	142.41	0.643	3.22
14X-3	ER	77	128.47	0.704	3.52	15X-7	ER	40	142.61	0.899	4.50
14X-3	ER	96	128.66	0.552	2.76	16X-1	ER	20	145.00	0.466	2.33
14X-3	ER	116	128.86	0.596	2.98	16X-1	ER	40	145.20	0.47	2.35
14X-4	ER	14	129.34	0.629	3.15	16X-1	ER	70	145.50	0.461	2.31
14X-4	ER	35	129.55	0.616	3.08	16X-1	ER	90	145.70	0.632	3.16
14X-4	ER	55	129.75	0.637	3.19	16X-1	ER	110	145.90	0.856	4.28
14X-4	ER	75	129.95	0.741	3.71	16X-1	ER	132	146.12	0.866	4.33
14X-4	ER	95	130.15	0.611	3.06	16X-2	ER	20	146.45	0.723	3.62
14X-4	ER	115	130.35	0.571	2.86	16X-2	ER	43	146.68	0.849	4.25
14X-4	ER	136	130.56	0.751	3.76	16X-2	ER	63	146.88	1.146	5.73
14X-4	ER	156	130.76	0.53	2.65	16X-2	ER	103	147.28	0.652	3.26
14X-5	ER	15	130.85	0.547	2.74	16X-2	ER	125	147.50	1.006	5.03
14X-5	ER	35	131.05	0.53	2.65	17X-2	ER	110	155.90	0.701	3.51
14X-5	ER	55	131.25	0.612	3.06	17X-2	ER	135	156.15	0.711	3.56
14X-5	ER	79	131.49	0.585	2.93	17X-3	ER	20	156.50	0.747	3.74
14X-5	ER	100	131.70	0.616	3.08	17X-3	ER	54	156.84	0.745	3.73
14X-5	ER	117	131.87	0.555	2.78	17X-3	ER	75	157.05	0.749	3.75
14X-5	ER	132	132.02	0.669	3.35	17X-3	ER	95	157.25	0.732	3.66
14X-6	ER	15	132.35	0.765	3.83	17X-3	ER	115	157.45	0.741	3.71
14X-6	ER	35	132.55	0.667	3.34	17X-3	ER	135	157.65	0.779	3.90
14X-6	ER	62	132.82	0.609	3.05	17X-4	ER	15	157.95	0.67877	3.39
14X-6	ER	80	133.00	0.606	3.03	17X-4	ER	53	158.33	0.77353	3.87
14X-6	ER	100	133.20	0.646	3.23	17X-4	ER	79	158.59	0.77353	3.87
14X-6	ER	122	133.42	0.689	3.45	17X-4	ER	102	158.82	0.73439	3.67
14X-7	ER	15	133.85	0.766	3.83	17X-4	ER	124	159.04	0.87035	4.35
14X-7	ER	18	133.88	0.72	3.60	17X-5	ER	15	159.45	0.799	4.00
14X-7	ER	32	134.02	0.654	3.27	17X-5	ER	26	159.56	0.822	4.11
14X-7	ER	52	134.22	0.627	3.14	17X-5	ER	53	159.83	0.824	4.12
15X-1	ER	21	135.41	0.71	3.55	17X-6	ER	20	160.90	0.989	4.95
15X-1	ER	36	135.56	0.684	3.42	17X-6	ER	40	161.10	0.845	4.23
15X-1	ER	51	135.71	0.652	3.26	17X-6	ER	60	161.30	0.825	4.13
15X-1	ER	71	135.91	0.678	3.39	17X-6	ER	95	161.65	0.773	3.87
15X-2	ER	20	136.21	0.639	3.20	17X-6	ER	112	161.82	0.854	4.27
15X-2	ER	40	136.41	0.633	3.17	17X-7	ER	20	162.40	0.848	4.24
15X-2	ER	60	136.61	0.631	3.16	17X-7	ER	35	162.55	0.808	4.04
15X-2	ER	80	136.81	0.69	3.45	17X-7	ER	47	162.67	0.861	4.31
15X-2	ER	100	137.01	0.65	3.25	18X-1	ER	20	164.50	0.822	4.11
15X-2	ER	120	137.21	0.626	3.13	18X-1	ER	46	164.76	0.668	3.34
15X-2	ER	140	137.41	0.616	3.08	18X-1	ER	66	164.96	0.626	3.13
15X-3	ER	20	137.71	0.685	3.43	18X-2	ER	18	165.21	0.549	2.75
15X-3	ER	40	137.91	0.76	3.80	18X-2	ER	40	165.43	0.63	3.15
15X-3	ER	60	138.11	0.82	4.10	18X-2	ER	60	165.63	0.631	3.16
15X-3	ER	80	138.31	0.862	4.31	18X-2	ER	80	165.83	0.586	2.93
15X-3	ER	100	138.51	0.978	4.89	18X-2	ER	100	166.03	0.625	3.13
15X-3	ER	120	138.71	0.769	3.85	18X-2	ER	120	166.23	0.625	3.13
15X-3	ER	140	138.91	0.863	4.32	18X-2	ER	140	166.43	0.742	3.71
15X-4	ER	20	139.21	0.98	4.90	18X-3	ER	20	166.73	0.687	3.44
15X-4	ER	38	139.39	0.778	3.89	18X-3	ER	40	166.93	0.747	3.74

Table 14. Wenner array electrical resistivity and formation factor results for Hole NGHP-01-18A. (To view the complete table, please see the ASCII files.)—Continued

Core, section	Sample	Top (cm)	Depth (mbsf)	Electrical resistivity (W×m)	Apparent formation factor	Core, section	Sample	Top (cm)	Depth (mbsf)	Electrical resistivity (W×m)	Apparent formation factor
NGHP-01-18A—Continued											
18X-3	ER	60	167.13	0.626	3.13	19X-6	ER	38	179.01	1.1	5.50
18X-3	ER	80	167.33	0.615	3.08	19X-7	ER	50	180.23	0.596	2.98
18X-3	ER	100	167.53	0.633	3.17	19X-7	ER	70	180.43	0.603	3.02
18X-3	ER	120	167.73	0.608	3.04	19X-8	ER	40	181.08	0.735	3.68
18X-3	ER	140	167.93	0.684	3.42	20X-1	ER	20	183.70	0.608	3.04
18X-4	ER	27	168.30	0.604	3.02	20X-1	ER	40	183.90	0.619	3.10
18X-4	ER	47	168.50	0.621	3.11	20X-1	ER	60	184.10	0.673	3.37
18X-4	ER	67	168.70	0.605	3.03	20X-1	ER	80	184.30	0.69	3.45
18X-4	ER	87	168.90	0.735	3.68	20X-1	ER	100	184.50	1.286	6.43
18X-5	ER	20	169.12	0.659	3.30	20X-1	ER	120	184.70	1.43	7.15
18X-5	ER	20	169.12	0.607	3.04	20X-1	ER	140	184.90	1.245	6.23
18X-5	ER	40	169.32	0.521	2.61	20X-2	ER	20	185.20	0.655	3.28
18X-5	ER	60	169.52	0.673	3.37	20X-2	ER	40	185.40	0.694	3.47
18X-5	ER	80	169.72	0.66	3.30	20X-2	ER	60	185.60	0.646	3.23
18X-6	ER	20	170.62	0.599	3.00	20X-2	ER	80	185.80	0.7	3.50
18X-6	ER	40	170.82	0.585	2.93	20X-3	ER	20	186.70	0.679	3.40
18X-6	ER	64	171.06	0.916	4.58	20X-3	ER	40	186.90	0.675	3.38
18X-6	ER	64	171.06	0.684	3.42	20X-3	ER	60	187.10	0.726	3.63
19H-1	ER	20	174.00	0.59	2.95	20X-3	ER	80	187.30	0.722	3.61
19H-2	ER	20	174.25	0.592	2.96	20X-3	ER	100	187.50	0.685	3.43
19X-2	ER	20	174.25	0.592	2.96	20X-3	ER	120	187.70	0.783	3.92
19X-2	ER	44	174.49	0.548	2.74	20X-3	ER	140	187.90	0.628	3.14
19X-2	ER	54	174.59	0.602	3.01	20X-4	ER	20	188.20	0.644	3.22
19X-2	ER	64	174.69	0.601	3.01	20X-4	ER	40	188.40	0.687	3.44
19X-2	ER	81	174.86	0.596	2.98	20X-4	ER	60	188.60	0.664	3.32
19X-3	ER	20	175.43	0.523	2.62	20X-4	ER	80	188.80	0.661	3.31
19X-3	ER	49	175.72	0.732	3.66	20X-4	ER	100	189.00	0.659	3.30
19X-3	ER	73	175.96	0.637	3.19	20X-4	ER	120	189.20	0.752	3.76
19X-3	ER	96	176.19	0.641	3.21	20X-4	ER	140	189.40	1.031	5.16
19X-3	ER	110	176.33	0.695	3.48	20X-5	ER	20	189.70	0.731	3.66
19X-3	ER	134	176.57	0.64	3.20	20X-5	ER	40	189.90	0.652	3.26
19X-4	ER	21	176.94	0.81	4.05	20X-5	ER	60	190.10	0.839	4.20
19X-4	ER	42	177.15	0.78	3.90	20X-5	ER	80	190.30	0.714	3.57
19X-4	ER	62	177.35	0.921	4.61	20X-5	ER	100	190.50	0.718	3.59
19X-4	ER	84	177.57	0.701	3.51	20X-5	ER	120	190.70	0.646	3.23
19X-5	ER	19	177.96	0.828	4.14	20X-5	ER	140	190.90	0.703	3.52
19X-5	ER	42	178.19	1.118	5.59	20X-6	ER	20	191.20	0.895	4.48
19X-5	ER	42	178.19	0.799	4.00	20X-6	ER	40	191.40	0.761	3.81
19X-5	ER	62	178.39	0.985	4.93						

Resistivity determined using the MSCL increase between 20 and 80 mbsf (fig. 24), which is at and below the depth of the SMI (20 mbsf). A possible explanation for this agreement is that methane is produced below the SMI and this gas expands upon core recovery disrupting the sediment structure.

The apparent formation factor is the ratio of the resistivity of a saturated sediment to the resistivity of the pore fluid and provides an indication of the relationships between sediment structure, void space, tortuosity, and other factors, and the ability of fluid to flow through the formation. Because pore water salinity typically varies a small amount in the recovered sediment and is similar to that of seawater (see "Inorganic Geochemistry"), we have normalized the measured Wenner resistivity values by that of seawater (approximately 0.2 ohm-mk) (table 14). Most values range from about 2.0 at the top of the core to 4.0 below 50 m (fig. 27). Other equations and methods exist for calculating formation factor, however, they require the use of empirical constants that have not yet been determined for the sediments at this location.

P-Wave Velocity

P-wave velocity (V_p) measured with the MSCL increased from 1.47 km/s in the top of the hole (fig. 24) to 1.54 km/s at a sub-bottom depth of 20 m, which represents the depth where gas and voids present in the sediment prevented further valid

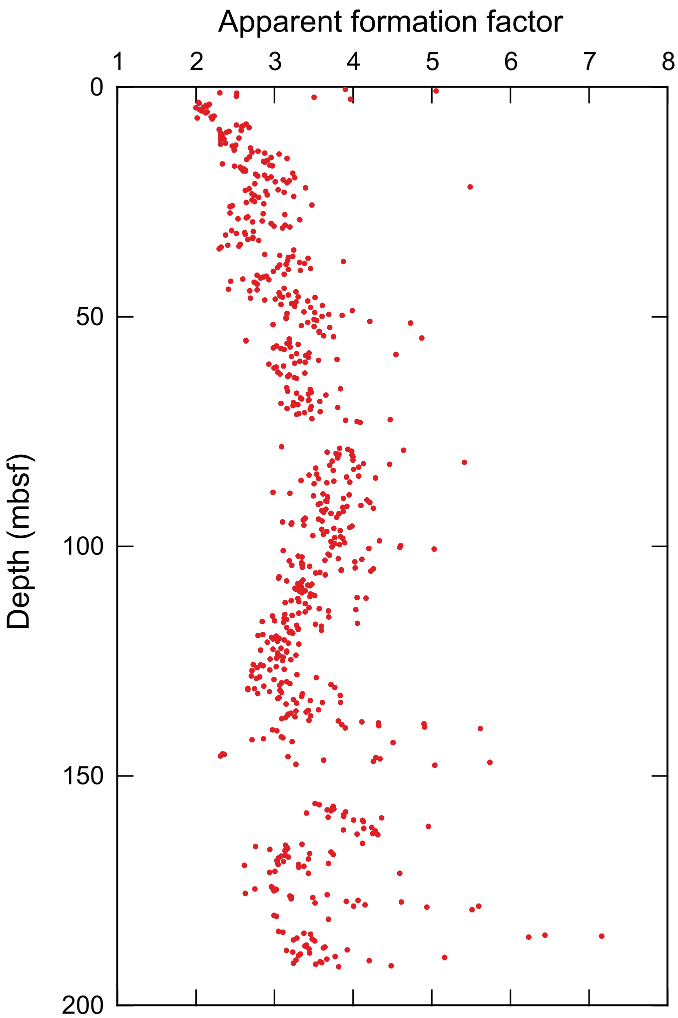

Figure 27. Apparent formation factor versus sub-bottom depth for Hole NGHP-01-18A.

Table 15. Contact *P*-wave velocity results determined on split cores sections from Hole NGHP-01-18A.

Core, section	Sample	Top (cm)	Depth (mbsf)	VP (m/s)	VP (km/s)
NGHP-01-18A					
1H-1	VP	104	1.04	1467.1	1.467
1H-2	VP	36	1.86	1468.7	1.469
1H-3	VP	115	4.15	1464.0	1.464
1H-4	VP	56	5.06	1476.2	1.476
1H-5	VP	56	6.56	1468.7	1.469
2H-1	VP	65	8.05	1492.4	1.492
2H-2	VP	75	9.65	1484.4	1.484
2H-3	VP	35	10.75	1482.8	1.483
2H-4	VP	75	12.65	1487.6	1.488
2H-5	VP	55	13.95	1482.8	1.483
2H-6	VP	90	15.80	1507.1	1.507
2H-7	VP	15	16.55	1489.2	1.489
3H-1	VP	55	17.45	1479.7	1.480
3H-2	VP	36	18.76	1492.4	1.492

measurements from being logged. The contact V_P values of 1.47 to 1.51 km/s (table 15) are in agreement with the MSCL values. Valid contact V_P measurements also could not be determined below 20 mbsf. Both techniques are adversely affected by the SMI located at about 20 mbsf (see "Organic Geochemistry" and "Inorganic Geochemistry"). Methane, which is typically produced below the SMI, may come out of solution if present in a high enough concentration and attenuate acoustic signals.

Magnetic Susceptibility

Except between 10 to 20 mbsf, magnetic susceptibility is uniform and low at this site compared to previous holes drilled to the S in the KG Basin during Expedition 01. These measurements reflect a lack of terrigenous magnetic minerals in the sediment (fig. 24 and see "Lithostratigraphy").

Thermal Conductivity

Thermal conductivities vary between 0.7575 and 1.077 W/(m×K) and average about 0.9 W/(m×K) with sub-bottom depth (table 16 and fig. 24). Such values are well within the range of marine sediments (for example, Novosel, and others, in press), although they are all lower than values determined by Davis and others (1990) for sediment from Cascadia and the Nankai Trough.

Table 16. Thermal conductivity results for Hole NGHP-01-18A.

Core, section	Sample	Top (cm)	Depth (mbsf)	Thermal conductivity (W/[m×K])
NGHP-01-18A				
1H-3	TC	70	3.70	0.9035
2H-7	TC	33	16.73	0.9035
3H-3	TC	55	20.45	1.077
3H-7	TC	35	25.75	0.8865
4H-3	TC	65	30.05	0.8475
5H-1	TC	75	36.65	0.86075
5H-4	TC	62	41.02	0.9035
5H-7	TC	47	45.37	0.85025
6H-1	TC	75	46.15	0.82875
6H-3	TC	75	49.07	0.99325
7H-3	TC	75	58.23	0.84725
8H-3	TC	66	67.99	0.9035
9H-3	TC	75	81.65	0.7575
10H-3	TC	75	91.15	0.88275
11H-3	TC	55	100.45	0.91075
12H-3	TC	73	109.29	0.88675
13X-3	TC	75	119.65	0.9035
14X-3	TC	75	128.45	0.879
14X-7	TC	33	134.03	0.94575
15X-3	TC	75	138.26	0.90925
16X-3	TC	75	148.50	0.867
17X-3	TC	75	157.05	0.9035
18X-3	TC	75	167.28	0.97725
19X-3	TC	75	175.98	0.87775
20X-3	TC	75	187.25	1.0145

Down-Hole Temperature Measurements

A number of different tools are available for determining downhole sediment temperature (see “Physical Properties” section of “Methods” chapter). At Site NGHP-01-18, four attempts were made to measure *in situ* temperature, and three provided usable *in situ* temperature data, although the two APC3 measurements showed several secondary frictional pulses, leading to large uncertainty (table 17). With only three measurements, we did not attempt to estimate the uncertainty in the thermal gradient. The seafloor temperature intercept was determined to be 5.4 °C and the geothermal gradient was determined to be 50 °C per km (fig. 28). The base of gas-hydrate stability is predicted at 210 mbsf assuming pure methane and porewater salinity of 35 ppt (Sloan, 1998) (shipboard calculated seafloor temperature 5.4 °C, geothermal gradient 50 °C per km).

Pressure Coring

No pressure cores were recovered at Site NGHP-01-18. The weather was too rough to deploy the pressure coring tools, with ship’s heave over 5 m.

Down-Hole Logging

No wire-line logging was performed at Site NGHP-01-18 due to rough weather and sea state.

Table 17. *In situ* temperature estimates for Hole NGHP-01-18A.

Depth (mbsf)	Core	Assumed thermal conductivity (W/m×K)	Tool	Temperature (°C)	Ad-hoc calibration correction	Corrected temperature (°C)	Estimated uncertainty	Data quality
26.4	A03H	0.95	APCT-3	6.56	0	6.56	0.2	fair-good
45.4	A05H	0.95	APCT-3	7.76	0	7.76	0.2	fair-good
NA	A14X	0.95	DVTP	NA	0.50	NA	NA	poor (no contact with formation)
191.4	A20X	0.95	DVTP	14.45	0.50	14.84	0.2	good

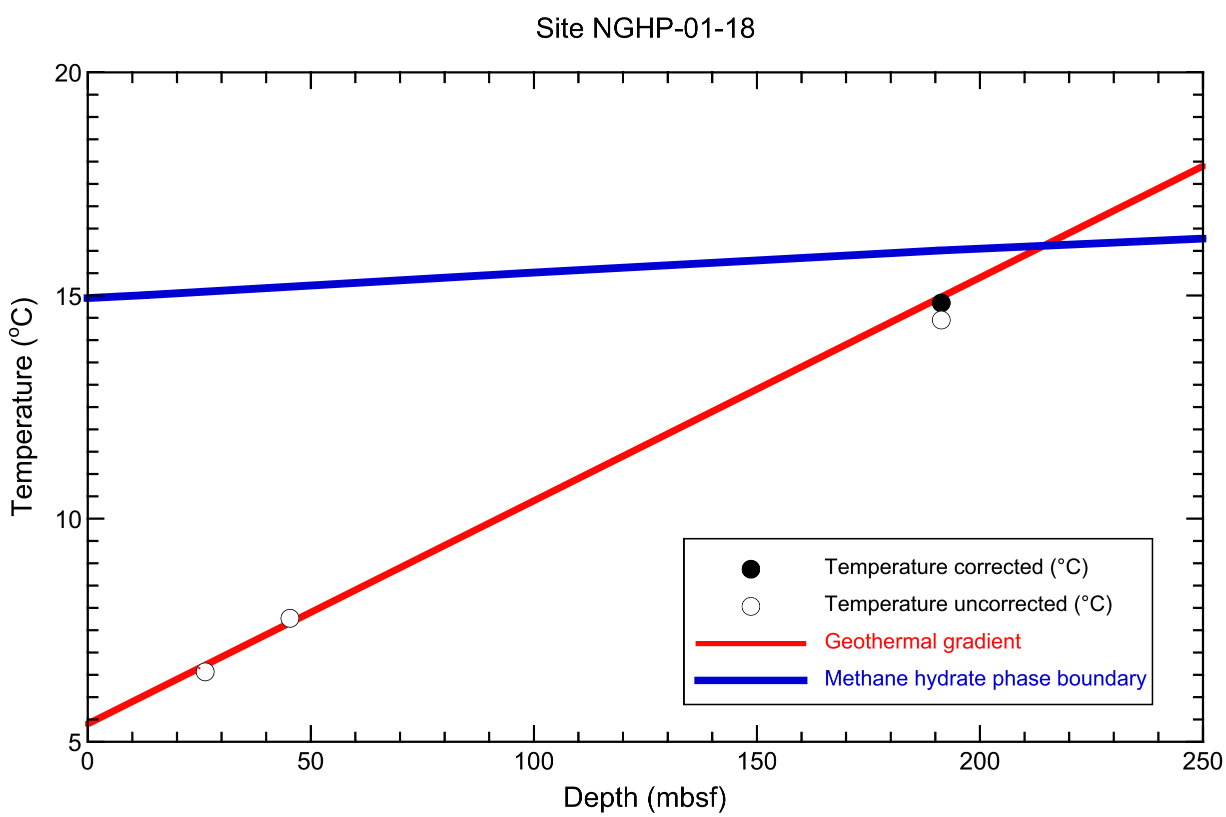

Figure 28. Geothermal gradient and estimated depth to the BSR from *in situ* temperature measurements for Hole NGHP-01-18A. [BSR, bottom-simulating reflector]

References Cited

Bjerrum, L., 1972, Embankments on soft ground, *in* ASCE Specialty Conference on Performance of Earth and Earth-Supported Structures, Lafayette, Ind., June 11–14, 1972, Proceedings: New York, American Society of Civil Engineers, v. 2, p. 1–54. [Held at Purdue University]

Davis, E.E., Hyndman, R.D., and Villinger, H., 1990, Rates of fluid expulsion across the northern Cascadia accretionary prism—Constraints from new heat flow and multichannel seismic reflection data: Journal of Geophysical Research, v. 95, p. 8869–8889.

Duan, Z., Møller, N., Greenberg, J., and Weare, J.H., 1992, The prediction of methane solubility in natural waters to high ionic strengths from 0° to 250°C and from 0 to 1600 bar: Geochimica et Cosmochimica Acta*,* v. 56, p. 1451–1460.

Holtz, R.D., and Kovacs, W.D., 1981, An introduction to geotechnical engineering: Englewood Cliffs, N.J., Prentice-Hall, Inc., 733 p.

Hunt, R.E., 1984, Geotechnical engineering investigation manual: New York, McGraw-Hill Book Company, 983 p.

Kvenvolden, K.A., and Lorenson, T.D., 2000, Methane and other hydrocarbon gases in sediment from the southeastern North American continental margin, *in* Paull, C.K., Matsumoto, R., Wallace, P.J., Black, N.R., Borowski, W.S.,Collett, T.S., Damuth, J.E., Dickens, G.R., Egeberg, P.K., Goodman,K., Hesse, R.F., Hiroki, Y., Holbrook, W.S., Hoskins, H., Ladd, J. ,Lodolo, E., Lorenson, T.D.,Musgrave, R.J., Naehr, T.H., Okada, H., Pierre, C., Ruppel, C.D., Satoh, M., Thiery, R., Watanabe, Y., Wehner, H., Winters, W.J.,and Wood, W.T., Gas hydrate sampling on the Blake ridge and Carolina rise—covering leg 164 of the cruises of the drilling vessel JOIDES Resolution, Halifax, Nova Scotia, to Miami, Florida, sites 991–997, 31 October–19 December 1995: Proceedings of the Ocean Drilling Program, Scientific Results*,* v. 164: College Station, Tex., Ocean Drilling Program, p. 29–36. [CD-ROM; available from: Ocean Drilling Program, Texas A&M University, College Station, Tex. 77845-9547, U.S.A.]

Ladd, C.C., Foote, R., Ishihara, K., Schlosser, F., and Poulos, H.G., 1977, Stress-deformation and strength characteristics, *in* State-of-the-Art Report, International Conference on Soil Mechanics and Foundation Engineering*,* 9th, Tokyo, Japan, July 1977, Proceedings: London, International Society for Soil Mechanics and Geotechnical Engineering, v. 2, p. 421–494.

Lambe, T. W., Whitman, R.V., 1969, Soil mechanics: New York, John Wiley and Sons, 553 p.

Musgrave, R.J., Bangs, N.L., Larrasoana, J.C., Gracia, E., Hollamby, J., and Vega, M.E., 2006, Rise of the base of the gas hydrate zone since the last glacial recorded by rock magnetism: Geology*,* v. 34, no. 2, p. 117–120.

Novosel, I., Winters, W.J., Boldina, O.M., Labails, C., and Geli, L., 2007, Thermal conductivity of sediment recovered from the IMAGES VIII/PAGE 127 Gas Hydrate and Paleoclimate Cruise on the R/V Marion Dufresne in the Gulf of Mexico, 2–18 July 2002, chap. 7 *of* Winters, W.J., Lorenson, T.D., and Paull, C.K., eds., Initial report of the IMAGES VIII/PAGE 127 gas hydrate and paleoclimate cruise on the RV Marion Dufresne in the Gulf of Mexico, 2–18 July 2002: U.S. Geological Survey Open-File Report 2004–1358, unpaged. (Also available at *http://woodshole.er.usgs.gov/pubs/of2004-1358/*)

Sloan, E.D., 1998, Clathrate hydrates of natural gases (2d ed.): New York, Marcel Dekker, 705 p.

Xu, W., 2002, Phase balance and dynamic equilibrium during formation and dissociation of methane gas hydrate, *in* International Conference on Gas Hydrates, 4th, Yokohama, Japan, May 2002, Proceedings: Yokohama, Japan, International Conference on Gas Hydrates, p. 195–200.

Xu, W., 2004, Modeling dynamic marine gas hydrate systems: American Mineralogist, v. 89, p. 1271–1279.